UNIVERSITY OF CALIFORNIA SAN DIEGO

Passive acoustic monitoring of Arctic cetaceans: Site-specific detection probability, species identification and discrimination, and underwater soundscape with increasing shipping

A dissertation submitted in partial satisfaction of the
requirements for the degree
Doctor of Philosophy

in

Oceanography

by

Joshua M. Jones

Committee in charge:

John A. Hildebrand, Chair
Peter J. S. Franks
Julie L. McClean
Mark D. Ohman
Ronghui (Lily) Xu

2021

The dissertation of Joshua M. Jones is approved, and it is acceptable in quality and form for publication on microfilm and electronically.

University of California San Diego

2021

DEDICATION

To the many people in the north who have shared so much to guide this work and to make it possible.

TABLE OF CONTENTS

LIST OF FIGURES

LIST OF TABLES

ACKNOWLEDGEMENTS

I thank the Mittimatalik Hunters & Trappers Organization, Pond Inlet, Nunavut and the Resolute Bay Hunters and Trappers Association, Resolute Bay, Nunavut for annual permission to carry out fieldwork and acoustic recording. Acoustic data collection and fieldwork could not have been completed without expert knowledge and technical, logistical, and vessel support provided by Randy Nungaq and Alex Ootoowak. I also thank Sheattie Tagak and Tagak Outfitters for additional vessel support. Kristin Westdal and Amanda Joynt of Oceans North were also instrumental in initiating and sustaining this research program. Thanks to Evan Richardson and Environment and Climate Change Canada, for substantial logistical support at the Pond Inlet Research Facility. This project is funded through a private foundation grant to the Marine Physical Laboratory at the Scripps Institution of Oceanography and by Oceans North, with additional support provided by Environment and Climate Change Canada through a grant from the World Wildlife Fund - Canada.

Thanks to the Alaska Department of Fish and Game, Sylvia Kreel and the Coastal Impact Assistance Program (CIAP) of the U.S. Fish and Wildlife Service and Craig George and Robert Suydam of the North Slope Borough Department of Wildlife Management for providing the funding to make the Chukchi Sea acoustic monitoring program possible. Thanks to Mati Kahru (SIO) for assistance with the acquisition and processing of satellite sea ice data. Bob Pickart (WHOI), John Kemp (WHOI), and Catherine Berchok (NOAA-NMFS), who provided ship time and invaluable at-sea support for Chukchi Sea mooring operations. We also thank the captain and crew of the US Coast Guard Cutters *Healy* and *Maple* for their professionalism and assistance at sea.

I thank members of the Scripps Whale Acoustics Laboratory, including E. H. Roth, B. J. Thayre, J. E. Mainez-Hurwitz, E. O'Neill-Mertz, J. Trickey, and S. Wager for assistance with HARP operations and data processing. Kait Frasier helped with many aspects of signal detection, data processing, and emotional well-being. Sean M. Wiggins, lead engineer and project scientist

at the Whale Acoustics Laboratory, developed the High-frequency Acoustic Recording Package upon which all acoustic data collection for my dissertation has depended. Sean has also provided countless hours of detailed feedback and guidance on all aspects of my research. I owe him a debt of gratitude that cannot be paid back, only forward. Special thanks to Andrew Mack, Marianne Marcoux, Jeff Hidgon, and Bruce Stewart, who provided helpful comments and critical review. Phil McGillivary, thank you for your abundant mentorship over 15 years and for your more than generous support in the form of detailed, line-by-line, looking at every word and phrase, reviews of the contents of this document. Dr. Julie D. Lee also provided extensive detailed critical feedback and guidance throughout the process of writing and finalizing my dissertation. Thank you, Dr. Lee for also being my Mom.

Thank you June, for your always support. Even more so, thank you for showing me what it looks like to take risk, to be vulnerable, and to turn toward discomfort even when you are afraid. Thank you to my children, Jewliet and Josh for your love without judgment and for always ever-so-gently encouraging me to become a better listener.

Chapter 2 is currently being prepared for submission for publication of the material. Jones, J. M.; Hildebrand, J. A.; Thayre, B. J.; and Wiggins, S. M. The dissertation author was the primary investigator and author of this material.

Chapter 3 is currently being prepared for submission for publication of the material. Jones, J. M.; Frasier, K. E.; Wiggins, S. M.; Hildebrand, J. A. The dissertation author was the primary investigator and author of this material.

Chapter 4 is currently being prepared for submission for publication of the material. Jones, J. M.; Hildebrand, J. A.; and Wiggins, S. M. The dissertation author was the primary investigator and author of this material.

VITA

2008	B. S. in Environmental Systems, University of California San Diego
2013-2020	Graduate Student Researcher Scripps Institution of Oceanography University of California San Diego
2021	Doctor of Philosophy, Oceanography Scripps Institution of Oceanography University of California San Diego

PUBLICATIONS

Stafford, K. M., Ferguson, M. C., Hauser, D. W., Okkonen, S. R., Berchok, C. L., Citta, J. J., Clarke, J. T., Garland, E. C., Jones, J. M., and Suydam, R. S. (2018). Beluga whales in the Western Beaufort Sea: Current state of knowledge on timing, distribution, habitat use, and environmental drivers, *Deep-Sea Research II*, 152,182-194.

Clark, C. W., Berchok, C. L., Blackwell, S. B., Hannay, D. E., Jones, J. M., Ponirakis, D., and Stafford, K. M. (2015). A year in the acoustic world of bowhead whales in the Bering, Chukchi, and Beaufort seas. *Progress in Oceanography*, 136, 223-240.

Miksis-Olds, J. L., Van Opzeeland, I. C., Van Parijs, S. M., and Jones, J. M. (2015). Pinniped sounds in the Polar Oceans. In Au, W. L., and Lammers, M. (Eds.) *Listening in the Ocean* (pp. 257-308). New York, Springer.

Jones, J. M., Mahoney, M., Thayre, B. J., Roth, E., Jackson, C., Zeller, C., Claire, M., Johnson, M., Kitka, K., Gentes, Z., Small, R. J., Stirling, I., Wiggins, S. M., and Hildebrand, J. A. (2014). Ringed, bearded, and ribbon seal vocalizations north of Pt. Barrow, Alaska: Seasonal presence and relationship with sea ice. *Arctic*, 67(2), 203-222.

Mack, A. L., and Jones, J. M. (2003). Low-frequency vocalizations by cassowaries. *AUK*, 120(4), 1062-1068.

ABSTRACT OF THE DISSERTATION

Passive acoustic monitoring of Arctic cetaceans: Site-specific detection probability, species identification and discrimination, and underwater soundscape with increasing shipping

by

Joshua M. Jones

Doctor of Philosophy in Oceanography

University of California San Diego, 2021

John A. Hildebrand, Chair

Arctic marine mammal habitats are changing rapidly while marine shipping is increasing in some areas of the Arctic. Passive acoustic monitoring can increase understanding of Arctic marine mammal responses to change and to stressors, like ship traffic. The strength of inference from underwater sound recordings is limited by several factors that I address in this dissertation with the aim of improving the usefulness of acoustic monitoring findings for Arctic marine resource management. I provide spatial context for acoustic detections of bowhead whale sounds, enabling direct comparisons of acoustic presence across different locations and environmental conditions. Ice cover and noise substantially reduce the predicted listening area around underwater

sound recorders. Spatially normalized acoustic detections reveal that bowhead whales utilize an area at least 140 km north of Alaska during their spring migration, migrating through large areas of > 90 % sea ice cover. I describe acoustic characteristics of beluga and narwhal echolocation clicks, which differ substantially in frequency content and rhythmic patterns. Sound absorption by seawater and apparent changes in animal orientation strongly affect frequency spectra of recorded clicks. Finally, I measure the underwater soundscape within a narwhal summer habitat and quantify underwater noise added by commercial ship traffic. The natural soundscape, excluding periods with nearby ships, is relatively quiet in an acoustically sheltered fiord. Distant sounds from regional shipping are apparent at a less-sheltered location open to long-range sound propagation. When ships pass the recording locations, sound levels are elevated above the median levels of natural sounds for periods ranging from 30 minutes up to > 4 hours with each transit. Icebreaker and tanker ships radiate more underwater noise than general cargo and bulk carrier ships. Ship sounds overlap with common social sounds produced by narwhals and ringed seals at distances of 5 to > 30 km from passing ships, possibly interfering with animal communication. Improved detection distance estimates and understanding of detection probability estimation coupled with increased confidence in detection and identification of beluga, narwhal, and bowhead sounds will facilitate passive acoustic density estimation of Arctic marine mammals, investigation of their relationships with habitat, and studies of their behavioral responses to ship traffic.

Chapter 1

Introduction

Climate change is impacting the world's marine ecosystems, altering patterns in ocean productivity and food web dynamics while shifting species distributions in many regions (Hoegh-Guldberg and Bruno, 2010). Concurrently, economic growth and globalization are increasing human maritime activities worldwide (Walsh et al., 2019). Some ecosystems are experiencing greater impacts from these two global processes creating a "double exposure" (O'Brien and Leichenko, 2000), where the simultaneous effects of multiple stressors reduce the resilience of species and ecosystems to impacts of climate change (Ramirez et al., 2018). The Arctic Ocean is one such region where climate and human activities are changing more rapidly than other areas of the ocean (Overland et al., 2019; Stroeve and Notz, 2018), with predicted impacts to unique assemblages of ice-adapted marine mammals that inhabit this region (Moore et al, 2008).

Marine mammals in the Arctic are closely tied to sea ice and the ecosystems that result from this prominent feature of Arctic waters (Moore and Laidre, 2006). Over the past 42 years of satellite-based earth observation, the extent of perennial Arctic sea ice has decreased about 11% per decade (Stroeve and Notz, 2018). Arctic sea ice is becoming thinner and melting earlier (Kwok, 2018; Stroeve and Notz, 2018). Across the Arctic, annual net primary production increased 57% between 1998 and 2018, with the largest changes occurring in the shallow marginal

seas (Lewis et al., 2020; Arrigo and van Dijken, 2015). Changes in marine mammal species composition and seasonal movements are occurring in the Arctic and have been attributed to sea ice loss and the related changes to marine food webs (Clarke et al., 2013; Silber et al., 2017).

Predicting marine mammal responses to climate change is complicated by a need to also understand their responses to increasing human activities. Shipping activity in the Arctic is increasing (Eguiluz et al., 2016), generating additional potential stressors to marine mammal species, particularly within the archipelagos and marginal seas. These areas are where most Arctic shipping occurs (Eguiluz et al., 2016) and Arctic marine mammal abundance and species richness are highest (Tittensor et al., 2010; Laidre et al., 2015). Among risks associated with commercial ship traffic, impacts to marine mammals resulting from underwater noise have been a major source of concern and subject of research (Southall et al., 2007). Marine mammal responses and risks from shipping include behavioral disturbance, injury to hearing, and masking of critical acoustic signals used for navigation, foraging, and communication. Each of these effects of underwater noise from shipping has the potential to impact the health of marine mammal species (Southall et al., 2007).

To understand and ultimately predict Arctic marine mammal responses to the dual stressors of climate change and increasing human activities, it is necessary to effectively monitor a range of spatial and temporal scales. Predicting species distribution and seasonal movements may be among the most important aspects for informing appropriate management and conservation decisions (Guisan et al., 2013). Many Arctic marine mammal species make large annual movements with the seasonal expansion and contraction of sea ice (Laidre et al., 2015). Their responses to human disturbance are measurable on smaller spatial and temporal scales, such as the transit of a ship within tens of kilometers of an individual or group of animals (Wartzok et al., 2003; Booth et al., 2020). Understanding noise impacts from shipping requires detailed knowledge of acoustic characteristics of ships and marine mammal behavioral responses to ships, particularly in regions where concentrated ship traffic overlaps with core use areas of marine mammal species.

At any spatial scale, marine mammal monitoring is inherently challenging. The remoteness of many marine mammal habitats, the cost and feasibility of accessing these areas using ships, and the fact the marine mammals spend much of their time submerged and out of visual range from the sea surface are all limiting factors in marine mammal research. In the Arctic, these challenges are exacerbated by the presence of sea ice, extreme low temperatures, and annual periods of limited sunlight. The use of passive acoustics to study marine mammals is helping to address some of these challenges. Passive acoustic methods are increasingly employed in studies of marine mammal distribution and seasonal movements (Stanistreet et al., 2018), habitat modeling (Sirovic and Hildebrand, 2011), and density estimation (Hildebrand et al., 2015). They are also proving useful for studies of behavioral responses to local stressors, such as underwater noise from ships (Pirotta et al., 2012), sonar (Melcón et al., 2012), and offshore petroleum exploration (Blackwell et al., 2015).

The use of acoustic methods to study marine mammals is limited by several factors, which if addressed will improve strength of inference from passive acoustic data. Often, Passive Acoustic Monitoring (PAM) is undertaken using single sensors mounted to the seafloor. Unlike visual or satellite telemetry methods for marine mammal studies, the precise location of individuals and the local density of animals is often not known from autonomous acoustic recording with a single sensor. Factors in the environment and the recording system can dramatically affect the recorded signals and their detectability. As sound travels through the water, it interacts directly with the water, seafloor, and sea surface. Properties of each, including bathymetry, water sound speed, seabed properties, and sea surface characteristics influence signals between the source and receiver. In polar regions, sea ice strongly scatters propagating acoustic energy in ways that are dependent upon characteristics of the ice, such as thickness and underside roughness, and on the frequency of the sound (Brown and Milne, 1967; Jin et al., 1994; Jensen et al., 1994).

Detection of acoustic signals depends on the received levels of signal and the noise within the frequency band of the signal. Noise may mask the presence of acoustic signals making

the signal-to-noise ratio (SNR) an important parameter in signal detectability, which can be complicated when noise levels vary in time (e.g., Helble et al, 2013). In Arctic waters, sea ice, wind, and surface waves cause substantial but variable underwater noise, significantly affecting ambient noise sound pressure measurements on timescales of months to seconds (Roth et al., 2012; Farmer and Xie, 1988).

Interactions between the instrument mooring hardware and ocean currents can cause episodic low-frequency oscillations (i.e., strum) and noise in the 0 to 500 Hz band; and the digital recording process can introduce electronic noise to the recordings. Unless addressed carefully, time-varying effects of the environment on signal propagation and noise levels on detection probability create substantial risks of misinterpreting the results of bioacoustic analyses and limit the value of acoustic recording for marine mammal studies.

There are two primary objectives of my dissertation. The first is to improve the acoustic detection and spatial context of autonomously recorded underwater sounds of bowhead whales, belugas, and narwhals. My second objective is to measure underwater noise from commercial ships and examine the impact of ship transits on the natural underwater soundscape in a region of the Arctic experiencing rapid increases in shipping traffic. The motivation for my research is the need to further our understanding of two pressing concerns about marine mammals in the Arctic: their responses to environmental change and the impacts of increasing levels of large ship traffic. In the case of bowhead whales, I improve a method to correct acoustic detections for the effects of the environment and noise on their detection. The result is a spatially explicit measure of the density of animal calls within a specified area around the recorder. For belugas and narwhals, I develop a method to acoustically detect their echolocation clicks and confidently discriminate between the two monodontid species. Finally, I study the effects of shipping traffic on the underwater soundscape and measure sounds from ships in units used to evaluate potential for behavioral disturbance and interference with communication. To accomplish this research, information about ship traffic and environmental variables including surface winds and sea ice

were combined with long-term acoustic recordings in two widely separated regions of the Arctic. The results are intended to provide support for current and future decision-making processes regarding levels of commercial shipping in the Alaskan and Canadian Arctic and their effects on populations of marine mammals considered in this study.

1.1 Study areas

1.1.1 Chukchi Sea shelfbreak and slope

The Chukchi Sea is an extensive marginal sea of the Arctic Ocean located between the northernmost coasts of Russia and the United States. The shelfbreak and slope at the northeastern boundary of the Chukchi Sea mark the transition into the abyssal Canada Basin. Oceanographically, this region receives inflow of nutrients, heat, and freshwater from the Pacific Ocean through the Bering Strait, influencing Chukchi Sea and Canada Basin circulation and ecosystems (Weingartner et al., 2005; Pickart et al., 2016). Sea ice decline in this region has intensified, with localized decreases in ice coverage of -6.57 d/yr in the northernmost region of the Chukchi Sea between 2000 and 2012 (Frey et al., 2015). This change represents one of the largest decreases in annual duration sea ice cover across the Arctic (Stroeve et al., 2014). Seasonal maximum Chl a (mg m^{-3}) increased in the Chukchi Sea 26.2% during 1998-2018 (Lewis et al., 2020), higher than all Arctic regions except for Baffin Bay (+26.4%) and the Barents Sea (+60.5%).

1.1.2 Eclipse Sound, Nunavut

Eclipse Sound is a deep body of that lies between north Baffin Island and Bylot Island in the eastern Canadian Arctic. The sound contains several bays and inlets and is habitat to several Arctic marine mammal species, including a summering population of narwhal, a year-round

ringed seal population, and the more occasional presence of bowhead whales. It is the location of the community of Pond Inlet and is situated within Canada's Sirmilik National Park.

Eclipse Sound in the eastern Canadian Arctic is a region where ship traffic is increasing due to tourism and industrial development. The community of Pond Inlet experienced almost triple the annual shipping traffic during 2011-2015 when compared to the decade 1990-2000 (Dawson et al., 2018). This was the largest proportional increase in shipping of any region in the Canadian Arctic during that period. The change was due to increasing numbers of tourism-related vessels (i.e., passenger ships and pleasure craft) and in bulk carrier and tanker ships. While increasing traffic by tourism-related vessels is widespread across the Canadian Arctic, the additional cargo ship traffic past Pond Inlet was associated with the 2010-2015 development of the Baffinland Iron Mines Corporation (BIMC) Mary River Mine on North Baffin Island (Dawson et al., 2018). Increased iron ore production proposed by the BIMC and under environmental impact review in 2018-20 would double bulk carrier transits through Eclipse Sound by 2022 (BIMC, 2020).

1.1.3 Marine mammal species

1.1.4 Bowhead whales

Bowhead whales (Balaena mysticetus) are the only baleen whale endemic to the Arctic and are closely associated with sea ice for much of the year. Annual migrations of bowhead populations generally follow the seasonal expansion and retreat of Arctic sea ice cover (Citta et al., 2015; Nielsen et al., 2015). The Bering-Chukchi-Beaufort (BCB) stock of bowheads migrates annually between the Bering Sea during winter, the Canadian Amundsen Gulf in summer, and the coast of Chukotka, Russia in the fall. This population may be the most well understood due to environmental impact assessments related to regional offshore oil and gas exploration and to generations of subsistence harvest by Inupiaq communities of Alaska's North Slope Borough.

Details of the seasonal distribution and movements of BCB bowheads have been provided by satellite telemetry studies of tagged bowheads (Citta et al., 2014), ice-based and aerial visual surveys (Givens et al., 2013), and traditional ecological knowledge shared by subsistence hunters (Huntington et al., 2016). Bowheads have shown behavioral responses to underwater noise, avoiding active seismic survey vessels at ranges $>$10 km (Ljungblad et al., 1988; Robertson et al., 2016) and changing their calling rates and source levels in response seismic survey sounds at $>$100 km distance (Blackwell et al., 2015).

The acoustic behavior of bowheads includes frequency modulated calls, usually less than 300 Hz, and broadband pulsed calls with energy up to 3.5 kHz (Clark and Johnson, 1984). Bowheads also produce songs, which can be more complex with repeated units and phrases (e.g., Delarue et al., 2009; Johnson et al., 2015). The characteristic sounds produced by bowheads have been used to indicate occurrence in several acoustic studies of the BCB bowhead population (Delarue et al., 2009; Moore et al., 2010). An increasing abundance of long-term acoustic recordings collected in the Alaskan Arctic has created opportunities to conduct acoustic studies of their seasonal movements and distribution on larger spatial scales (Clark et al., 2015).

1.1.5 Monodontids (beluga and narwhal)

Belugas (*Delphinapterus leucas*) and narwhals (*Monodon monoceros*) are the two members of the odontocete family *Monodontidae* and are the only toothed whale species endemic to Arctic waters. Belugas have a circumpolar range (Skovrind et al., 2019). Narwhals have a more limited range, significantly overlapping with beluga (Skovrind et al., 2019). Both make migrations with seasonal expanse and retreat of sea ice (Dietz et al., 2008, Hauser et al., 2014). These deep-diving whales produce high-frequency echolocation clicks for navigation and foraging. Their clicks have acoustic energy between 20 and 120 kHz and have been described in several bioacoustic studies (Au et al., 1985; Miller et al., 1995; Roy et al., 2010; Rassmussen et al., 2015; Koblitz et al., 2016). Both species have shown sensitivity to underwater noise and have exhibit

behavioral responses to underwater noise from ships (Southall et al., 2007).

1.2 Data sources

1.2.1 Passive acoustic recordings

Passive acoustic recordings included in this research were obtained using High-frequency Acoustic Recording Packages (HARPs; Wiggins and Hildebrand, 2007). Recordings were analyzed from HARPs deployed at five Arctic locations. Two locations were along the shelf and slope in the NE Chukchi Sea at depths of 100 m and 320 m, respectively. Two HARPs were deployed in Eclipse Sound in the eastern Canadian Arctic at depths of 670 and 313 m. One day of data was analyzed from a HARP deployed in Barrow Strait in the central Canadian High Arctic at a depth of 170 m. The instruments recorded underwater sound either continuously or on a recording schedule at a sampling rate of 200 kHz (effective bandwidth 10 Hz - 100 kHz). The hydrophone consisted of a low-frequency stage with six cylindrical transducers (Benthos AQ-1; http://teledynebenthos.com) with a combined sensitivity of -193.5 dB re: V/µPa and preamplifier gain of 50 dB, and a high-frequency stage with a single spherical transducer (ITC 1042; http://www.piezo-kinetics.com) with a relatively flat (±2 dB) sensitivity of -200 dB re: V/µPa from 1 Hz to 100 kHz. Combined sensitivity of the two stages was consistent with published specifications (Wiggins and Hildebrand, 2007). Acoustic data were corrected for the calibrated preamplifier response during analysis.

1.2.2 Ship positional information

Satellite Automated Information System (AIS) data were obtained from ExactEarth (www.ExactEarth.com) on ship traffic within 100 km of the two acoustic recording stations. Locations were extracted from AIS data for all ships transiting past the recording sites, including

time, latitude and longitude, speed, heading, maximum draft, Maritime Mobile Service Identity (MMSI) number, vessel name, vessel type and cargo class. Additional ship specification data, including gross and deadweight tonnage (i.e., weight carrying capacity), were obtained from Lloyd's Registry of Ships. Distances between ship location and the recording location were used to calculate the radius along the sea surface from the acoustic recording location to the ship reported position.

1.2.3 Sea ice concentration

Daily Advanced Microwave Scanning Radiometer 2 (AMSR2) 6.25 km spatial resolution sea ice maps were obtained from the University of Bremen (https://seaice.uni-bremen.de/sea-ice-concentration/amsre-amsr2/). Values were extracted and processed using Windows Image Manager (WIM) and Windows Automation Module (WAM) software (Kahru, 2000) to produce a time series of mean daily Sea Ice Concentration (SIC) within radii matching estimated species acoustic detection ranges.

1.2.4 Sea surface winds

Wind speed within a 100 km radius of the recording sites was estimated from 25 km resolution Advanced Scatterometer (ASCAT) 10 m height ocean surface wind measurements processed by the National Oceanic and Atmospheric Administration, National Environmental Satellite Data and Information Service (https:
manati.star.nesdis.noaa.gov/products/ASCAT.php). These data were limited to time periods without sea ice cover because ASCAT wind vectors are inaccurate over sea ice. Wind speed was correlated with 1-min average received broadband sound pressure level by selecting all available wind vectors within radius 100 km and time +/- 60 min of SPL_{BB} measurements.

1.3 Dissertation outline

In Chapter 2, I develop and test a method to estimate spatially normalized bowhead whale acoustic density, accounting for the environmental and noise effects on detection probability with and without the presence of sea ice. The outputs are site-specific detection probability maps for bowhead whale calls that account for sound propagation with and without a sea ice layer and at varying levels of ambient noise within the frequency range of bowhead acoustic behavior. I use these maps to create a model that generates spatially normalized time series of bowhead whale acoustic detection density as a function of recording location, ambient sound levels, and sea ice state. Additional sound transmission loss resulting from sea ice cover and increasing ambient sound levels both result in underestimation of bowhead whale presence in uncorrected detection time series.

In Chapter 3, I detect and categorize echolocation clicks in year-long recordings made at two widely separated locations in the Arctic: one in the northeast Chukchi Sea; and one in the eastern Canadian Arctic. Only belugas are expected at the Chukchi Sea site and only narwhals at the Canadian Arctic location, allowing detailed description of the clicks of each species. Click characteristics were significantly different from one another and a method for acoustic discrimination between the species was developed. I test the method on recordings from a third location in the central Canadian High Arctic where the species overlap and there are characteristic echolocation signals of both narwhal and beluga. The recorded click characteristics from both species are substantially influenced by the received sound pressure level of the clicks, indicating that sound propagation and behavioral factors must be integrated when interpreting detection time series of these species.

In Chapter 4, I opportunistically measure underwater radiated noise from commercial ships transiting Eclipse Sound in the Eastern Canadian Arctic by combining ship position and operational information with acoustic data recorded from the seafloor at two different locations

along the shipping route. Acoustic characteristics of the most common ship types are described using measures relevant to potential disturbance and acoustic masking for the two most abundant marine mammal species inhabiting the study area: narwhals and ringed seals. I also measure and characterize the underwater soundscape of each recording location including and excluding the time periods with local ship traffic present. The estimated natural (ship-excluded) soundscape is much quieter in all months at the site protected from long-range sound propagation. Sounds emitted from ships transiting the acoustically sheltered site result in greater relative increases in sound levels compared to times when ships are not present, suggesting that increased acoustic masking of marine mammal communication signals occurs in this location.

In Chapter 5, I summarize the main findings of the dissertation and provide an overview of technical issues addressed, improving the use of PAM for studies in the Arctic. I also propose next steps for the research, which will help answer questions about Arctic marine mammals and their responses to change.

Chapter 2

Bowhead whale (*Balaena mysticetus*) call detection probability in ice-free and ice-covered Arctic Ocean

2.1 Abstract

Marine mammal passive acoustic monitoring in the Arctic is influenced by changes in the environment and in ambient sound pressure levels, both of which affect call detection probability. Acoustic modeling and Monte Carlo simulation were used to estimate site-specific detection probability for sounds produced by bowhead whales in the northeast Chukchi Sea with and without sea ice cover under various ocean noise conditions. A time series of daily acoustic detection probability was produced for two recording sites, one on the outer shelf and the other on the continental slope, from modeled transmission loss for daily sea ice coverage and average ambient sound pressure levels. The daily detection probability was applied to recorded bowhead whale call detections between 2012 and 2013 to correct for the effects of ice cover and noise. The resulting corrected index of acoustic density suggests a decrease in whale presence with

the retreat of sea ice within a 40 km radius of the recording sites. Acoustic density of bowhead detections increased during the two weeks leading up to and two weeks following the onset of sea ice formation in October. In both ice-covered and ice-free conditions, variability in observed acoustic detection rate and modeled detection probability track closely with changing ambient sound and instrument self-noise levels. These results highlight the importance of accounting for the effects of the environment and changing ambient sound pressure levels when interpreting results of passive acoustic monitoring.

2.2 Introduction

Passive acoustic monitoring (PAM) is a useful tool for studying marine mammal seasonal distribution, migration, and behavior, especially in remote locations such as polar regions, where sea ice cover and light limitations prevent ship access and visual surveys for much of the year (e.g. Stirling et al., 1983; Sirovic et al., 2004; Moore et al., 2012; Jones et al., 2014; Clark et al., 2015). PAM also is being used for estimating population densities for a variety of marine mammals to help with stock assessment and management (e.g., Marques et al., 2011; Hildebrand et al., 2015; von Brenda-Beckmann et al., 2018; Hildebrand et al., 2019). Distance sampling is one of the more widely used methods with PAM for density estimation and requires knowledge of the distance between the source (e.g. calling marine mammal) and the receiver (e.g. PAM sensor) (Marques et al., 2013). The influence of environmental factors on sound propagation can substantially alter the effective listening area around a recording location, complicating distance estimation and evaluation of marine mammal density using PAM. Factors in the environment that can influence the propagation of underwater sounds produced by marine mammals include sea water and seabed physical properties, bathymetry, and sea ice coverage. These influences on acoustic transmission are specific to hydrophone location and some, like sea state or ice cover, are temporally variable. Ambient sound pressure levels as well as recording system self-noise

are also temporally variable and may significantly affect the detectability of recorded signals by reducing the signal-to-noise ratio. If not accounted for, influences of the sound propagation environment and noise limit the strength of inference that can be drawn from PAM detection time series about marine mammal abundance and relationships with habitat or other ecological variables.

Acoustic propagation modeling can help account for environmental effects on detection of marine mammal sounds by incorporating site-specific environmental data to estimate distance to signals of known source sound pressure level (e.g. Helble et al., 2013a, Frasier et al., 2016). When combined with measurements of recorded ambient and instrument self-noise levels, it is possible to estimate and correct for time-varying acoustic detection probability, resulting in spatially-explicit estimates of acoustic density (Helble et al., 2013b).

In Arctic waters, rapid changes in sea ice and increases in human activities, such as commercial shipping and mineral resource exploration, have motivated extensive marine mammal research in the region. Bowhead whales (Balaena mysticetus) are closely associated with sea ice and have been the object of considerable research efforts, especially in the Chukchi and Beaufort Seas where bowheads are harvested for subsistence by Inupiat communities and commercial exploration for offshore petroleum reserves has raised concerns about underwater noise impacts on the Bering-Chukchi-Beaufort (BCB) bowhead population.

Bowheads make characteristic calls underwater (Clark et al., 1984; Blackwell et al., 2007; Johnson et al., 2015), including frequency modulated calls, usually less than 300 Hz, and broadband pulsed calls with energy up to 3.5 kHz (Clark and Johnson, 1984). Bowhead calls are readily identifiable in autonomous acoustic recordings and have been used to indicate their seasonal presence in numerous acoustic PAM-based studies across much of the BCB bowhead range (Moore et al., 2010; Stafford et al., 2012; Delarue et al., 2009; Clark et al., 2015; Blackwell et al., 2007; Thode et al., 2017), contributing to knowledge of their seasonal movements and distribution.

The effects of environmental properties, ocean noise, and recording system characteristics on detection probability can be large for marine mammal sounds at frequencies below 1 kHz (Helble et al., 2013a,b). In the Arctic, the presence of sea ice further complicates interpretation of PAM results. Sea ice strongly scatters propagating acoustic energy in ways that are dependent upon characteristics of the ice, such as thickness and underside roughness, and on the frequency of the sound, reducing the effective listening radius around the recorder. Across the band of frequencies used by bowheads, there is substantially higher attenuation with sea ice cover when compared to ice-free conditions (Diachok, 1976; Yang and Votaw, 1981). Previous experiments in the Arctic have found scattering strength in full sea ice cover to be between -10 and -15 dB for frequencies between 70 and 200 Hz at grazing angles of 10-20 deg (Milne, 1964; Brown and Milne, 1967; Duckworth et al., 2001).

Ambient sound pressure levels may mask the presence of acoustic signals making the signal-to-noise ratio (SNR) an important parameter in signal detectability, which can be complicated when noise levels vary over time. Sea ice, wind, and surface waves cause substantial but variable underwater noise (Greene and Buck, 1964), significantly affecting ambient sound pressure measurements on seasonal and shorter temporal scales. Mean monthly sound pressure spectrum levels in the bowhead whale call frequency band (80-180 Hz) along the NE Chukchi Sea continental slope are highest during September ice-free conditions (open water; 70-78 dB dB re 1 μPa^2/Hz) and lowest during May (55-60 dB re 1 μPa^2/Hz; Roth et al., 2012). Across the call band, ambient sound pressure levels are typically highest at the lowest frequencies, and instrument electronic self-noise is 40 – 35 dB re 1 μPa^2/Hz. Sound pressure spectrum levels at 250 Hz increase with wind speed by 1dB/m/s in open water and by 0.5 dB/m/s during 75-100% ice cover (Roth et al., 2012). Episodic events in the sea ice layer, such as ice motions, ice field deformation and fracturing, also introduce broadband underwater noise (Farmer and Xie, 1988; Kinda et al., 2015). In open water, man-made noise from seismic surveys can increase sound pressure spectrum levels significantly; for example, recordings from the Chukchi Sea during

2006-09 found sound pressure spectrum levels increased by 3-8 dB in the 80-180 Hz band during extended seismic survey periods (Roth et al. 2012). Ocean currents can also cause episodic low-frequency oscillations (i.e., strum) and noise in the 1 to 500 Hz band.

In this study, we use underwater acoustic modeling and detection simulations to develop site-specific, time-dependent corrections to year-long time series of bowhead whale acoustic detections at recording sites in the northeast (NE) Chukchi Sea outer shelf (shelf) and continental slope (slope). The corrected detections of bowhead whale acoustic presence were examined with respect to major factors affecting detection probability and factors which may be influencing the presence and behavior of the whales. The sound propagation loss for bowhead whale calls is substantially greater during ice-covered conditions than during ice-free conditions. Both changes in propagation and time-varying ambient sound pressure levels must be considered to provide reliable detection probability estimations, which can then be used for quantitative assessment of bowhead whale population densities during changing environmental conditions, such as sea ice variation.

2.3 Methods

2.3.1 Acoustic recordings

High-frequency Acoustic Recording Packages (HARPs) were deployed at two locations along the shelf (Site D) and slope (Site C) in the NE Chukchi Sea between October 2012 and October 2013 at depths of 100 m and 320 m, respectively (Fig.2.1). The instruments recorded underwater sound at a sampling rate of 200 kHz (effective bandwidth 10 Hz - 100 kHz) with a schedule of 10 min recording every 15 min. The hydrophone consisted of a low-frequency stage with six cylindrical transducers (Benthos AQ-1; http://teledynebenthos.com) with a combined sensitivity of -193.5 dB re: V/μPa and preamplifier gain of 50 dB, and a high-frequency stage with a single spherical transducer (ITC 1042; http://www.piezo-kinetics.com) with a relatively

flat (±2 dB) sensitivity of -200 dB re: V/ μPa from 1 Hz to 100 kHz. Combined sensitivity of the two stages was consistent with published specifications (Wiggins and Hildebrand, 2007). All acoustic recordings were converted into an adapted wav file format (XWAV) for analysis. To minimize computational requirements, XWAV files were decimated by a factor of 20 using an eighth-order Chebyschev type I filter (new bandwidth: 10-5000 Hz) for the detection of bowhead calls. Analyses were conducted using the Triton program, based in MATLAB (MathWorks Inc., Natick, MA), to calculate and display long-term spectral averages (LTSA) and spectrograms, to perform audio playbacks, and to log call detections (Wiggins and Hildebrand, 2007).

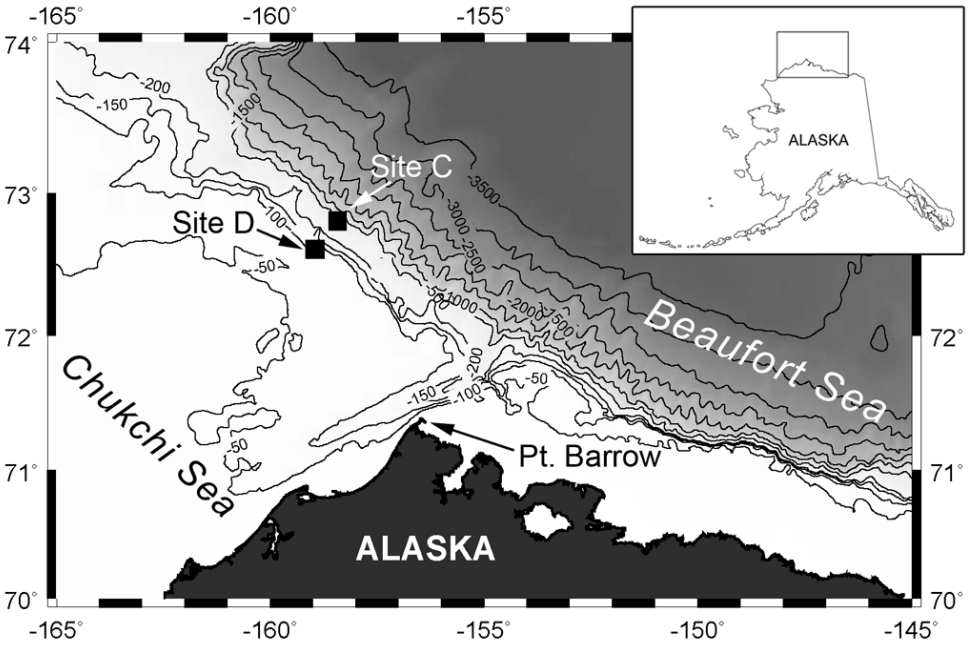

Figure 2.1: Chukchi Sea acoustic recording sites along the continental slope NNW of Pt. Barrow, Alaska from 2006 through 2014. Contour depths in meters with darker shading indicating deeper depths. Hydrophones at sites C (slope) and D (shelf) were at depths of 320 and 100 m, respectively.

2.3.2 Call detection

Expert judgement was applied when visually scanning 30-minute LTSAs for the characteristic calls of bowhead whales. Previously described acoustic behavior for bowhead whales (Clark

and Johnson 1984; Blackwell et al., 2007) was compared with calls detected in the HARP recordings. To simplify identification, only frequency modulated non-song type calls were accepted as initial detections of bowhead whales (Fig. 2.2). When a possible call was detected in the LTSA, a spectrogram of 60 s or less was visually inspected to verify the identity of the call. A minimum of one call was logged for each hour in which bowhead calls were present, providing acoustic presence or absence of bowheads at a temporal resolution of one-hour. Finally, spectrograms of the logged calls were visually inspected for identification errors, and misidentified calls were removed from the detection database.

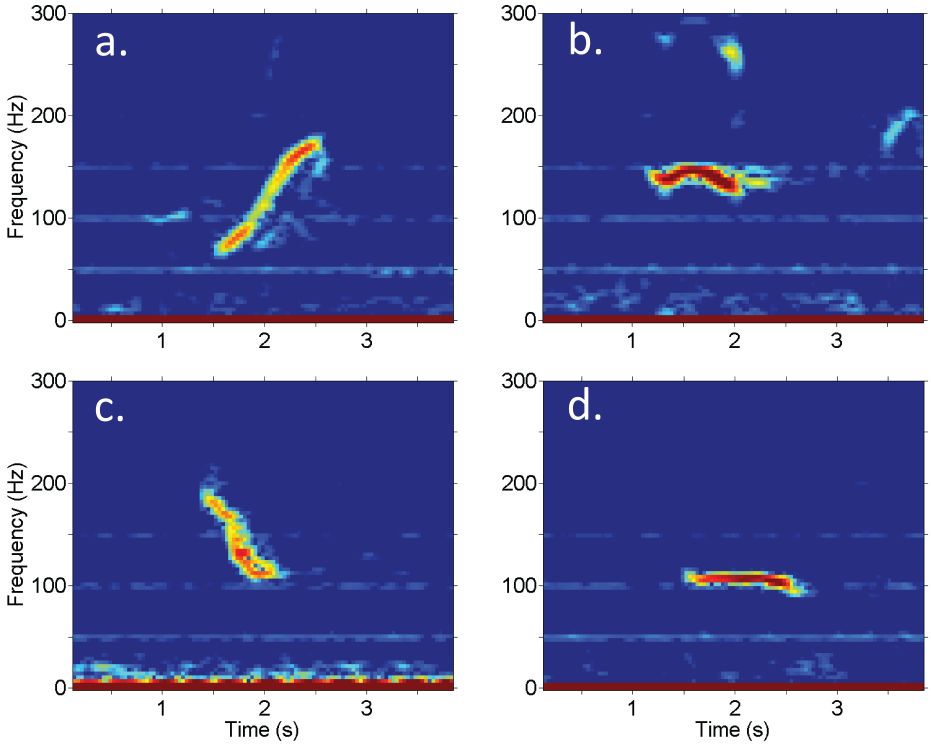

Figure 2.2: Spectrogram (time versus frequency) examples of bowhead calls recorded in the Chukchi Sea include the call types (a) upsweep, (b) undulating n, (c) downsweep, and (d) constant. Undulating u call type not shown. Sample rate: 2000 Hz, FFT length: 550 samples, window overlap: 87%, window type: Hanning.

2.3.3 Detection probability

To convert acoustic occurrence to a spatially explicit model for inference about density, the area monitored must be estimated. This can be accomplished for a single sensor by understanding detection probability as a function of horizontal range from the hydrophone. Detection probability for calling bowhead whales was estimated using methods similar to those of Kusel, et al., (2011) and with adaptation of a method used for site-specific probability of detecting humpback whale calls (Helble et al., 2013a). Detection probability ($\hat{P}$) for an area within some radius (ω) can be calculated as a function of range (r) and azimuth (θ) from the recording location (Buckland et al., 2001),

$$\hat{P} = \int_0^w \int_0^{2\pi} \rho(r,\theta) g(r,\theta) r dr d\theta \tag{2.1}$$

$\rho(r,\theta)$ is the probability density function for whale locations and $g(r,\theta)$ is the detection function. If a random homogeneous distribution of whales within the detection area is assumed, then the probability density function becomes $\rho(r,\theta) = 1/\pi w^2$. Detection probability can be estimated for all r and θ within a radius w by developing a parametric model for $g(r,\theta)$ using a Monte Carlo simulation (e.g. Helble et al., 2013a; Frasier et al., 2016). This method includes characteristics of bowhead whale acoustic behavior and the seasonal acoustic environment, including source level and depth characteristics for calling bowhead whales, time-varying ambient sound pressure levels, observed signal to noise ratio for bowhead whale call detections in the acoustic recordings, recording site properties, and sound propagation modeling to predict signal transmission.

Signal source level and depth

Estimated root mean squared (RMS) source levels of bowhead whale frequency modulated calls exhibit a roughly normal distribution with a peak at 160 dB RMS re 1 μPa @ 1 m (Cummings

and Holliday, 1987; Thode et al., 2016). Bowhead vocalizations exhibit some directivity pattern of radiated energy, which could explain this distribution of source level estimates. Blackwell et al., (2012) studied directionality of migrating bowhead whale sound production and estimated that whales traveling toward the receiver resulted in RMS received levels averaging 4.2 - 4.8 dB higher than whales moving away. Random horizontal orientation of the animals with respect to the receiver was assumed. The detection function dependence on the depth of calling animals was simplified by assuming a constant calling depth of 26 m for bowhead whales. This value was chosen from the peak of a probability density function of bowhead whale source depths estimated by Thode et al. (2016) from a full propagation model of manually detected calls in the Beaufort Sea.

Hourly ambient sound pressure levels

To estimate time-varying ambient sound pressure levels (SPL) for the 80-180 Hz band, we performed a time series analysis of LTSA files to calculate the hourly 10^{th}, 50^{th}, and 90^{th} percentile received levels within the 80-180 Hz bowhead call frequency band. Received levels in 1 Hz bins were summed across the frequency band to produce an estimate for received sound pressure level. Percentiles were calculated for each hour from the received SPL of all LTSA slices in that hour. The first three and last three of the five second (s) time bins from each 75 s raw file were excluded from percentile and SPL calculations to remove instrument self-noise associated with writing to hard disk.

Call received levels and SNR

To evaluate signal-to-noise thresholds for detection at the two recording sites, an additional analysis was performed to calculate the received sound pressure level and signal-to-noise ratio for a representative subset of calls from each site across the range of detectable received sound pressure levels. The start and end times and frequencies were logged for every detectable call

for the last one-week period before sea ice breakup with mean weekly ice concentration greater than 90% (ice-covered), the week centered on the last day with 50% sea ice concentration before open water (transitional), and the last full week with sea ice no greater than 10% (ice-free). The peak-to-peak (p-p) and RMS received sound pressure level for each call were calculated as follows:

$$RL_{p-p} = 20log_{10}\Big(max(P(t)) - min(P(t))\Big) \tag{2.2}$$

$$RL_{RMS} = 20log_{10}\sqrt{1/T\int_0^T p^2(t)dt} \tag{2.3}$$

where pressure, P, of the signal is evaluated over the duration, T, in which the energy is between 5% and 95% of the total integrated energy in the signal bandwidth (80 - 180 Hz). To estimate ambient sound pressure level, p-p received levels were also calculated during the one second prior to each call.

A simplified equation for signal-to-noise ratio (SNR) was used to determine the SNR threshold for signal detection,

$$SNR = RL - NL \tag{2.4}$$

where SNR for each call is estimated from the p-p call received level (RL) and the ambient sound pressure level one s prior to the call (NL). The detection threshold was estimated from the SNR distributions for each site and ice state and a single threshold of 2 dB chosen to represent the SNR level that would result in fewer than 5% of the detected calls being missed. Calls falling below this SNR of 2 dB were assumed to be not reliably detectable.

Recording site properties

The outer shelf and continental slope of the northeast (NE) Chukchi Sea is a transition zone between the shallow Chukchi Sea shelf (avg. depth 50 m) and abyssal Canada Basin (avg. depth 3600 m). The region is covered by seasonal sea ice, typically present from October

through August, with substantial interannual variability in timing of ice formation and breakup (Markus et al., 2009). Sea ice is primarily first-year with interannually variable proportions of thicker multi-year ice (Kwok and Cunningham, 2015). The water column characteristics in the NE Chukchi Sea slope vary seasonally and are strongly influenced by sea ice, extreme low air temperatures, sea ice melt, and Atlantic water at depth. A two-layer profile of temperature and salinity often exists, with a cold (-2° C) relatively fresh upper layer during periods with ice cover, saltier relatively warmer underlying water column, and a weak thermocline (e.g. Krishfield et al., 2008; Gong and Pickart, 2015). The seafloor consists of relatively thick fine silt, sand, and clay, especially on the shallow shelf (Xiangmei et al., 2015).

Available data on acoustically relevant properties of the surface, water column, seafloor, and seabed from time periods as close to the recordings as possible were compiled (Table 2.1) to create a seasonally appropriate model prediction of sound propagation around the recording sites. Vertical CTD profiles from the NE Chukchi Sea were obtained during acoustic recording in ice-covered and ice-free periods of the acoustic recording years. The hydrographic data were collected during 100% ice cover by an Ice Tethered Profiler (ITP-62; Toole et al., 2011) in May, 2013, and during open water from the USCGC Healy in October, 2013. Sound speed profiles (Fig. 2.3) were calculated from pressure, salinity, and temperature using the Equation of State (TEOS-10; Millero et al., 2008).

Bathymetric data were extracted from the International Bathymetric Chart of the Arctic Ocean (Jakobsson et al., 2012) at a spatial resolution of 1 km and adopted seafloor acoustic properties and a sub-bottom sound speed profile from previous studies on the Chukchi Shelf (Xiangmei et al. 2015; Warner et al. 2015). All surface to sub-bottom physical properties included in sound propagation modeling are listed in Table 2.1.

Daily AMSR2 sea ice maps were obtained from the University of Bremen (http://www.iup.uni-bremen.de:8084/amsr2data/asi_daygrid_swath/n6250/) and processed using Windows Image Manager (WIM) and Windows Automation Module (WAM) software (Kahru, 2000) to produce an

Table 2.1: Acoustic model parameters.

Location	Parameter	Symbol	Value(s)	Units	Source
Sea ice	Sea ice thickness	z_i	2.7	m	Goff, 1995
	Ice-water RMS roughness		1.38	m	(Ibid.)
	Ice-air RMS roughness		0.45	m	Gavrilov & Mikhalevsky, 2006
	Sea ice density	ρ_i	0.89	g/cm^3	Alexander et al., 2013
	Sea ice compressional speed	c_i	3000	m/s	Gavrilov & Mikhalevsky, 2006
	Sea ice shear speed		1800	m/s	(Ibid.)
	Compressional wave attenuation		0.45	dB/λ	(Ibid.)
	Shear wave attenuation		0.9	dB/λ	(Ibid.)
Water column	Surface sound speed	c_w	1435		ITP-62; HLY1303
	Seafloor sound speed	c_w	1465		ITP-62; HLY1303
	Range-independent water depth	z_w	2500	m	
	Density and sound speed profile shelf	-	-		ITP-62; HLY1303
	Density and sound speed profile basin	-	-		ITP-62; HLY1303
	Absorption		Negligible		Fisher & Simmons, 1977
Seafloor	Seafloor mean grain size	d	3.0, 3.6	μm	Xiangmei et al., 2015
	Depth (bathymetry)	z_b	-		IBCAO v.3 1-min grid
Subbottom	Number of subbottom steps		5		Warner et al., 2015
	Step depths		2, 5, 10, 20, 40	m	(Ibid.)
	Layer compressional speed	c_b	1465, 1555, 1605, 1750, 2200	m/s	(Ibid.)
	Layer shear speed				(Ibid.)
	Layer density	ρ_b	1.49, 1.77, 1.87, 2.06, 2.2	g/cm^3	(Ibid.)
Basement	Compressional speed	c_b	2300	m/s	(Ibid.)
	Shear speed				(Ibid.)
	Density	ρ_b	2.3	g/cm^3	(Ibid.)

annual time series of mean daily Sea Ice Concentration (SIC) within a 20 km radius mask about each recording site. The 20 km radius was selected as a conservative detection range for bowhead whale calls based on previous studies (Blackwell et al., 2007) and distance within which most interactions with the surface would likely occur. WAM software was used to compute the daily arithmetic mean, variance, and median of the sea ice concentration as a percent of the total mask area.

Sound propagation modeling

Acoustic modeling techniques were employed to predict the sound propagation transmission loss of bowhead calls due to recording site properties under ice-free and ice-covered conditions within a 1 km resolution spatial grid of 40 km radius about each recording site. The predicted transmission loss allowed for creation of model simulations of call detection probability

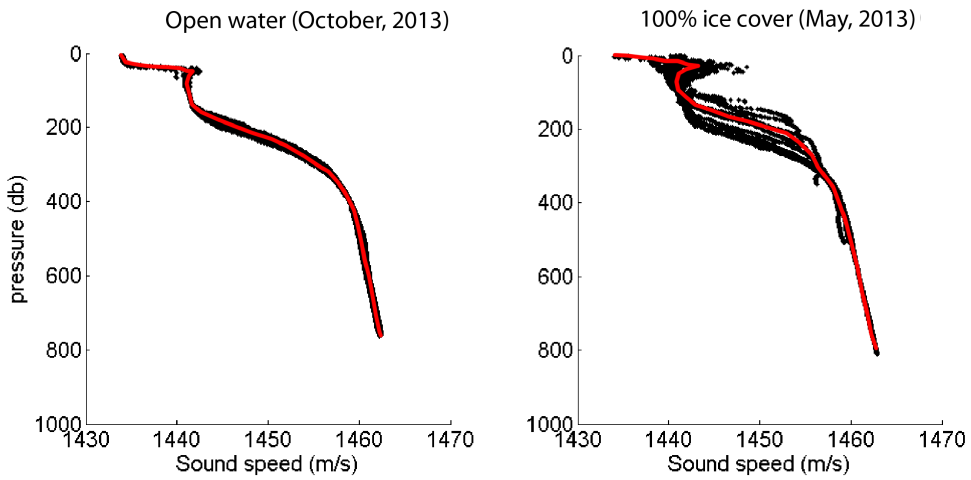

Figure 2.3: Density and sound speed profiles calculated from CTD measurements during 2013 October (left)and May (right). Black dots are CTD measurements. A curve is also fit to the data (red line) and used as a single representative sound speed profile. Open water and ice-covered measurements were made from the USCGC Healy and an Ice Tethered Profiler (ITP Mission 62; Toole et al., 2011), respectively.

under the two ice states across the range of ambient sound pressure levels for the 80-180 Hz band measured at the recorders (50 – 85 dB re 1 μPa).

Transmission loss (TL) grids were created using the Acoustics Toolbox User Interface and Post-processor (AcTUP v 2.2L; Duncan and Maggi, 2006), which provides a Matlab-based graphical user interface for the Acoustics Toolbox (M. Porter, Acoustic Toolbox) and RAMS Parabolic Equation Models (Collins, 1993). A parabolic equation sound propagation model for was used (RAMGEO) because it is well suited for shallow water environments and for frequencies less than one kilohertz (Alexander et al. 2013) and can incorporate water column, seabed, sea surface and sea ice input parameters. Representative sound speed profiles were selected from hydrographic data collected in ice-covered (ITP-62) and ice-free (HLY1303) conditions (Fig.2.3). The sea ice layer was assumed from an April 1992 survey to be uniform first-year ice with no ridging, layer thickness 2.7 m, underside RMS roughness 1.38 m (Goff, 1995), compressional speed 3000 m/s, and shear speed 1800 m/s (Gavrilov and Mikhalevsky, 2006). Table 2.1 lists all acoustic model parameters, chosen from a review of published literature and hydrographic data

sets local to the recording location.

The propagation transmission loss models were executed on sixteen transects at 22.5 degree angular intervals originating at the recording site. Models were executed in one Hz steps from 80 to 180 Hz (the bowhead band) with source depth 26 m below the sea-air surface and receiver depth 10 m above the seafloor. The models were incoherently averaged across frequency (Alexander et al. 2013) and a 100-point moving average filter was applied with range, to smooth each transect. Using linear interpolation between transect points, transmission loss was estimated for each location within a 1 km resolution grid centered on each recording site. Grid locations were mapped to geographic coordinates using a polar stereographic projection, yielding 40 km radius transmission loss grids for each site and ice condition. An additional range-dependent loss term of -0.26 dB/km was applied to all locations in the transmission loss grids to approximate excess loss observed for the Chukchi Shelf region (Keen et al., 2018; Cate et al., 2014).

Monte Carlo detection probability estimation

A simulation method was used to estimate detection probability for different ocean noise levels and ice states. Seven ambient sound pressure levels were simulated from 50 to 85 dB re 1 μPa in 5 dB steps to represent the observed range for the 80-180 Hz frequency band in the 2012-13 recordings. For each noise level, two simulations were run using the modeled transmission loss grids for ice-free and ice-covered states. For each combination of site, noise level, and ice state, a simulation randomly placed 100,000 bowhead call source level values within the 40 km radius transmission loss grid. Simulated source levels were randomly generated from a probability distribution fit to source level estimates for bowhead frequency modulated calls reported by Cummings and Holliday (1987) which ranged from 126 to 178 dB (RMS) re 1 μPa @ 1m (mean 157, +/- 10 dB re 1 μPa @ 1m). Each 1 km x 1 km cell in the simulated detection grid was scored with the proportion of simulated calls originating at that location resulting in received levels at the hydrophone with a threshold greater than 2 dB above the noise level for that simulation run. The

detection probability, $\hat{P}$, for each pixel in the grid was calculated as the proportion of detected to total simulated calls originating from that location. The mean detection probability for each site, ice condition, and noise level was calculated by weighted average of the detection probability values for all pixels in the 40 km radius grid. Finally, a spline interpolation was used to fit a curve to detection probability as a function of noise level for both ice conditions.

2.3.4 Estimating density of occurrence

The detection probability for each hour of acoustic data was estimated by using the detection probability from the modeling simulation for the measured hourly 50^{th} percentile noise level and the corresponding mean daily sea ice state for that hour. Assuming the probability of false detection, $\hat{c}$ is zero and the probability of animals calling during each one-hour period is 1, $\hat{D}_T$, the daily detection density for each site can be calculated as,

$$\hat{D} = (N_T \frac{(1-\hat{c})}{\pi w^2 \hat{P}_T}) \tag{2.5}$$

where $\hat{N}_T$ is the number of hours per day with acoustic detection of bowhead whales and $\hat{P}_T$ is the average detection probability of all hours in day T. To evaluate uncertainty in $\hat{D}$ due to noise, detection probability was calculated for the hourly averaged 10^{th} and 90^{th} percentiles and input to Eqn. 5 to yield lower and upper bounds, $\hat{D}_{10}$ and $\hat{D}_{90}$ for detection density. A threshold of 20% ice cover was set to determine whether the detection probability function for the ice-covered or ice-free model would be used for each hour.

2.4 Results

Density of bowhead whale acoustic occurrence was estimated from detection probability simulations run with acoustic propagation model results. Detection probability was influenced strongly by sea ice concentration and local bathymetry. Bowhead whale call detection time series

showed substantially different patterns when corrected for detection probability. Spatial normalization of detection density estimation resulted in comparable estimates of acoustic occurrence across sites and seasons.

2.4.1 Acoustic propagation and detection probability

Modeled sound propagation transmission losses in the bowhead whale calling frequency band were substantially higher in the presence of ice cover than for ice-free conditions (Figs. 2.4,2.5). For instance, there was greater average transmission loss within the 40 km radius at the slope site than at the shelf site in both ice states, partly due to the slope site's greater exposure to deep water (Fig. 2.4). Likewise, at a range of 20 km, losses were 25-30 dB greater with ice cover than for ice free conditions (Fig. 2.5). At both sites, sounds traveling upslope toward more shallow water had the lowest predicted propagation losses with ice-free conditions and greatest losses with ice cover. This spatial pattern of propagation losses with depth contour was reversed for sounds traveling toward deeper water. Down slope propagation loss was lower relative to upslope during ice cover and higher during ice-free conditions.

Average detection probability for calls within the 40 km radius follow similar patterns to transmission loss. Detection probability is substantially reduced in the presence of sea ice when compared to the ice-free modeled state. In both ice states, spatial patterns in detection probability correspond with bathymetry (Fig. 2.6). In open water, modeled detection values are higher at greater ranges for sources positioned along and up slope than for those downslope from the recorders. This pattern is reversed with ice-cover and detection probability greater downslope than upslope from the recorder.

Averaging detection probability across all azimuths for each radial distance gives detection probability as a function of distance for each noise level (Fig. 2.7). The probability of detecting a call falls off with increasing distance from the recording site and with increasing ambient sound pressure level (SPL) both with and without sea ice (Fig. 2.7). Detection probability decreases

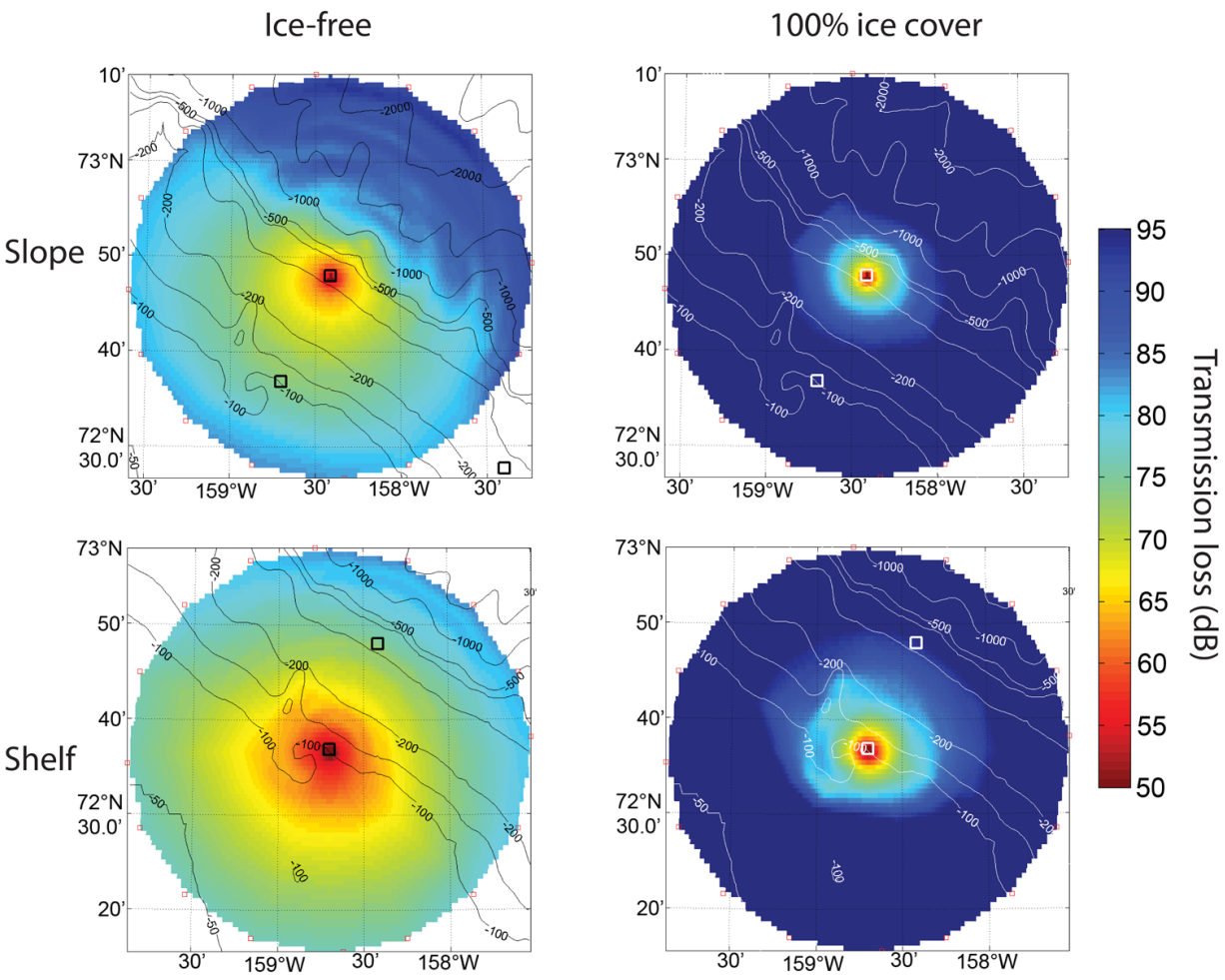

Figure 2.4: Transmission loss in dB for: ice-free (left panels) and ice-covered (right panels) conditions for Chukchi slope (upper panels) and shelf (lower panels) sites with receivers at 320 and 88 m, respectively. Contour lines in m.

slowly with increasing distance in open water, decreases more rapidly at higher noise levels, and is greater on the shelf than on the slope.

We also estimate detection probability as a function of noise level for each site and ice state from the mean detection probability across all modeled grid locations within the 40 km radius for each detection simulation (Fig. 2.8). With sea ice cover, average detection is substantially lower than open water at both sites and all noise levels, and, as with open water, it is higher on the shelf than the slope, and decreases more rapidly as distance and noise levels increase. The 40

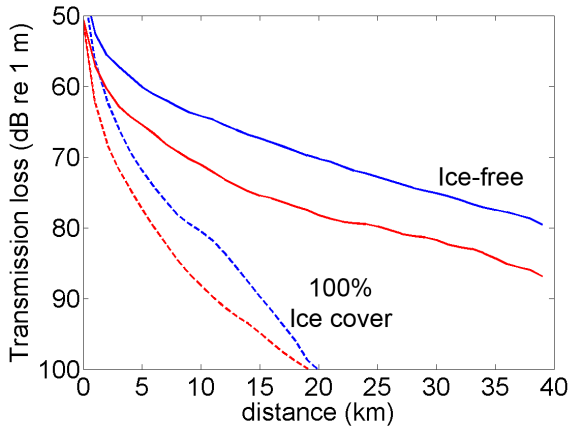

Figure 2.5: Transmission loss in dB for: ice-free (left panels) and ice-covered (right panels) conditions for Chukchi slope (upper panels) and shelf (lower panels) sites with receivers at 320 and 88 m, respectively. Contour lines in m.

km average detection probability is 20 – 60% lower with the sea ice layer. In open water at the shelf site, detection probability remains above 70% even at high ambient SPL up to 75 dB re 1 μPa (blue line in Fig. 2.8). At the slope site, detection probability drops to less than 50% at the 75 dB re 1 μPa noise level (red line in Fig. 2.8). With the sea ice layer (dashed lines in Fig. 2.8), average detection probability was similar at both locations and ranged from 50% at the lowest noise levels (50 dB re 1 μPa) down to less than 5% with the highest noise levels. Overall, adding the sea ice layer results in substantially lower detection probabilities and a decreased detection area.

Received levels for recorded bowhead whale calls ranged from approximately 75 - 105 dB_{RMS} re 1 μPa in both ice-covered and ice-free conditions. Assuming a 160 dB RMS source level, propagation losses for detected bowhead whale calls can be estimated to range between 55 to 85 dB. The transmission loss models for the slope and shelf sites predict average radial distances (fig. 2.5) of approximately 0.5 to 13 km for this range of propagation losses during ice cover and about 0.5 to greater than 40 km radial distances to calling whales during ice-free conditions.

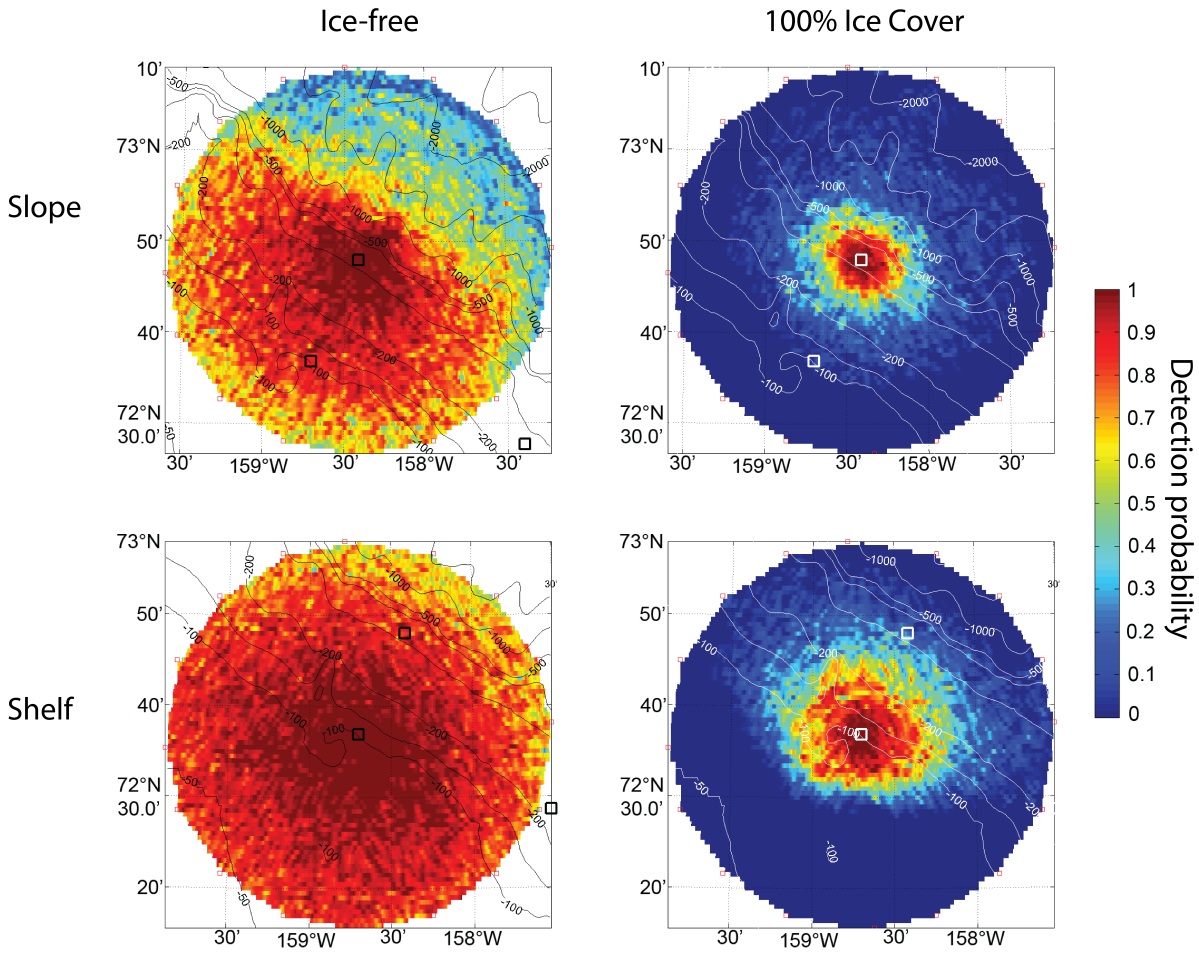

Figure 2.6: Detection probability for ice-free (left panels) and ice-covered (right panels) conditions for slope and shelf recording sites (upper and lower panels) with 70 dB re 1 μPa noise spectrum level in the 80-180 Hz band.

2.4.2 Ambient sound pressure levels and detection probability

Measured ambient sound pressure levels in the 80-180 Hz frequency band are higher with less ice coverage (Figs. 2.9.a and 2.10.a). Annual average noise levels were lower at the slope (63 +/- 6 dB re 1 μPa) than on the shelf recorder (70 +/- 7 dB re 1 μPa) due to current-induced strumming of mooring hardware noise at the shelf recorder. This resulted in overall higher detection probability on the slope than the shelf site (mean 0.52 +/- 0.17 and 0.42 +/- 0.23, respectively). The highest detection probability values approached 100% at both sites and

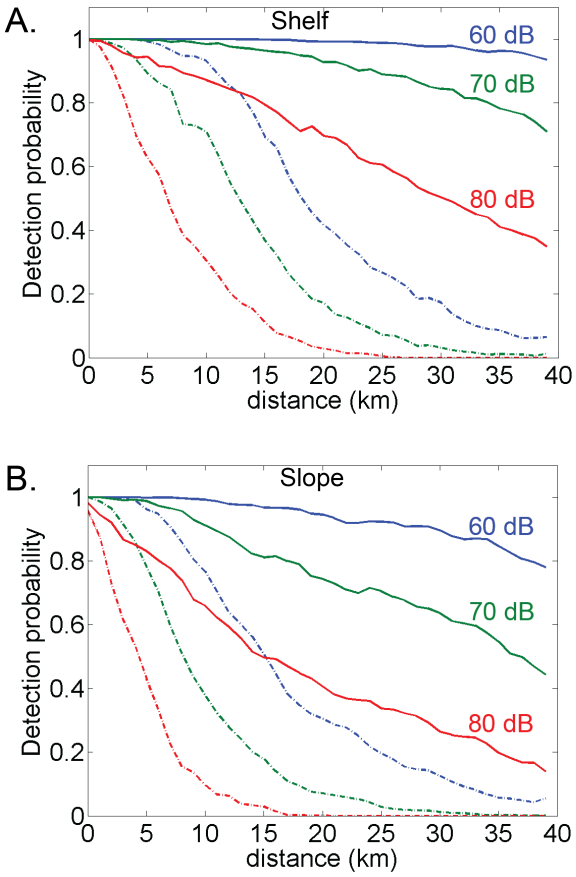

Figure 2.7: Detection probability as a function of radial distance for Chukchi (A) shelf and (B) slope sites at ambient sound pressure level 60, 70, and 80 dB re 1 μPa (blue, green, and red lines) in the 80-180 Hz frequency band with open water (solid line) and ice-covered (dashed line) conditions.

occurred during open water low-noise periods. With ice cover and low noise, detection probability peaked at 48% on the shelf and 75% at the slope recorder.

2.4.3 Density of bowhead acoustic occurrence

Applying the detection density function (Eqn. 2.5) to the uncorrected call detection time series (hrs/day) provides acoustic occurrence in estimated density form, relative to area covered (hrs/10^3km^2/day). Both uncorrected and corrected call detections indicate that bowhead whales were acoustically present at both sites during most open water periods, in spring and early summer

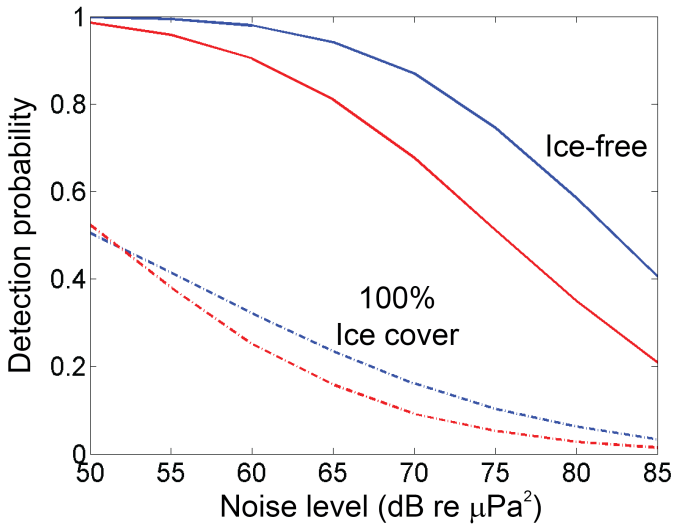

Figure 2.8: Modeled average detection probability ($\hat{P}$) within a 40 km radius of the recording site as a function of noise (ambient sound pressure) level in the 80-180 Hz band for each ice state and site for input to the detection density function (Eqn. 5). Blue and red lines represent the shelf and slope sites, respectively in ice-free (solid line) and ice-covered (dashed line) conditions.

during high ice cover, and during freeze-up in October and November (Figs. 2.9.c and 2.10.c). Corrected density of acoustic occurrence increased in October leading up to and during sea ice formation, ending abruptly as sea ice concentration reached 100%. From April through July, as sea ice concentration varied between 90 and 100%, bowhead acoustic density increased with substantial variability on daily and weekly time scales. At both sites, there was a decline in estimated acoustic density following the breakup of sea ice (Fig. 2.9).

2.5 Discussion

Analysis of passive acoustic monitoring data needs to incorporate the significant effects of the environment on acoustic propagation and noise variability on the probability of detection. In the Arctic, seasonal sea ice cover dramatically decreases the range over which calls can be detected, especially when comparing across multiple sensors with different surrounding bathymetry and noise characteristics. With the presence of a sea ice layer, sound attenuates to

undetectable levels over much shorter distances than in open water. This has the largest effect on detection probability, yielding a bimodal distribution over the course of a year. Without the correction for the effects of sea ice on sound propagation, acoustic presence is overestimated during open water periods and underestimated when sea ice is present.

The effect of variability in noise level on detection probability is greatest at mid-ranges relative to the total propagation distance over which detection is possible. The noise characteristics near the recorder can also have a large influence on detection probability. The average noise levels at the shelf site were 10 dB higher than at the slope, resulting in substantially lower detection probability in the presence of the sea ice layer. The correction method presented here, therefore has the effect of normalizing the estimates of detection density across the two sites, including differences in environmental and internal characteristics. This opens the possibility of comparing detection densities between sites.

2.5.1 Acoustic propagation and detection probability

Acoustic modeling results of this study were consistent with theoretical predictions and experimental results from previous studies of sound propagation in the Arctic. Long-range propagation of 80-180 Hz signals is predicted during open water and rapid attenuation with the addition of a sea ice layer. Optimum frequency for acoustic propagation in shallow open water is highly dependent on depth. In temperate oceanographic conditions, optimum frequencies for depths from 100 to 300 m are about 220 to 50 Hz, respectively (Jensen and Kuperman, 1983). Optimum frequency decreases for the same depth with the upward refracting sound speed profile characteristic of the Arctic. Loss to the seafloor resulting from thick sediment layers in the Chukchi Sea may raise the lower end of the optimum frequency band relative to other areas. The combined effects of these factors may act to narrow the bandwidth of frequencies that propagate best within the study area.

Adding the sea ice layer dramatically increased transmission loss, consistent with theoret-

ical predictions and previous studies of Arctic long-range sound propagation. Diachok (1976) found transmission loss of 95 dB for 200 Hz at 40 km with sea ice, compared with a theoretical prediction of 76 dB with ice-free conditions. Results for the slope site are closest to these levels, with TL of 76 dB at 40 km of in open water and 105 dB with ice cover. The shelf site had substantially lower TL in open water (68 dB) and higher with ice cover (110 dB) at 40 km range. The increased TL with sea ice cover is likely due to the shallower depth of the sites, increasing reflections off the seafloor which then interact with the underside of the sea ice. The low up-slope and along-slope TL at the shelf versus slope site may also be related to bathymetry, with depth changing more slowly with range up slope at the shelf site. Combined with the upward sound speed profile, this may result in an acoustic waveguide during open water.

Scattering of acoustic energy is also affected by the number and depth of ice keels under pressure ridges (Diachok, 1976) and in the marginal ice zone (Jin et al., 1994), and seafloors with low shear strength may attenuate signals further in shallow water waveguides as compressional waves are converted to shear waves, but not into water column compressional waves (e.g., Duncan et al., 2013). Future models should develop additional parameters to account for these factors in acoustic propagation.

One factor not addressed in this study is the effect of sea state on transmission loss during open water. Surface scattering strength increases as a function of wind speed (Chapman and Harris, 1962). Our model uses an RMS roughness of 1.38 m for the sea surface in open water, which would correspond to typical wind speeds observed in the region. Much higher wind velocities do occur regularly during open water and would result in greater surface roughness and increased ambient sound pressure levels at the high end of the bowhead call frequency band (e.g., Wenz 1962). At higher wind speeds, scattering strength increases significantly for bowhead whale call frequencies at grazing angles up to 25 deg (Gauss et al., 2005). This effect of surface roughness could substantially reduce the high detection probability we predict for open water conditions and should be incorporated into future models.

2.5.2 Ambient sound pressure level effect on detection probability

For a given site and ice state, temporal variability in detection probability was primarily a function of noise level. With no ice layer, detection probability was less sensitive to changes in noise at relatively low noise levels than at higher levels (e.g. >70 dB). With ice cover, detection probability had a more linear relationship with noise from the lowest to highest levels. The relatively higher noise levels during ice-free conditions counteract somewhat the effect of lower transmission loss during these conditions. Noise levels are higher all year at the shelf site and we see a more dramatic effect of the presence of the sea ice layer on detection probability. These results underscore the importance of noise levels on detection probability. A 23 dB decrease in noise level at the slope site in early April results in a >50% increase in detection probability; whereas, a 23 dB decrease in noise level in June at the shelf site caused only a 33% increase in detection probability. Site-specific differences in propagation caused the magnitude of the effect to be higher at the shelf site.

2.5.3 Density of bowhead acoustic occurrence

Applying the detection density function with the input of hourly estimated detection probability had the effect of normalizing acoustic occurrence across the two sites that differ in both sound propagation environment and noise characteristics. The uncorrected daily occurrence of bowhead whale calling suggests a greater presence of bowheads around the slope than the shelf site during ice cover, with many June and July days with nearly 24 hours of presence at the slope site and few days above 12 hours of presence at the shelf site. Examining the acoustic density at both sites, corrected for site-specific sound transmission, ice state, and the ambient SPL time series, this apparent difference in magnitude of bowhead presence between the two sites disappears. Detection probability is substantially lower at the shelf site during ice cover due to the relatively higher instrument self-noise, which occurred as a result of strumming of the

mooring hardware specific to that instrument deployment. The slope mooring did not experience the same level of self-noise during the relatively low environmental noise of June-July ice cover. Additionally, the shallower depth of the shelf site brought it closer to noise from the sea surface associated with sea ice dynamics and noise from wind generated waves, also increasing noise relative to the deeper slope site. With the model-derived correction applied, the density of acoustic occurrence at the two sites is comparable during the same time period, with both sites fluctuating around a density index of 7.5 hrs/$10^3 km^2/day$ within a 40 km radius of the recorders.

Examining bowhead acoustic density with respect to sea ice, the annual patterns of presence are similar at both sites are similar, with whales appearing in April during full ice cover and again approximately two weeks before the onset of ice formation through freeze-up. A sustained period of acoustic density occurs at the shelf site prior to freeze up and increases during ice formation. This fall density of occurrence does not appear as pronounced at the slope. Both sites exhibit peaks in acoustic density in June and July, which decreases around the onset of sea ice break-up. This pattern does not appear in the uncorrected acoustic detection time series and is consistent with satellite telemetry results showing seasonal movements of bowheads extending to areas of their range outside of the majority of previous surveys of their abundance and distribution (Citta et al., 2014).

2.6 Conclusions

Detection of acoustic signals from bowhead whales in Arctic shelf and slope waters result from an interaction of environmental factors that affect the transmission of the sounds through the water and factors that affect the levels of ambient noise. To help interpret results from passive acoustic monitoring detections, it is necessary to address these factors and account for them. Acoustic detection time series can be corrected for the effects of sound transmission during ice-free and ice-covered conditions as well as the effects of time-varying noise levels. This approach

approximates the seasonal conditions in the Arctic. Applying these tools to multi-year time series of acoustic data will substantially improve the use of passive acoustic monitoring in estimating abundance and distribution of marine species and to investigate ecological relationships with environmental factors, such as sea ice.

2.7 Acknowledgements

The author and co-authors thank Robert Small and the Alaska Department of Fish and Game, Sylvia Kreel and the Coastal Impact Assistance Program (CIAP) of the U.S. Fish and Wildlife Service, and Craig George and Robert Suydam of the North Slope Borough Department of Wildlife Management for providing the funding and additional support to make this study possible. Thanks to Mati Kahru (SIO) for assistance with the acquisition and processing of satellite sea ice data. Bob Pickart (WHOI), John Kemp (WHOI), and Catherine Berchok (NOAA) provided ship time and invaluable at-sea support for Chukchi Sea mooring operations. We also thank the captain and crew of the US Coast Guard Cutter Healy for their professionalism and assistance at sea. Special thanks to Mike Porter (HLS Research) for development of the Acoustic Toolbox and Alec Duncan (Curtin University), who wrote the Acoustic Tolbox User interface and Post processor (AcTUP V2.2L). We thank members of the Scripps Whale Acoustics Laboratory, including B. J. Thayre, J. Hurwitz, E. O'Neill-Mertz, and S. Wager for assistance with HARP operations and data processing. Thank you, Dr. Julie D. Lee for substantial assistance with editing and review of this manuscript.

Chapter 2 is currently being prepared for submission for publication of the material. Jones, J. M.; Hildebrand, J. A.; Thayre, B. J.; and Wiggins, S. M. The dissertation author was the primary investigator and author of this material.

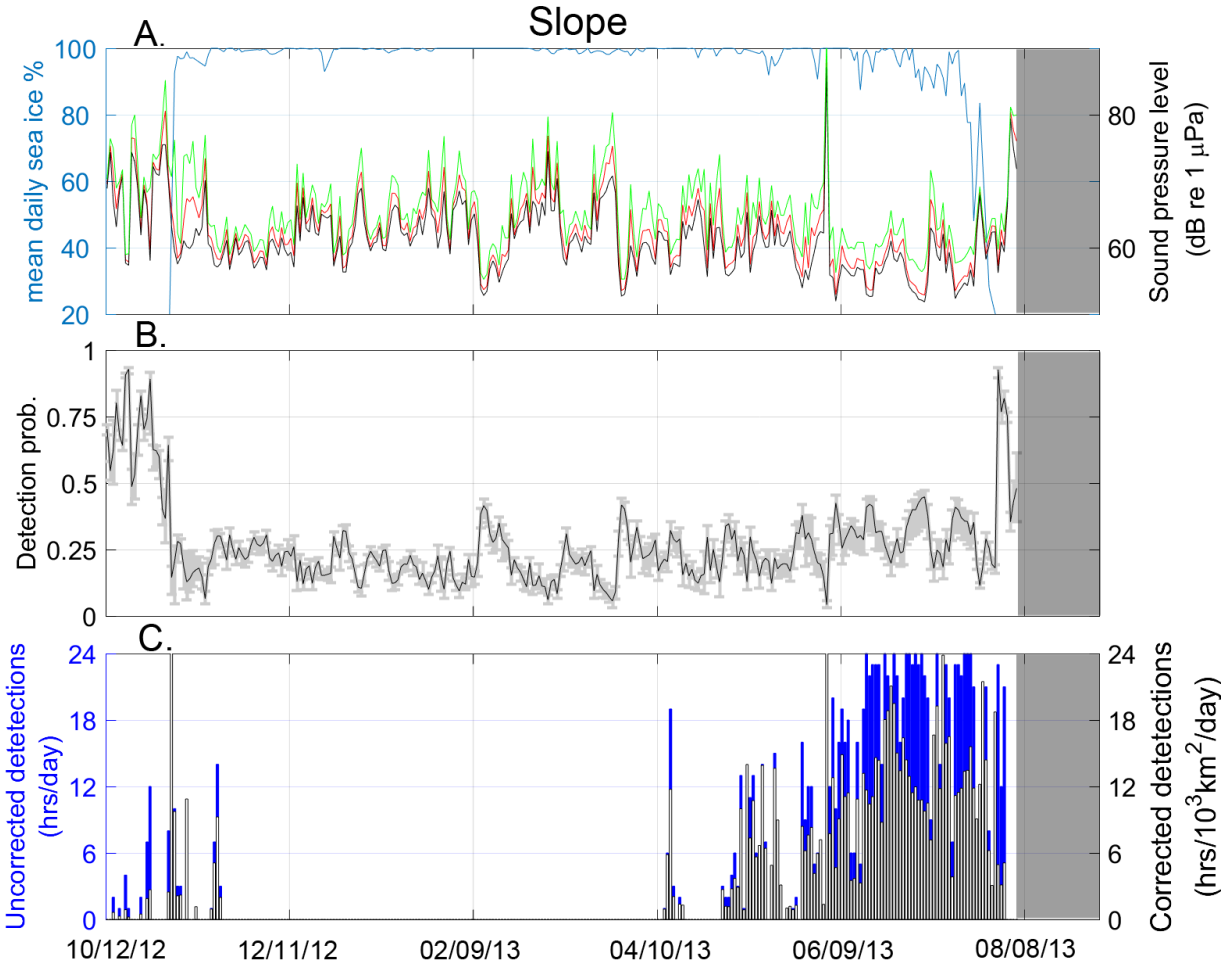

Figure 2.9: Average daily sound pressure levels (SPL) and mean daily sea ice concentration (blue line) at the slope site from October 2012 to October 2013. SPL values are the daily 10^{th} 50^{th}, and 90^{th} percentiles (black, red, and green lines, respectively) for the bowhead whale call 80-180Hz frequency band. (B) Daily averaged detection probability ($\hat{P}$) within a 40 km radius with gray bars showing range of $\hat{P}$ within the 90^{th} and 10^{th} percentile noise level for the day. (C) Bowhead whale call detections as the uncorrected daily detection hours (blue bars) and corrected detection density (black and white bars). Gray shaded areas indicate period of no recording.

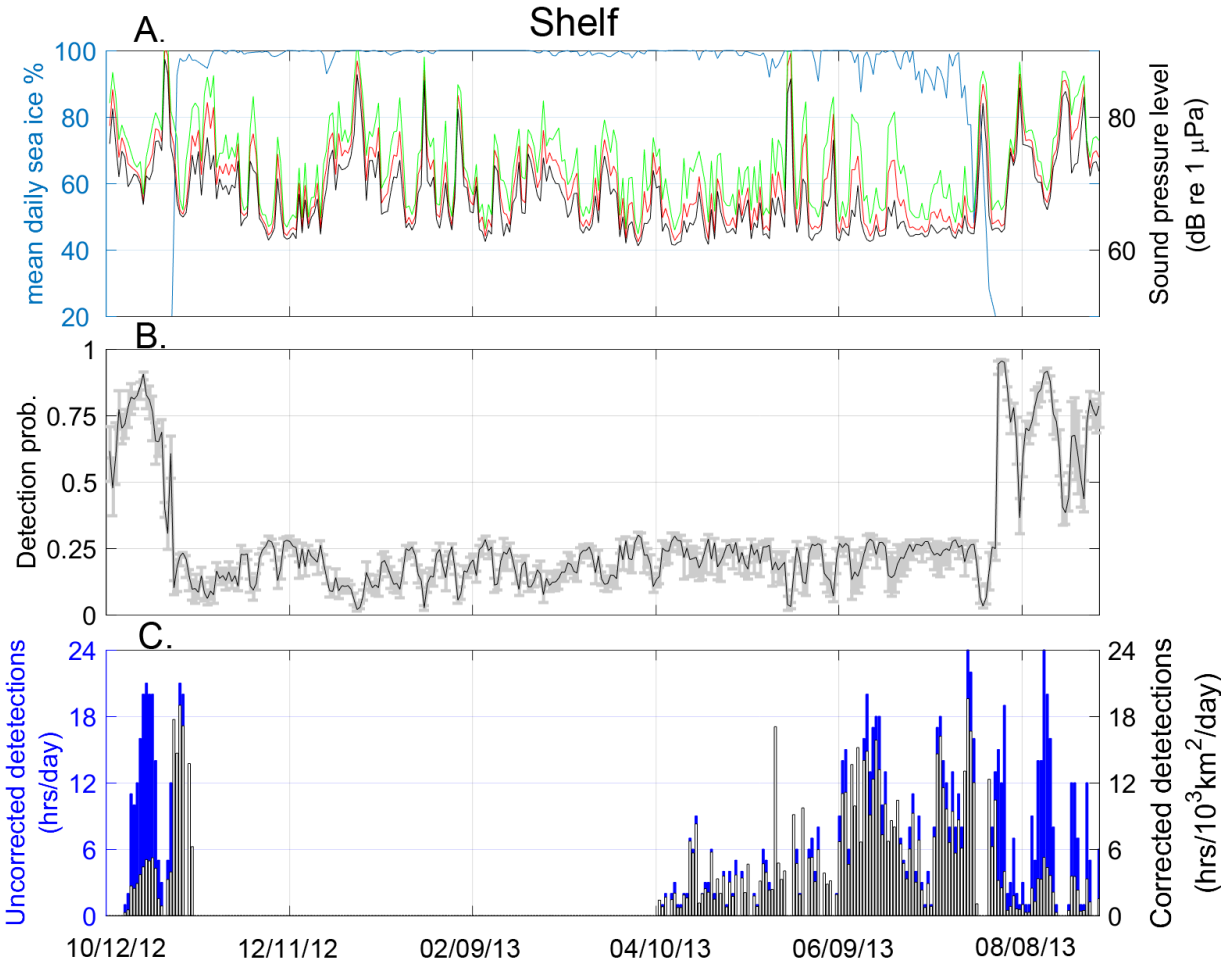

Figure 2.10: Average daily sound pressure levels (SPL) and mean daily sea ice concentration (blue line) at the shelf site from October 2012 to October 2013. SPL values are the daily 10^{th} 50^{th}, and 90^{th} percentiles (black, red, and green lines, respectively) for the bowhead whale call 80-180Hz frequency band. (B) Daily averaged detection probability ($\hat{P}$) within a 40 km radius with gray bars showing range of $\hat{P}$ within the 90^{th} and 10^{th} percentile noise level for the day. (C) Bowhead whale call detections as the uncorrected daily detection hours (blue bars) and corrected detection density (black and white bars). Gray shaded areas indicate period of no recording.

Chapter 3

Beluga (*Delphinapterus leucas*) and narwhal (*Monodon monoceros*) echolocation click detection and differentiation from long-term Arctic acoustic recordings

3.1 Abstract

Beluga (*Delphinapterus leucas*) and narwhal (*Mondon monoceros*) echolocation signals have been described in numerous acoustic studies but reported characteristics of their clicks vary across studies. Here, a year of acoustic recordings was collected in the Chukchi Sea where belugas are abundant, and narwhals are not present. A second year was recorded in Eclipse Sound, Nunavut, where beluga sightings are rare and narwhals abundant. The same calibrated hydrophone was used at both locations to facilitate data comparison. Click detection and signal parameter measurements were carried out using a single analysis method. Peak frequency of detected clicks decreased with peak-to-peak received sound pressure level (received level; RL)

for both species. High RL beluga clicks (n=24,097) and narwhals clicks (n=15,764) had a modal peak frequency of 56 kHz. Lower RL modal peak frequency of beluga clicks (n=699,916) was 53 kHz and for narwhal clicks (n=399,341) was 22.5 kHz. Modal inter-click interval (ICI) for beluga clicks (n=872,336) was 49 ms. Narwhal ICI distribution (n=791,905) was bimodal and right skewed with modal values of 4 and 144 ms. A test recording of 24-hour duration was analyzed from a Barrow Strait (BS), Nunavut location where the range of belugas and narwhals overlap. At BS clicks of both belugas and narwhals were readily distinguishable by frequency spectra and ICI distribution. These parameters provide a reliable way to discriminate between the monodontid species in large acoustic datasets where distributions of click characteristics can be determined. It is also important to consider the received sound levels of clicks when using frequency spectra as an identifying characteristic of monodontids. Due to the frequency-dependent acoustic absorption of seawater, longer propagation and detection distances are predicted for narwhal clicks that show greater energy below 30 kHz than found in beluga click spectra.

3.2 Introduction

Toothed whales produce impulsive sounds, or clicks, for navigation, foraging, and for social communication. Acoustic characteristics of these echolocation clicks can be used to identify and discriminate among some odontocete species in underwater acoustic recordings, making them valuable inputs for studies of click-producing species using passive acoustic methods. Most odontocete families contain species which can be positively identified from characteristics of their echolocation signals, including sperm whales (Morrissey et al., 2006), dwarf and pygmy sperm whales (Hildebrand et al., 2019), dolphins (Frasier et al., 2017), and beaked whales (Baumann-Pickering et al., 2013). Echolocation characteristics particularly useful for species identification include frequency spectrum, pulse duration, and rate of click production, often measured as inter-click-interval (ICI). These features of odontocete sound production have enabled the study

of their seasonal movements and distribution using passive acoustic monitoring (PAM) methods in remote locations where other methods of marine mammal research, such as aerial or ship-based observations are problematic or impractical. In recent studies, echolocation click detections have been increasingly used for density estimation where species identification is also known with confidence (Hildebrand et al., 2019; Küsel et al., 2011; Marques et al., 2009).

Two critical components in utilizing PAM for studies of echolocating marine mammals are the attribution of detected echolocation clicks to their species of origin and an understanding of the differences between characteristics of the received versus the source signal. Differences in the received signal can be caused by physiological attributes and swimming behavior of the animals, and effects of the environment on propagating sounds. Characteristics of the recording system can also cause differences in received signals unrelated to changes in the acoustic behavior of the animals producing the sounds. High frequency echolocation clicks with energy $>$30 kHz attenuate rapidly in the ocean due to frequency dependent absorption (Ainlie, 2013), changing the frequency content of the received signals. Odontocetes often exhibit highly directional projection of acoustic energy with more energy directed forward in the direction the head is oriented. Both horizontal and vertical beam patterns have been measured experimentally in species including Monodon monoceros (Koblitz et al., 2016), Delphinapterus leucas (Au et al., 1987), Tursiops truncatus (Au et al., 1986), and Pseudcorca crassidens (Au et al., 1995). And finally, hydrophone and recording system sensitivity must be well understood to translate recorded signals back to the sound pressure environment outside the hydrophone during recording. These aspects of acoustic monitoring produce challenges for marine mammal studies that must be addressed to improve the quality of passive acoustic detections as inputs to modern acoustic monitoring methods, such as studies of seasonal presence and acoustic density estimation.

In the Arctic, autonomous passive acoustic monitoring provides opportunities to monitor and study odontocete species from their echolocation clicks. Belugas (Delphinapterus leucas) and narwhals (Monodon monoceros), the two members of the odontocete family Monodontidae,

are the only toothed whales endemic to Arctic waters. These deep-diving whales produce high-frequency echolocation clicks with energy between 20 and 120 kHz that have been described in several bioacoustic studies (Au et al., 1985; Miller et al., 1995; Roy et al., 2010; Rassmussen et al., 2015; Koblitz et al., 2016; Frouin-Muoy et al., 2017). Arctic waters present unique challenges to studying the behavior and seasonal movements of these species due to the remoteness of much of their range, the inaccessibility to ships during months of sea ice cover, and absence of sunlight during winter. These factors make belugas and narwhals excellent species for passive acoustic monitoring with autonomous underwater acoustic packages that can record data for months in remote areas where other research methods are problematic.

Although descriptions exist for echolocation signals of belugas and narwhals, differences in characteristics of the hydrophones and recording systems, as well as differences in methods used to analyze acoustic recordings, make discriminating between these species acoustically challenging. A literature review of beluga and narwhal echolocation signals yielded a range of values for frequency spectra, ICI, and pulse duration (Au et al., 1985; Miller et al., 1995; Roy et al., 2010; Stafford et al., 2012; Rassmussen et al., 2015; Koblitz et al., 2016). More recently, a novel approach to differentiation between the echolocation clicks of the two species was developed, focusing on the frequency spectra of detected clicks (Frouin-Muoy et al., 2017). Narwhal clicks consistently contained significantly more energy than beluga clicks in the 15,849 Hz and 19,953 Hz $1/3^{rd}$ octave band sound pressure levels (SPL). This characteristic, when combined with the increased presence of whistle-type signals from belugas, allowed discrimination between the two species in autonomous underwater acoustic recordings.

To improve confidence in identification of beluga and narwhal echolocation signals, we analyze a large number of clicks detected with the same acoustic sensor and recording system deployed at two Arctic locations where overlap between the species is minimal and their seasonal presence is well known. A full year of underwater recordings are analyzed from one location in the Northeast Chukchi Sea where belugas are present, but narwhals are absent. Another year

of acoustic recordings are analyzed from the Eastern Canadian Arctic in a summering location for narwhals where presence of belugas is minimal. These data allowed characterization of echolocation clicks with special attention to the variability in the signals likely caused by animal behavior and environmental effects on sound propagation. This work shows that the clicks of the two species can be reliably differentiated across detection events based on frequency spectra and rhythmic patterns in the aggregated clicks.

3.3 Methods

3.3.1 Acoustic recording

Acoustic recordings were collected at two locations in the Arctic (Fig. 3.1), each with only one monodontid species commonly present - either beluga or narwhal. One recording location in the eastern Chukchi Sea (Fig. 3.1, 'CS') was 160 km north-northwest of Pt. Barrow, Alaska at seafloor depth 323 m along the continental slope between the Chukchi Sea shelf and Canada Basin. Beluga annual presence between May and November has been established at this location through acoustic detection of echolocation clicks and whistles in year-round acoustic recordings and from satellite telemetry locations of tagged animals (Stafford et al., 2017; Hauser et al., 2017). Belugas are the only odontocete commonly detected in the area of the CS recorder, with occasional annual presence of killer whales closer to the north coast of Alaska (Hannay et al., 2013). The second recording site (Fig. 3.1, 'PI') was in northwest Baffin Bay, 60 km east of the north Baffin Island community of Pond Inlet at the eastern entrance to Eclipse Sound at seafloor depth 670 m. Narwhal annual presence occurs in the Eclipse Sound region between July and November, with an estimated summering population of approximately 10,400 narwhal (Doniol-Valcrose et al., 2020). Narwhal are the dominant odontocete species in the region, with occasional presence of sperm whales (Physeter macrocephalus) and killer whales (Orcinus orca) (Frouin-Muoy et al., 2017; LeFort et al., 2020). Both recording locations are covered with sea ice

for approximately nine months annually, with freeze-up and break-up occurring in October-Nov and July-Aug, respectively (Stroeve et al., 2014, Tivy et al., 2011).

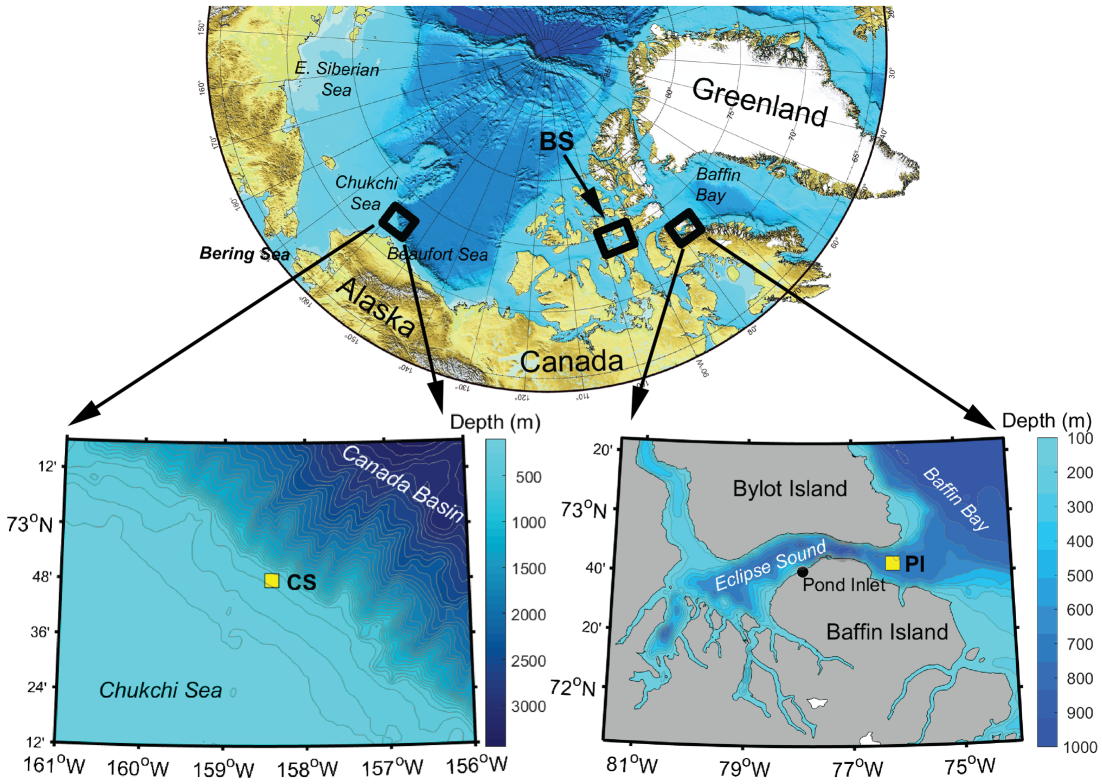

Figure 3.1: High-frequency Acoustic Recording Packages (HARPs; yellow squares) were deployed at locations in the eastern Chukchi Sea, northeast Baffin Bay, and Barrow Strait. The Chukchi Sea HARP (CS) was deployed to depth 323 m on the Chukchi Sea outer shelf. The Pond Inlet HARP (PI) was deployed to depth 670 m 60 km east of the community of Pond Inlet, Nunavut, at the eastern entrance to Eclipse Sound. The Barrow Strait HARP (BS) was deployed to depth of 190 m 30 km south of the community of Resolute Bay, Nunavut.

Acoustic recordings were made using High-frequency Acoustic Recording Packages (HARPs; Wiggins and Hildebrand, 2007), which are bottom-mounted acoustic recorders that record underwater sound for periods of up to a year at a time. The HARP units recorded at a sampling rate of 200 kHz. The CS HARP recorded on a schedule of 10 min recording followed by 5 min of non-recording, for a duty-cycle of 66.7% between July 21 and October 10, 2014 while the PI HARP recorded continuously between May 28 and Oct 3, 2016. The same hydrophone was used during both HARP deployments. These two deployments of the same hydrophone were

selected from among other years of acoustic data collected at the CS and PI locations to simplify comparisons of acoustic measurements between the recording sites. The hydrophone consisted of two stages, one for low-frequency (<25 kHz) and one for high-frequency (>25 kHz). The low-frequency stage was composed of six cylindrical transducers (Benthos AQ-1) wired in series and parallel, providing a hydrophone sensitivity of -187 decibels (dB) re: V/μPa and with 55 dB of preamp gain. The high-frequency stage consisted of a spherical omni-directional transducer (ITC-1042; www.itctransducers.com) with an approximately flat frequency response of -200 dB root mean squared (RMS) re 1V/μPa between 1Hz and 100 kHz with about 50 dB of preamplifier gain.

3.3.2 Signal detection and description

High-frequency echolocation clicks were detected and characterized using a combination of automated signal detection confirmed with visual validation. All signal processing was performed using custom software written for MATLAB (Mathworks). To facilitate visual validation of acoustic detections, Long-term Spectral Averages (LTSAs) were assembled from consecutive 5 s averaged sound pressure spectrum level estimates with 100 Hz frequency bins. All received sound pressure level (SPL) measurements are reported on a logarithmic scale in units of decibels (dB) with reference pressure of 1 μPa. Sound pressure spectrum levels reported in units of dB re 1 μPa^2/Hz.

Individual echolocation clicks (clicks) were detected within the full set of recordings from each site using a two-stage process. In the first stage of analysis, a simple suite of energy detection criteria were implemented to identify impulsive signals meeting a set of pre-determined parameters (Frasier, 2017). Prior to detection of impulsive signals, acoustic data were processed using a band-pass filter between 5 and 90 kHz. A 200-sample window centered on the peak of each impulse was analyzed for each detection. The band-pass filtered pressure time series was saved for each detected impulse for subsequent analyses. Inter-click interval (ICI) was estimated

from successive signal window start times. Spectrum of each detected impulse was calculated from the 200-sample window using a Hanning window to yield a sound pressure spectrum level measurement with frequency bin spacing of 500 Hz. Impulses that had peak frequencies between 15 and 85 kHz, received levels higher than 120 dB pp, and inter-click intervals less than 1 s were retained for the second stage of analysis.

In the second stage of analysis, detected signals were classified into impulse types using an unsupervised learning technique based on impulse spectral shape and ICI distributions (Frasier et al., 2017). The process was utilized to assist in the removal of false detections from the first stage of analysis. Distinct impulse types were identified by automatically stepping through detection time series windows in 5-min time bins, grouping detections within each time bin based on a similarity in ICI and spectrum, then using an agglomerative clustering routine to determine similar impulse types across all the time bins with detections (Frasier et al., 2017). The output from this process yielded a set of clusters, each containing impulsive detections with similar features in spectra and ICI. Example detection times from each cluster were examined visually in the LTSA and recording time series to evaluate whether the cluster of similar detections contained echolocation clicks. Impulses in clusters with no obvious echolocation clicks were discarded. All detections with peak frequency greater than 20 kHz within each retained cluster were assumed to be echolocation clicks and the rest were labeled false detections. Finally, all echolocation detections for each site were grouped and parameters estimated for click duration, ICI, averaged spectrum, peak and center frequency, and -3 and -10 dB bandwidth.

Click duration was estimated by fitting an envelope function over the absolute value of the linear pressure time series in the 200-sample signal window of each detected click (Fig. 3.2). Clicks with more than 10% of total envelope energy in the first 40 or the last 40 samples of the window were removed to reduce inclusion of noise in estimation of click duration. Only clicks with peak-to-peak (pp) amplitude of 140-160 decibels (dB) were retained for duration estimation to minimize effects of attenuation and increase signal to noise ratio in the click window. These

received level criteria increased the signal-to-noise ratio while avoiding potential clipping in the instances when there were clicks with received levels above 160 dB. The start of each selected click was determined to be the point at which energy in the 60-sample window prior to the peak reached 5% of total click energy. Click end points were determined from the point at which the energy under the envelope function, starting from 60 samples after and moving toward the peak, reached 5% of total energy. This effectively yielded a click duration in which 90% of total click energy was within the start and end points.

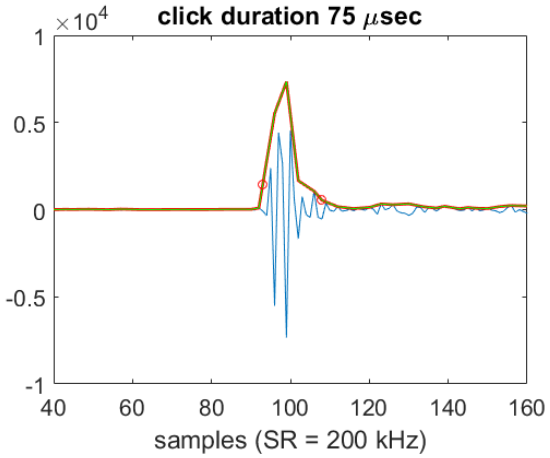

Figure 3.2: Representative click detection window of duration 0.75 milliseconds (ms) centered on the detected echolocation click waveform (blue line). First and last 40 samples of window contain less than 10%, respectively of total energy. Envelope function (orange line) is drawn over the absolute value of all peaks in window. Estimated start and end times of the click (red circles) contain 90% of the total energy within the click window.

Detected click events were defined as periods with presumed beluga or narwhal echolocation signals during which no more than 15 min passed between click detections. After more than 15 min passed with no click detected, the next set of clicks was assigned a new event number. Mean, mode, and standard deviation of click event duration were calculated from the set of events for each recording location.

3.3.3 Discriminating between monodontids and other odontocete echolocation signals

The two recording locations provided a unique opportunity to describe the echolocation of each monodontid species with confidence due to the lack of other common odontocete species in the areas. Both locations are covered with sea ice for up to 10 months per year, restricting access of other species not adapted to Arctic waters. During open water months there is a possibility of overlap with other occasional or extralimital odontocete species, so a set of criteria were developed to help avoid misidentification. Killer whales seasonally inhabit both the northeast Chukchi Sea and north Baffin Bay, with some evidence of increasing incursions of this species into Pacific and Atlantic sectors of the Arctic (Willoughby et al., 2020; Higdon et al., 2013; LeFort et al., 2020). There is overlap in acoustic characteristics of the echolocation clicks of killer whales and monodontids. Clicks are highly directional and similar in frequency content among two North Atlantic and three North Pacific ecotypes of killer whales, with peak frequency lying between 15 and 80 kHz (Au et al., 2004; Simon et al., 2007; Barrett-Lenard et al., 1996; Eskesen et al., 2011; Gassmann et al., 2013). Recording and analysis methods differ among studies of killer whale echolocation, making it difficult to confidently determine a single set of acoustic characteristics that would be diagnostic in their identification in autonomous acoustic datasets. Killer whales making incursions into the NE Chukchi Sea and N Baffin Bay are known to be mammal eaters (Willoughby et al., 2020; LeFort et al., 2020). The killer whale ecotypes foraging on mammals are known to produce far fewer echolocation clicks than other fish-eating ecotypes (Barrett-Lenard et al., 1996; Deecke et al., 2005; Matkin et al., 2007). Sightings of this species are most often reported during summer months in ice-free conditions or when ice has broken up (Higdon et al., 2013; Stafford, 2019). Echolocation clicks were detected in large numbers during times of the year with ice cover and not were accompanied by readily distinguishable social sounds of killer whales. The north Baffin Bay region is occupied seasonally by other odontocete

species, including sperm whales, white beaked dolphins, and bottlenose whales (Frouin-Muoy et al., 2017), but echolocation clicks of narwhals are more readily distinguished from these non-monodontid species based on their published acoustic characteristics or their lack of overlap in seasonal distribution with Eclipse Sound narwhal. Similarly, beluga occupy north Baffin Bay but are rarely sighted in the Eclipse Sound region where the acoustic recorder was located. In contrast, the utilization of Eclipse Sound by narwhals as a summering area is well known (Doniol-Valcrose et al., 2020).

3.3.4 Testing the detection and identification of beluga and narwhal clicks in Barrow Strait, Nunavut

A test analysis was performed on one day of acoustic recordings made with a HARP deployed at a location in Barrow Strait (BS; Fig 3.1), 30 km S of the community of Resolute Bay, Nunavut, to evaluate detection and identification of echolocation clicks where beluga and narwhal ranges overlap. The recording location is a core summer use area for belugas of the Eastern High Arctic – Baffin Bay population (COSEWIC, 2004) and for narwhals of the Somerset Island stock (Doniol-Valcrose et al., 2020). We perform the two-stage detection and analysis steps on these data to look for presence of each species. Click detections were validated aurally and by visual inspection of spectrograms, looking for characteristic whistles of belugas and burst-pulse sounds of narwhals to accompany echolocation events detected using the semi-automated process developed in this study.

3.3.5 Environmental data acquisition and processing

Daily Advanced Microwave Scanning Radiometer 2 (AMSR2) 6.25 km spatial resolution sea ice maps were obtained from the University of Bremen (https://seaice.uni-bremen.de/sea-ice-concentration/amsre-amsr2/) and processed using Windows Image Manager (WIM) and Windows

Automation Module (WAM) software (Kahru, 2000) to produce a time series of mean daily Sea Ice Concentration (SIC) within a 10 km radius mask about each recording site during the time periods analyzed. The 10 km radius was selected to exclude sea ice data pixels that included land near site PI but was large enough to include several pixel values in the estimation of daily mean around the recording site. WAM software was used to compute the daily arithmetic mean, variance, and median of the sea ice concentration as a percent of the total mask area.

3.4 Results

3.4.1 Acoustic detection of echolocation clicks

Impulsive signals consistent with previous descriptions of the echolocation clicks produced by monodontids were detected at both Arctic recording locations. Click events at the recording locations followed a similar pattern, with relatively lower received level (RL) at the start of the event increasing to some maximum RL before falling off relatively rapidly after the maximum RL was reached (e.g. Figs 3.3,3.4). Within events, individual trains of clicks were apparent and had a consistent tendency to change RL by 5-10 dB within a click train for clicks with RL less than 140 dBpp and by up to 30 dB for clicks with RL greater than 140 dBpp. This pattern can be observed in the series of vertically aligned set of clicks in the RL plot of representative click events at both sites (Figs. 3.3.a and 3.4.a).

At CS, a consistent modal ICI of approximately 0.06 s was apparent in many click events (Fig. 3.3c). ICI tended to be relatively longer and more variable in events at PI (Fig.3.4.c). Presumed narwhal click ICI at site PI was bimodal, with the most common interval of less than 0.01 sec and a second mode with a peak at approximately 0.14 sec.

A total 572 events of presumed beluga echolocation clicks were detected at site CS during the July 21 to Oct 10, 2014, analysis period. Mean click event duration at CS was 28 +/- 30 min and modal event duration was 2 min. At site PI, 179 presumed narwhal click events were

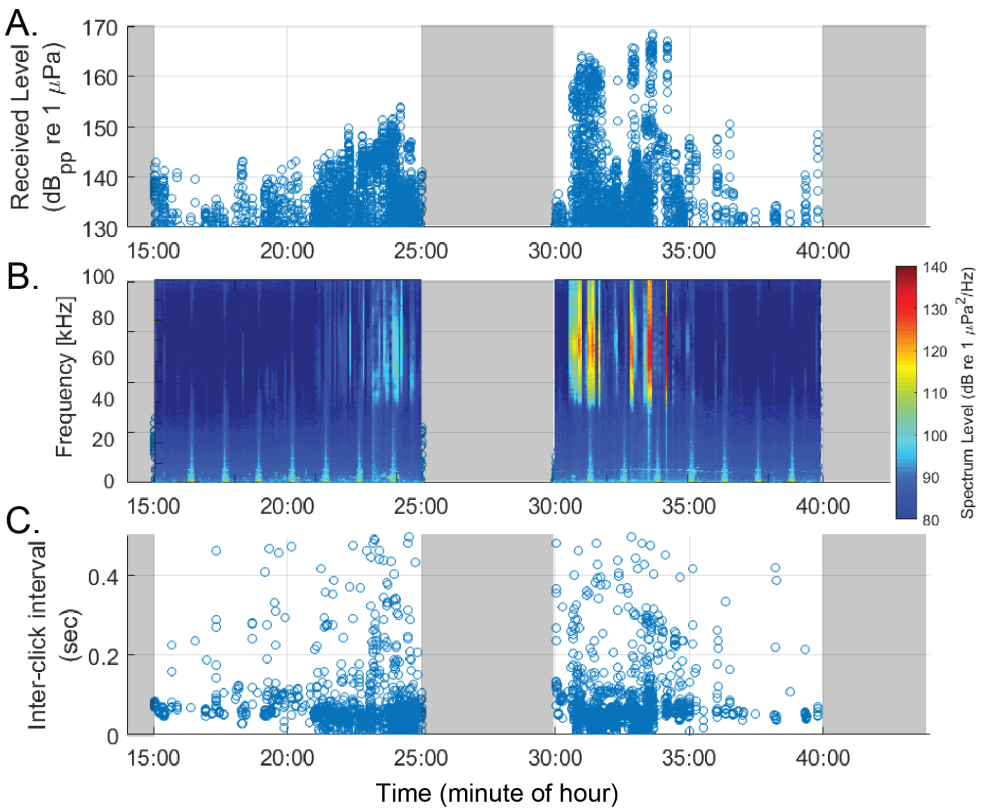

Figure 3.3: Representative beluga echolocation event July 28, 2014 at the Chukchi Sea recording location. Time series plot of n=3505 click received levels (a.; blue circles) and spectrogram (b) show levels increasing as group approaches the recording location. Inter-click interval is commonly about 0.06 sec throughout the event and becomes saturated as RL reaches maximum. Gray bars indicate scheduled periods of no recording.

detected. Mean narwhal event duration was 36 min +/- 47 min and modal event duration was 1 min. Across both sites, events were most commonly one to five min in duration with modal event duration of one to two min.

3.4.2 Click characteristics

A two-sample t-test was conducted to compare the distributions of click durations at CS and PI (Fig. 3.5). Presumed beluga click durations at CS (M=74.9 μs, SD=14.5 μs, n=5779) were significantly shorter than durations of presumed narwhal clicks at PI (M=80.3 μs, SD=21.1 μs, n=925); $t(6702) = 9.78$, $p<0.00001$. This difference can also be observed in the cumulative

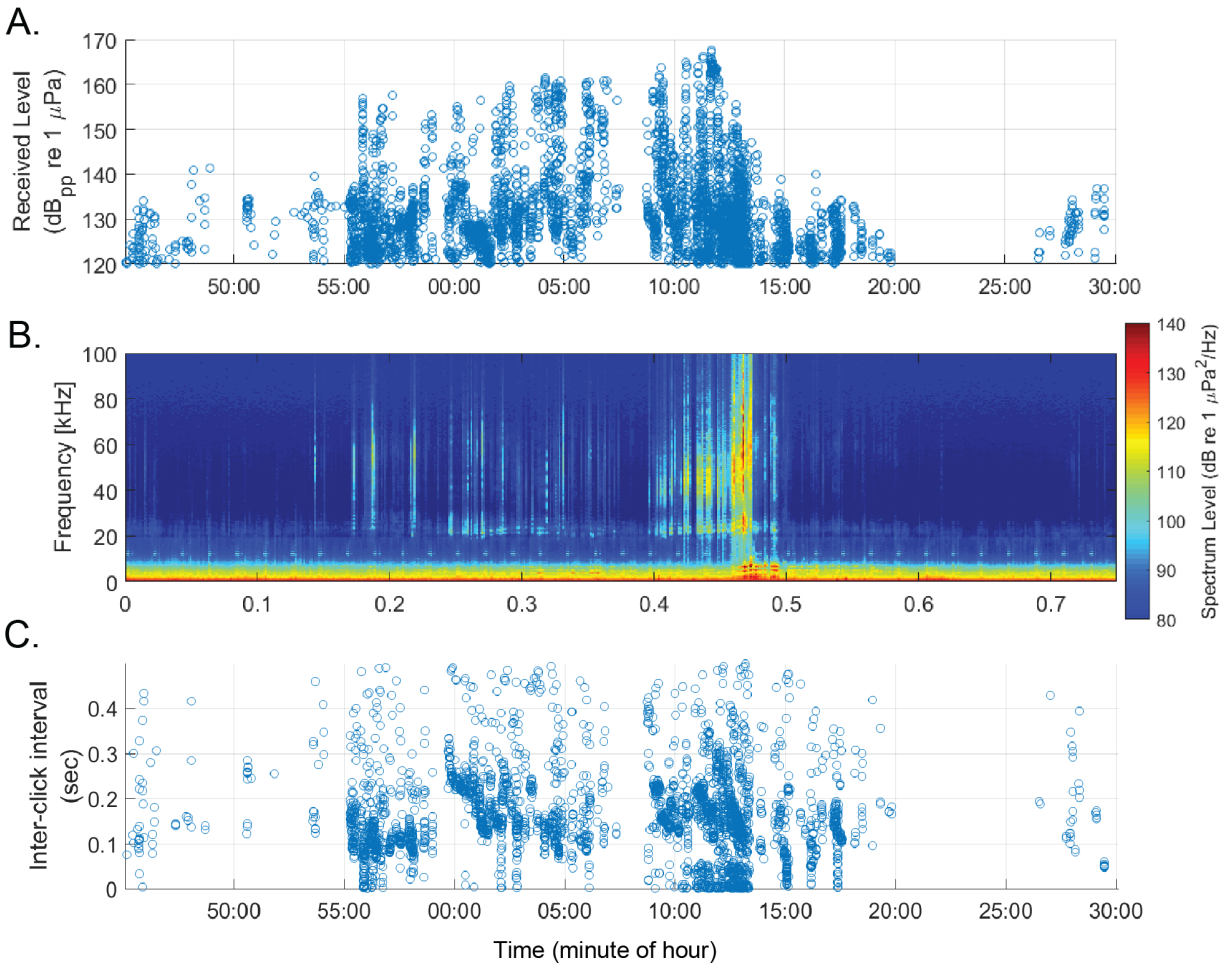

Figure 3.4: Representative narwhal echolocation event July 18, 2016 at the Pond Inlet recording location. Time series plot of n=1313 click received levels (A; blue circles) and spectrogram (B) show levels increasing as group approaches the recording location. Inter-click interval (C) is variable throughout the event and becomes saturated as RL reaches maximum.

distribution function for durations of clicks at both sites (Fig. 3.6).

Peak frequencies of echolocation clicks with RL >150 dBpp (Fig. 3.7.e,f) were between 50 and 60 kHz at both recording locations, with click spectra containing more energy at lower frequencies when RL was less that 150 dBpp. Among detections at each site, sound pressure spectrum levels changed with received level (Fig. 3.7.a-d). At higher received levels, peak frequencies were relatively higher and -3, -10 dB bandwidths were narrower (3.1). As RL decreased, clicks became more broadband and the peak frequencies shifted downward. At CS,

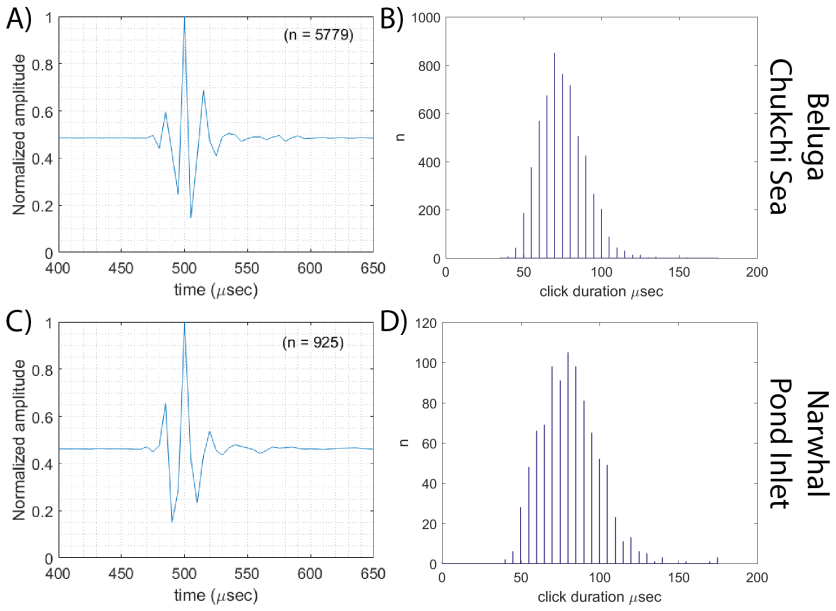

Figure 3.5: Normalized click waveform (panels A and C) and histogram of click duration (panels B and D) for select clicks between RL 140 and 160 dBpp from the CS (beluga) and PI (narwhal) recording sites. Mean click durations of beluga and narwhal were 74.1 +/- 15.2 μsec (n=5779) and 81.7 +/- 13.8 μsec (n=925) respectively.

spectra of beluga clicks exhibited a steep increase in received energy above 35 kHz with peak energy at approximately 55-60 kHz (Fig. 3.7.c). Narwhal clicks at PI also had peak energy at approximately 55 kHz, but with more energy extending below 35 kHz and a secondary peak at 23 kHz (Fig. 3.7.d). At lower received levels, this secondary peak in energy at 23 kHz was more prominent, becoming the peak frequency when RL was below 130 dB_{pp}. The relationship between click peak frequency and received level can be seen more clearly in figure 3.8. Median peak frequency of the received echolocation clicks increased with RL at both recording locations. At all received levels, detected narwhal clicks have more energy than beluga clicks at frequencies below 40 kHz.

Distributions of ICI differed substantially between the two sites. ICI of presumed beluga at CS (Fig. 3.9.a) was distributed around modal value 0.05 sec (Table 3.1). At PI, ICI was longer and more variable (Fig. 3.9.b), with local maxima at 0.003 sec and 0.14 sec.

Table 3.1: Descriptive statistics for beluga and narwhal echolocation clicks.

		Beluga: Chukchi Sea			Narwhal: Ecplise Sound		
Received Level (dB_{pp})		120-130	130-140	140-150	120-130	130-140	140-150
Peak frequency (kHz)	mean	53.2	58	63	37.9	45.3	52.2
	std	12.3	11.5	10.9	13.2	12.3	9.6
	mode	53	56	56	22.5	23.5	56
	median	52	55.5	60.5	37	48	53
Pulse duration (µs)	mean	87.6	80.3	74.9	85.1	83.7	80.3
	std	17.4	15.9	14.5	18.4	20	21.4
	mode	85	75	70	85	85	80
	median	85	80	75	85	85	80
ICI (ms)	mean	78	62.4	86.5	151.8	151.1	159.5
	std	88.9	55.6	91.1	118.8	114.3	113.6
	mode	48.6	49.5	1.6	2.5	5.7	84.5
	median	54.1	53.3	58.4	131.4	134	142.7
-3 dB bandwidth (kHz)	mean	12.7	11.1	7.1	4.3	4	4
	std	7.3	6.6	4.9	4.3	3.5	3.2
	mode	3	2.5	2.5	2	2	2
	median	12	11	6	2.5	2.5	3
-10 dB bandwidth (kHz)	mean	35.6	33.5	31.1	16.5	16.4	16.6
	std	15	15	13.5	14.3	13	12.2
	mode	35	31	25.5	3	3	5
	median	35	33	30	11.5	12.5	12.5
	n	699916	84891	24097	399341	104167	15764

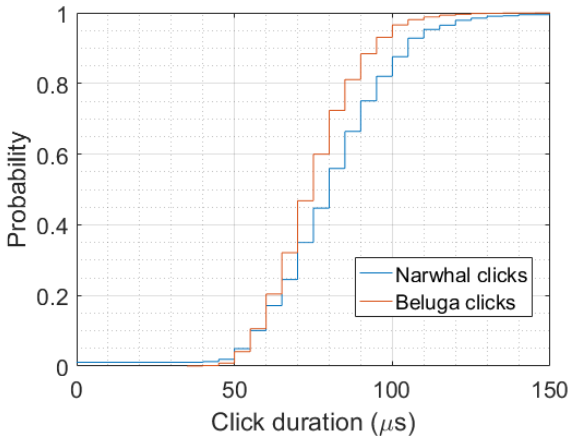

Figure 3.6: Cumulative distribution functions for duration of clicks at CS (red line; beluga clicks) and PI (blue line; narwhal clicks).

3.4.3 Time series of click detections

An average of 8,000 clicks with RL >120 dB were detected each day with acoustic presence of belugas echolocation during the May 28-Nov 1, 2014 recordings at the CS site (Fig. 3.10). The highest day of acoustic presence had 39,000 clicks. Beluga clicks were present in 124 of 135 days of recording, including periods with 100% sea ice cover during May and June and throughout the ice-free periods of August-October. Daily counts of click detections were higher during ice-free months than in periods of ice cover. At site PI, an average of 12,000 >120 dB RL clicks were detected per day with acoustic presence of narwhal (Fig. 3.11). Narwhal echolocation clicks were only present in 20 of 121 days analyzed (May-Nov). Acoustic presence of narwhal coincided with sea ice breakup at site PI, while beluga echolocation clicks were detected during all sea ice conditions, including 65 days of open water.

3.4.4 Discrimination between narwhal and beluga clicks at a single recording location

Clicks consistent with both beluga and narwhal echolocation were detected at the BS location in recordings analyzed from August 20, 2018. Click RL, spectra, and ICI are plotted

for a representative time period during which both presumed beluga and narwhal clicks were recorded (Fig. 3.12).One click event was consistent with narwhal echolocation. This can be identified from the secondary peak in sound spectrum level at 23 kHz across all RLs (Fig. 3.12.b.) and the broader range of ICI values (Fig. 3.12.c.). Beluga clicks are apparent after the narwhal clicks. These exhibit the steeper roll-off in energy below 35 kHz and shorter, less variable ICI. Canary-like whistles, typical of beluga acoustic presence, become audible during the period with beluga-like echolocation signals.

3.5 Discussion

3.5.1 Similarities in beluga and narwhal echolocation clicks

Two consistent patterns are apparent in received levels during beluga and narwhal detection events. Received level variability within individual click trains increases (e.g. Figs. 3.3 and 3.4) and peak frequencies increase (Fig. 3.8) as a traveling group apparently swims closer to the recorder. As detection events progress, the variability in RL within click trains increases from +/- 5 dB as the running maximum RL of the event reaches 120-125 dB_{pp} up to +/- 15 dB for clicks as the maximum event RL exceeds 140 dB_{pp}. The pattern of increased variability in received level within click trains as the overall event RL increases is likely due to scanning movements of the animals heads coupled with the beam pattern of clicks as they are produced. Beluga and narwhal clicks are directional and the highest energy is directed straight in front of the melon. Within 15 deg off-axis, the click energy is reduced by $>$20 dB (e.g. Koblitz et al., 2016). As orientation of animals change during dive behavior, RL would be expected to vary at the hydrophone. This pattern of received level variability has been observed in free-ranging narwhal as rapid changes in received level during click trains acoustically tracked to individual animals (Koblitz et al., 2016). The observed smaller range of click RL when the detected group is apparently farther from the hydrophone is consistent with expectations since more distant clicks would need to be closer to

on-axis to propagate to the hydrophone. As the group apparently moves closer to the recording location, a larger number of off-axis clicks would have enough energy to reach the hydrophone.

There is a strong relationship between click received levels and frequency content at both locations. As received level decreases, clicks have less relative energy at higher frequencies. This general pattern is likely caused by sound transmission loss due to frequency-dependent absorption by seawater. Measured absorption at 25 kHz in standard seawater is around 3 dB/km, increasing to 10 and 20 dB/km at 50 kHz and 75 kHz, respectively (Mellen et al., 1987; Macaulay et al., 2020). Lower-frequency energy from both species clicks travels farther than the higher frequency components of the clicks. With more energy below 30 kHz than beluga clicks, theoretical absorption spectra predict narwhal click detection will occur at greater ranges from the recorder than beluga clicks.

3.5.2 Discriminating features of beluga and narwhal clicks

The primary differences between beluga and narwhal clicks are in frequency content and rhythmic patterns of the inter-click intervals. Narwhal clicks contain more energy in the 20-30 kHz range and this difference becomes more pronounced as clicks travel away from the source. This difference between the two species has been used to differentiate between beluga and narwhal clicks, but from less than 200 representative clicks for each (Frouin-Muoy, 2017). By including a much larger set of click detections across a greater range of received levels, we substantially improve the confidence in using this characteristic for species identification and enable greater spatial context for received clicks.

ICI differed between beluga and narwhal, with beluga clicks tightly distributed around modal ICI of 50 ms. Narwhal ICI was much more variable and had a bimodal distribution, with one mode below 10 ms and a secondary mode at 140 ms. While a small number of detected clicks may limit the usefulness of this characteristic for discrimination between the species, it is diagnostic when coupled with frequency spectra in larger sets of click detections where

distributions of ICI can be determined with confidence. The difference in ICI is evident in the example detection of beluga and narwhal clicks in the recording at BS. Peak frequencies and ICI of the two species at lower received levels were easier to tell apart than during the apparent closest points of approach of the groups. The characteristic canary-like whistles of belugas were also present during the event attributed to beluga, adding confidence to the identification of the species.

3.5.3 Detection time series of belugas and narwhals

Narwhal presence at the PI site coincided closely with the short periods of sea ice breakup and freeze-up in July and Oct, respectively. The Eclipse Sound population of narwhal are known to enter Eclipse Sound around the time of sea ice break-up and exit again for the year around freeze-up (Ariak and Olson, 2019; Golder, 2018). Animals in this population spend the ice-free summer months within Eclipse Sound and its interior inlets and bays. The strongly pulsed seasonal signal to narwhal detection matches the expected acoustic presence of the species at the PI site, which is at the eastern entrance to Eclipse Sound. Dates of narwhal entry and exit from Eclipse Sound are relevant for management of this population with respect to regional shipping and this annual timing may be reliably detected acoustically from the PI recording location.

Beluga presence at CS began in early May during 100% sea ice coverage at the recording site. Belugas were present at this offshore location in >90% sea ice cover for 1.5 months before the onset of continuous melt occurred. Their seasonal acoustic presence agrees with known movements of two populations of belugas that inhabit the Chukchi Slope region between early sea ice breakup and well into freeze-up in October and November (Hauser et al., 2017). Although click detection spanned May-October, daily click detection counts were higher during open water periods than with ice cover. This could be due to the scattering effects of sea ice on beluga clicks, which reduces the probability of detection. A similar study on detection probability of echolocation clicks in the Gulf of Mexico demonstrated that propagation loss is a significant

factor in detection probability (Frasier et al., 2016). The results of this study confirm that effect of sea ice scattering on beluga and narwhal click detection ranges and detection probability is an area that should be further investigated.

3.6 Conclusions

Echolocation clicks of beluga and narwhal can be detected in long-term acoustic recordings using a relatively simple semi-automated process. These detected clicks can be used to discriminate between the species' signals acoustically, provided a sufficient sample size of clicks are recorded to observe distributions of key characteristics including peak frequency, sound pressure spectrum levels, and inter-click interval. Effects of sound propagation and the behavior and physiology of the animals must be accounted for when evaluating the results of click detection. This is needed to increase confidence in the species identification and make use of passive acoustic recordings as inputs to models for acoustic estimation of population density.

Received level variability in individual click trains may also provide insight into animal dive behavior. If sound propagation is accounted for, these characteristics of recorded echolocation events likely reflect dive behavior (scanning motion) and physiology of sound production (beam pattern). Similarly, increasing understanding of narwhal and beluga dive behavior and underwater movements could improve strength of inference about group composition and behavior from time series of acoustic detections. Density estimation using acoustic methods requires understanding of the source signal, the effect of propagation on the received signal characteristics, group composition and behavior, and detailed information on the dive behavior, physiology, and rates of sound production in individual animals. For this study, most detections occurred during periods of mostly open water or ice-free conditions. The influence of sea ice on received characteristics of echolocation clicks should also be further investigated in the future to help clarify and improve acoustic observations of beluga and narwhal presence in long-term acoustic recordings.

The success in detecting and discriminating between the species using the methods developed in this study will permit additional research using passive acoustic monitoring to study the seasonal movements and distribution of these species. In particular, it would be useful to focus further on developing acoustic methods for beluga and narwhal abundance estimates using echolocation clicks, similar to studies of *Mesolplodon* and *Kogia* species in the Gulf of Mexico (Hildebrand et al., 2015; Hildebrand et al., 2019).

3.7 Acknowledgements

We thank the Mittimatalik Hunters & Trappers Organization, Pond Inlet, Nunavut, Canada, for annual permission to carry out fieldwork and acoustic recording. Acoustic data collection and fieldwork could not have been completed without expert knowledge and technical, logistical, and vessel support provided by Alex Ootoowak. We also thank Sheattie Tagak and Tagak Outfitters for additional vessel support. Kristin Westdal and Amanda Joynt of Oceans North were also instrumental in initiating and sustaining this research program. Thanks to Evan Richardson and Environment and Climate Change Canada, for substantial logistical support at the Pond Inlet Research Facility. Special thanks to the Captain and crew of the US Coast Guard Cutter, MAPLE, for ship support in Alaska and Canada. This project is funded through a private foundation grant to the Marine Physical Laboratory at the Scripps Institution of Oceanography and by Oceans North, with additional support provided by Environment and Climate Change Canada through a grant from the World Wildlife Fund - Canada. We thank members of the Scripps Whale Acoustics Laboratory, including B. J. Thayre, J. Hurwitz, E. O'Neill-Mertz, and S. Wager for assistance with HARP operations and data processing. Special thanks to Dr. Julie D. Lee, Andrew Mack, and Phil McGillvary, who provided helpful comments on this manuscript.

Chapter 3 is currently being prepared for submission for publication of the material. Jones, J. M.; Frasier, K. E.; Wiggins, S. M.; Hildebrand, J. A. The dissertation author was the primary

investigator and author of this material.

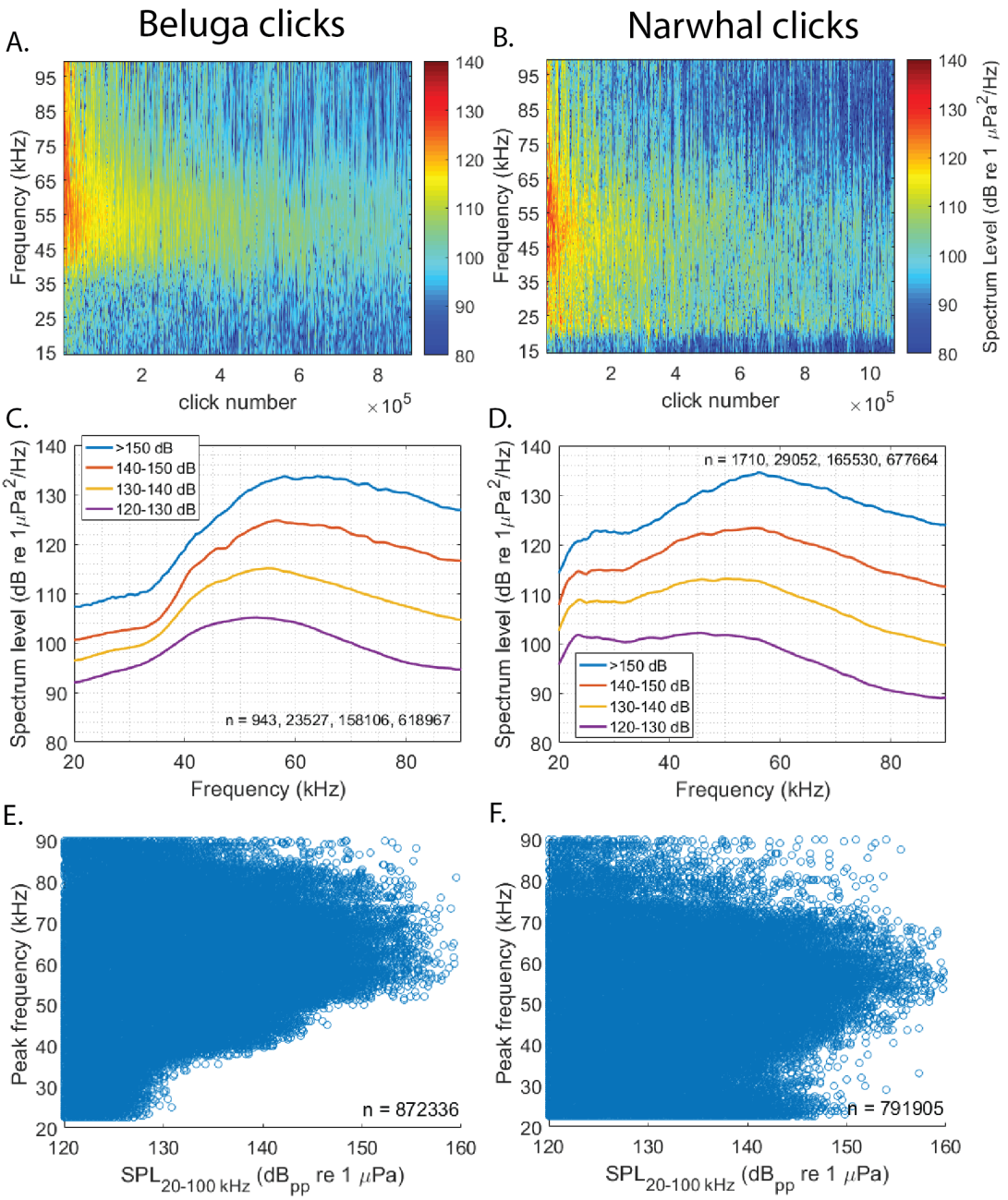

Figure 3.7: Concatenated spectrograms of detected beluga (A) and narwhal (B) clicks are sorted by click received level (dB_{pp}). Average sound pressure spectrum levels are plotted for beluga (C) and narwhal (C) clicks in 10 dB received level bins. Colored lines in average sound pressure spectra represent 120-130 dB (purple), 130-130 dB (orange), 140-150 dB (red) and >150 dB peak-to-peak sound pressure level. Bottom plots show peak frequency for beluga (E) and narwhal (F) clicks.

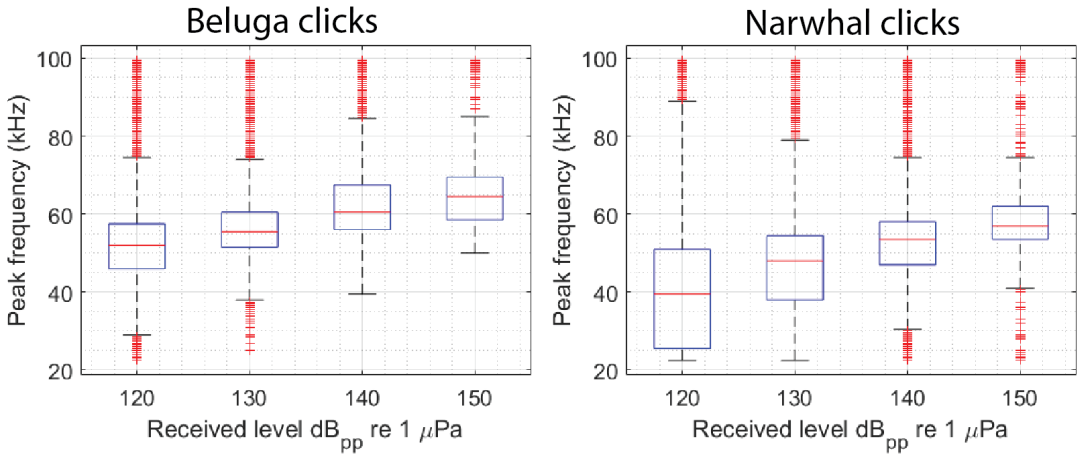

Figure 3.8: RL versus peak frequency for clicks within 10 dB RL bins (120-130, 130-140, 140-150, >150 dB$_{pp}$) for beluga and narwhal echolocation clicks. Peak frequency of the received echolocation click increased with RL at both recording locations. Box plot shows median (red line), 25^{th} and 75^{th} percentile (blue box), and range of values (whiskers). Outliers plotted as red 'plus' sign.

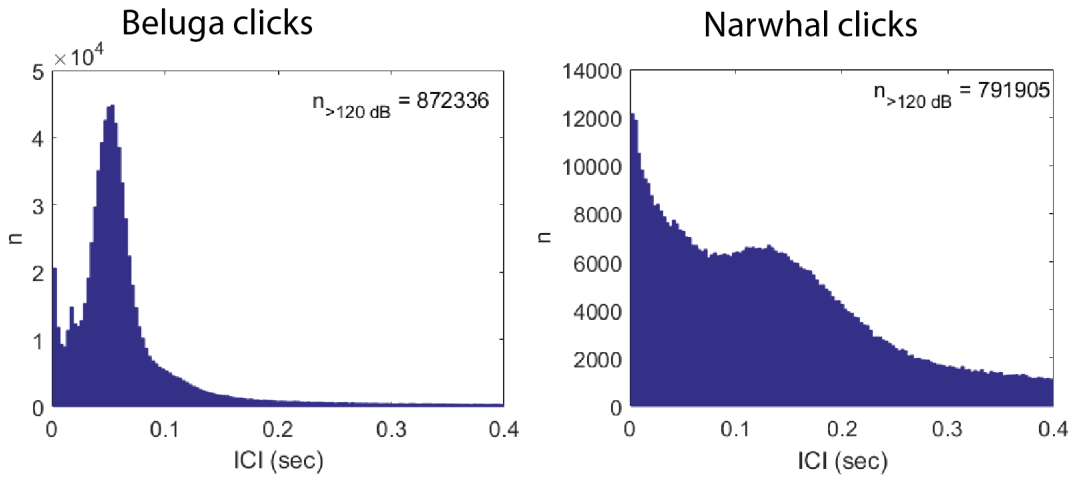

Figure 3.9: ICI of beluga (a) and narwhal (b) clicks. Beluga clicks distributed around 0.06 s while narwhal ICI are more variable.

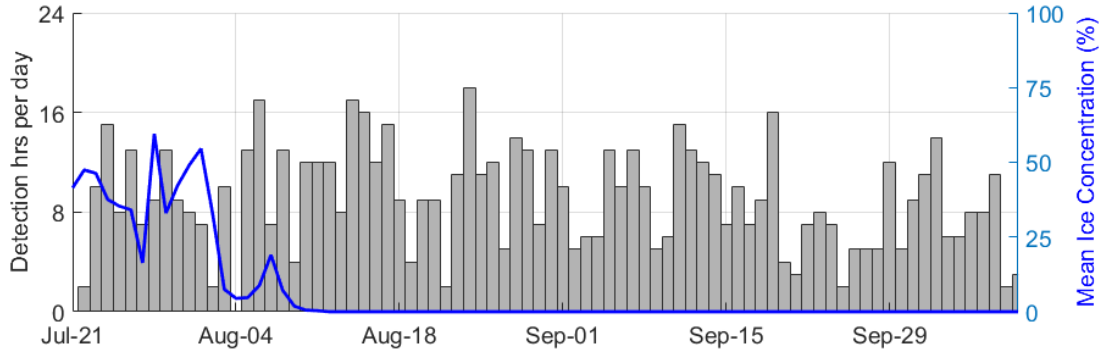

Figure 3.10: Number of beluga echolocation click detections per day (gray bars) at the CS site during the 81-day recording period analyzed. Mean daily sea ice concentration (blue line) decreased from Jul 21 through Aug 7, followed by open water for the remainder of the analysis period.

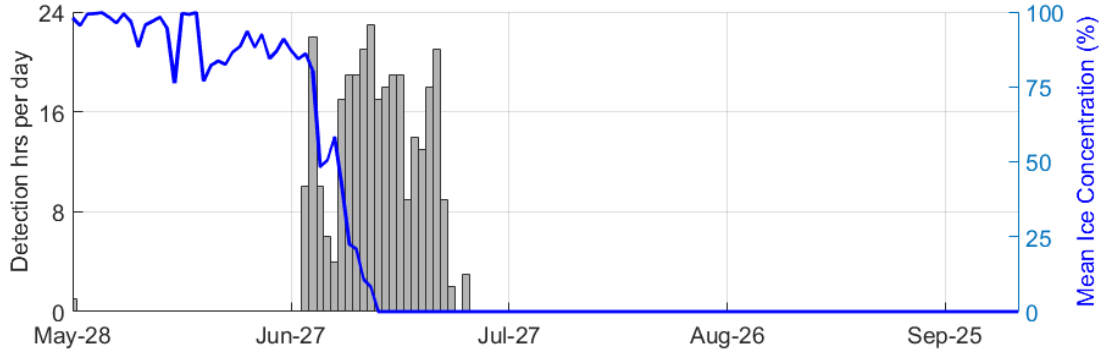

Figure 3.11: Number of narwhal echolocation click detections per day (gray bars) at the PI site during the 130-day recording period analyzed. Mean daily sea ice concentration (blue line) decreased from May 28 through Jul 10, followed by open water for the remainder of the analysis period.

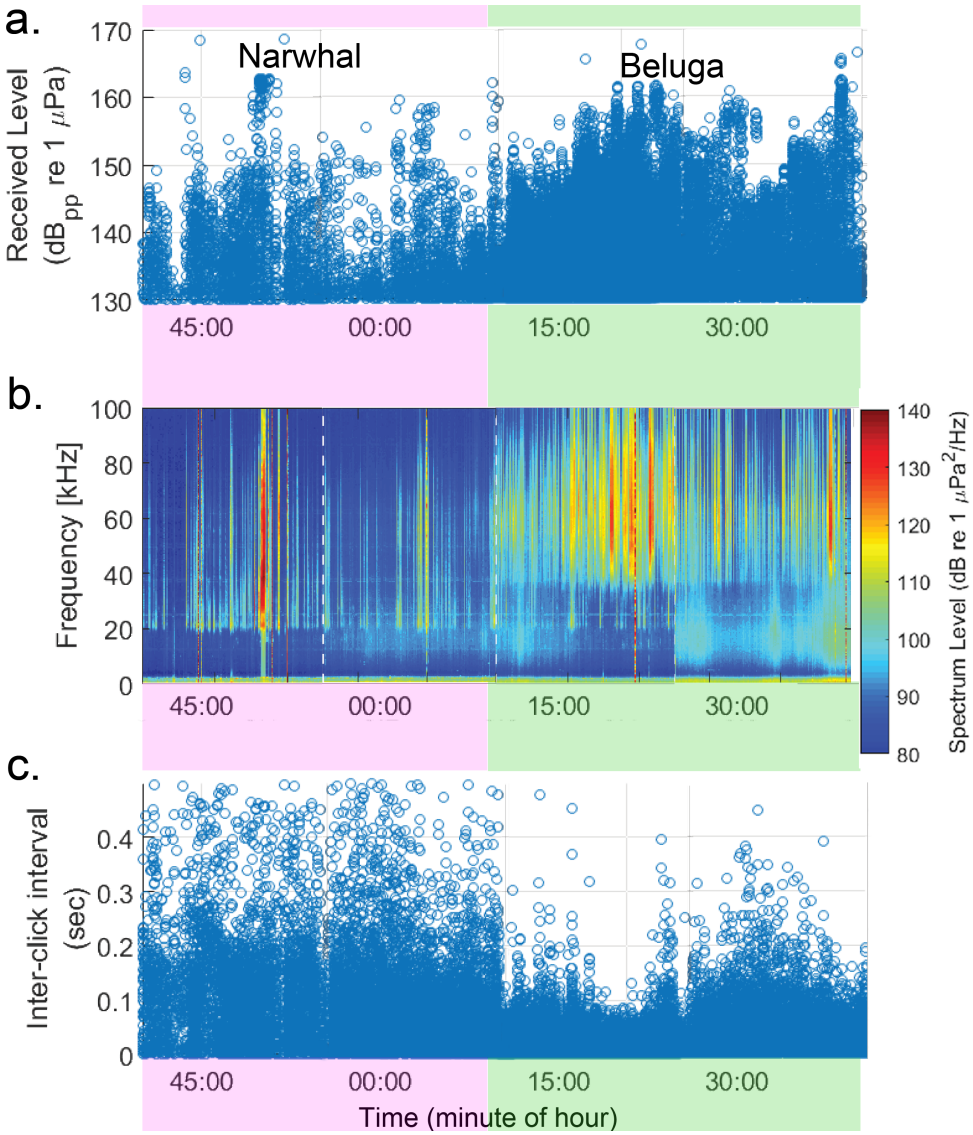

Figure 3.12: Representative echolocation detection event including clicks characteristic of both narwhals (pink area) and belugas (green area). Recording from in Barrow Strait, 30 km south of Resolute Bay, Nunavut on Aug 30, 2018 at 04:40 GMT. RL pattern (a) consistent with detection of two distinct groups of odontocetes. Spectra (b) and ICI (c) of the two groups suggest the first is composed of narwhal and the second group composed of beluga.

Chapter 4

Underwater soundscape and radiated noise from ships in Eclipse Sound, Northeast Canadian Arctic

4.1 Abstract

Increasing commercial shipping in the eastern Canadian Arctic is raising concerns about changes to the marine soundscape and potential impacts to Arctic marine mammals. Underwater radiated noise was measured for four types of commercial ships (bulk carrier, general cargo, fuel and chemical tankers, and an icebreaker) transiting Eclipse Sound, Nunavut during shipping months from October, 2018 through September 2019. Acoustic data were collected from two locations along the regular shipping route using seafloor-mounted acoustic recorders located 20 meters off the seafloor at depths of 313 m and 670 m, respectively. Ship location and operational information were combined with received sounds to calculate acoustic characteristics of individual ship transits. Ship sound measurements included broadband (20 Hz-4 kHz) sound pressure level (SPL), sound pressure spectrum level (SPSL) at the closest point of approach, and SPL in three

frequency bands to evaluate masking of communication signals produced by narwhals and ringed seals. Monthly (July, August, September, Oct) measurements were also calculated for periods selected to exclude sound from ships and for all recorded periods to compare the soundscape excluding and including sounds from nearby ships. Sound levels in all frequency bands were elevated for minutes to hours with each ship transit. The icebreaker and tankers had the highest sound levels, followed by the general cargo and bulk carrier. Noise was greater at the stern than the bow aspect for all ship types (e.g. the icebreaker reached SPL_{BB} 120 dB at range 4 km from the bow and 15 km from the stern). Long-range ship sound <200 Hz was present in median monthly SPSL excluding and including nearby ships at the deeper site. The shallower more acoustically sheltered site had substantially lower sound levels in all months, except during ship transits. The results presented provide a baseline description of the natural soundscape in the Eclipse Sound, Nunavut, and by assessing contributions of ship noise facilitate prediction of underwater sound levels with future increases in shipping traffic.

4.2 Introduction

Throughout the world's oceans, commercial ships are a significant source of underwater sound (Ross, 1976; Hildebrand, 2009), raising concerns about potential impacts these sounds have on aquatic ecosystems and species (Clark et al., 2009; Nowacek et al., 2007). Ship traffic is increasing rapidly in some areas of the Arctic (Dawson et al., 2018) and is projected to accelerate as decreasing sea ice coverage (Smith and Stephenson, 2013) opens new opportunities for industrial development, commercial shipping, and tourism across the region (Theocharis et al., 2018). From 2005 to 2015, vessel traffic in the Canadian Arctic increased by an estimated 75% (Pizzolato et al., 2016). Reductions in sea ice and the use of icebreaking ships can extend periods of shipping noise by lengthening the Canadian Arctic shipping season (Stroeve et al., 2014; Smith and Stephenson, 2013), whereas other factors such as tourism and industrial development may

play a larger role in contributing to shipping noise in some areas.

Eclipse Sound in the eastern Canadian Arctic is a region where ship traffic is increasing due to tourism and industrial development. The community of Pond Inlet, located on Eclipse Sound north Baffin Island (Fig. 4.1), experienced almost triple the annual shipping traffic during 2011-2015 when compared to the decade 1990-2000 (Dawson et al., 2018). This was the largest proportional increase in shipping of any region in the Canadian Arctic. The change was due to increasing numbers of tourism-related vessels (i.e. passenger ships and pleasure craft) and in bulk carrier and tanker ships. While increasing traffic by tourism-related vessels is widespread across the Canadian Arctic, the additional cargo ship traffic past Pond Inlet was associated with the 2010-2015 development of the Baffinland Iron Mines Corporation (BIMC) Mary River Mine (MRM) on North Baffin Island.

Starting in 2015, bulk carrier ships began service to the newly constructed Milne Port (BIMC, 2015), a deepwater shipping terminal in Milne Inlet at the southeast end of Eclipse Sound (Fig. 4.1). Iron ore from the MRM is loaded onto bulk carriers in Milne Port and shipped to market via northern sea routes. Reported annual ore production has increased from 0.92 million metric tons (MT) in 2015 to 5.86 MT in 2019. Annual mining-related shipping has increased proportionately with ore production and includes bulk cargo ships, tugs, general cargo and tanker ships (Appendix I). Eclipse Sound ship traffic occurs primarily during open water months from August through September, with an extension of the shipping season created in 2018 by the addition of an ice management vessel to escort ships servicing the MRM during July and October periods of ice cover. Increased ship traffic has raised concerns among community members, marine resource managers, and other stakeholders about the potential impacts of those sounds on the natural underwater soundscape and marine mammals (Ariak and Olson, 2019). The intensity of shipping in the Eclipse Sound region is projected to become substantially higher with a proposed 2021 increase to 12 MT/yr iron ore production at the MRM (BIMC, 2018).

Sources of sound in the ocean are abundant and varied, but generally can be classified as

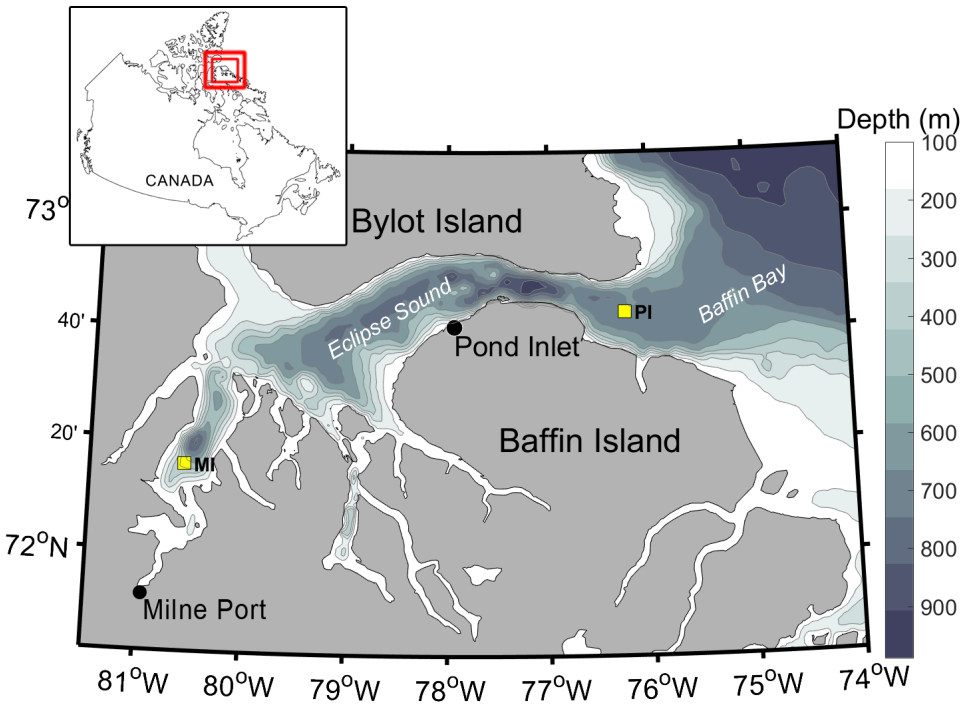

Figure 4.1: Long-term acoustic recording sites in Eclipse Sound, N. Baffin Island, Nunavut Territory, Canada. High-frequency Acoustic Recording Packages (HARPs) were deployed at the Pond Inlet site (PI; seafloor depth 670 m) from September 28, 2018 through September 21, 2019. A second location in Milne Inlet (MI; seafloor depth 313 m) recorded acoustic data from September 29, 2018 to August 18, 2019. The Baffinland Mary River Mine shipping terminal is located at Milne Port. Depth contour intervals 100 m.

natural in origin or man-made. Low-frequency natural sounds less than 200 Hz are produced by earthquakes and surface wave interactions (Hildebrand, 2009). Wind-driven waves are a major contributor to underwater sound above 200 Hz and levels decrease by about 6 dB/octave above 500 Hz (Wenz, 1962; Urik, 1983). In Arctic waters, a positive strong relationship between sound pressure level and wind speed occurs during ice-free conditions, but is weaker during periods of ice cover (Roth et al., 2012; Halliday et al., 2020). Sounds associated with mechanical activity of sea ice can also be a major component of the underwater soundscape across frequencies from 20 Hz to >4 kHz (Milne and Ganton, 1964; Kinda et al., 2015). Sounds produced by marine animals, particularly marine mammals, can also be significant features of the natural underwater Arctic soundscape. For example, sound pressure levels between 50 Hz and 10 kHz increase with greater

presence of bearded seal vocalizations in the Western Canadian Arctic (Heimrich et al., 2020).

Marine mammals produce underwater sounds for navigation, foraging, socializing, and reproduction. In the Eclipse Sound region, the most abundant marine mammal species are ringed seals (Pusa hispida), which are present year-round (Yurkowski et al., 2018), and narwhal (Monodon monoceros), which are present annually from July-Oct (Marcoux et al., 2019; Richard et al., 2010). Ringed seals produce barks and growls in the 50-400 Hz range and yelps at frequencies to >1 kHz (Jones et al., 2014; Stirling et al, 1983; Stirling, 1973). Narwhals produce high-frequency echolocation clicks from 20 kHz to >100 kHz (Koblitz et al., 2016; Rassmussen et al., 2015). They also produce sounds for communication, including whistles from about 600 Hz up to 14 kHz and burst-pulse sounds from 800 Hz to 10 kHz (Marcoux et al., 2012; Shapiro, 2006; Ford and Fischer, 1978).

Sounds from distant ships are a major underwater sound source from 10-200 Hz (Hildebrand, 2009; Wenz, 1962). Low-frequency sounds are generated by cavitation of the ship's propeller and can be measured in ambient noise levels throughout the world's oceans at great distances from any shipping traffic (Širović et al., 2016; McDonald et al., 2006). Shipping traffic is also a source of higher-intensity short-term (transient) noise events as ships pass closer to a listener's location. At closer ranges, ship sounds occupy frequencies to above 10 kHz (McKenna et al., 2012; Gassmann et al., 2017). These transient sounds from ships can be detected above the ambient sound levels when ships are at ranges of tens to >100 km (e.g. Zhu et al., 2018). Evaluations of the effects on marine mammals resulting from underwater ship sounds generally address two areas. One is the effect of long-range sound propagation on the ambient sound environment. As additional shipping traffic occurs within a region, ambient sound levels increase.. The other is the effect of transient noise caused by ships transiting within an area of habitat. Noise from a transiting ship may have direct effects on individuals and groups of marine mammals along the ship's track.

Two concerns about how underwater noise from ships impacts marine mammals stem

from noise-induced alteration of physiology or natural behavior (acoustic disturbance) and the potential for masking of biologically important signals where ship sounds overlap in frequency (Southall et al., 2007; Gomez et al., 2016; Erbe et al., 2016). Acoustic disturbance of marine mammals has been extensively studied through observation of animal behavior at various levels of underwater noise from ships. Generalized guidelines have been developed to help predict threshold broadband sound pressure levels (SPL_{BB}) at which behavioral disturbance or avoidance of the sound source may occur for several taxonomic groups of marine mammal species (Southall et al., 2007). Narwhal and ringed seals are classified in this system as mid-frequency cetaceans and pinnipeds, respectively. The generalized received SPL_{BB} at which behavioral disturbance is expected to occur for those taxonomic groupings is 120 dB, although actual observed behavioral disturbance has occurred at a wider range of received levels in published studies for narwhal and ringed seal (Golder, 2020; Golder, 2019; Golder, 2018; Southall et al., 2007; Finley et al., 1990). Masking of acoustic signals caused by the introduction of underwater sound from ships is evaluated at discrete frequency bands that overlap with biologically important signals, such as echolocation or social communication, and with consideration for the hearing systems of the species of interest. Although a signal, such as a whistle produced by narwhals, might occupy a narrow frequency band, there is some critical band around that frequency where other sounds from the environment may interfere with the ability of another animal to hear it. To account for these hearing system effects, sound levels are evaluated in $1/3^{rd}$ octave frequency bands around the biologically relevant frequency being considered (Erbe et al., 2016). Acoustic masking caused by changing levels of noise in the environment can be estimated as Listening Space Reduction (LSR; Erbe et al., 2016), which is a function of the amount of potentially masking noise added by a source, such as a transiting ship, relative to some reference background sound level, such as the mean sound level of that frequency band in the absence of the additional sound source (Erbe et al., 2016; Pine et al, 2018).

This study reports levels of underwater sound associated with the natural acoustic en-

vironment and with man-made noise from shipping at two locations in Eclipse Sound on N. Baffin Island in the region of the community of Pond Inlet, Nunavut. Analyses of 2018 to 2019 regional Automated Information System (AIS) ship tracks and underwater acoustic recording data were undertaken to determine quantity and spatial patterns of ship traffic and to estimate underwater sound levels emitted by ships. Measurements of underwater sound levels during the July-Oct shipping season are presented for periods excluding and including times when ships transited past the recording site. Monthly sound pressure spectrum levels (SPSL) of periods selected to minimize recorded sounds from transiting ships are representative of the 'natural' acoustic environment. Monthly SPSL from all recorded periods, including ship transits and inter-ship periods, represent the soundscape including the total contribution of underwater sound from ships. Acoustic characteristics of transient underwater sound from commercial ships are quantified in relation to vessel design and operational parameters for the most common ship types. Characteristics were selected to prioritize evaluation of underwater shipping noise with respect to narwhal and ringed seal behavioral disturbance and potential masking of communication signals.

4.3 Methods

4.3.1 Ship transit information

Satellite Automated Information System (AIS) data were obtained from ExactEarth (www.ExactEarth.com) on ship traffic within 100 km of two acoustic recording stations. Locations were extracted from AIS data for all ships transiting past the recording sites, including time, latitude and longitude, speed, heading, maximum draft, Maritime Mobile Service Identity (MMSI) number, vessel name, vessel type and cargo class. Additional ship specification data, including gross and deadweight tonnage (i.e. weight carrying capacity), were obtained from Lloyd's Registry of Ships. The ship location was used to calculate the distance along the sea surface from the acoustic recording location to the ship reported position.

Ship transits were defined as periods of continuous presence of a ship (i.e. unique MMSI number) within a maximum radius of each acoustic recording location (Fig. 4.1) during which a ship's closest point of approach (CPA) occurred within 15 km of the recorder. Continuous presence was defined as having no greater than 60 min between AIS position updates during a 6 h time period centered on the CPA of each transiting ship. A 100 km maximum radius was selected for AIS ship transit data at the Pond inlet site (PI) to include vessels of speeds up to 18 knots, the maximum speed in the AIS data included in this study, within the 6 h transit window. A 30 km maximum radius was selected for AIS data at the Milne Inlet site (MI) to prioritize transiting ships while excluding ships engaged in port-related operations near the shipping terminal at southern terminus of Milne Inlet and ships anchored at a designated cargo ship anchorage 30 km northeast near Ragged Island. Due to irregularity in satellite transit and vessel transmission, all ship tracks and ship information were interpolated linearly to a uniform temporal resolution of 5 s.

4.3.2 Acoustic recording and data processing

Underwater acoustic recordings were collected at two locations in the Eclipse Sound region (Fig. 4.1). One recording location was at depth 640 m between Baffin and Bylot Islands in eastern Eclipse Sound and will be referred to as the Pond Inlet (PI) recording site. The second recording location was at depth 313 m in Milne Inlet (MI) near the southwest end of Eclipse Sound. Recordings at both sites were made using High-frequency Acoustic Recording Packages (HARP; Wiggins and Hildebrand, 2007; Fig. 4.2), which recorded acoustic data at a sampling rate of 200 kHz. Recordings were made continuously at PI from September 28, 2018 to September 21, 2019 and on a schedule of 25 min recorded of every 30 min at MI from September 29, 2018 to August 19, 2019. The HARPs were deployed to the seafloor and the hydrophone sensor was suspended approximately 20 m above the seafloor. The MI hydrophone consisted of two stages, one for low-frequency ($<$2 kHz) and one for high-frequency ($>$2 kHz). The low-frequency stage was composed of six cylindrical transducers (Benthos AQ-1) with a sensor

sensitivity of -202 decibels root mean squared (dBrms) re: 1 V/μPa. The high-frequency stage consisted of a spherical omni-directional transducer (ITC-1042; www.itctransducers.com) with an approximately flat (± 2dB) frequency response of 200 dBrms re 1 V/μPa between 1Hz and 100 kHz. The hydrophone transducer signals were fed into a preamplifier with approximately 50 dB of gain. The PI hydrophone used the same high-frequency stage and single omni-directional transducer as MI, but did not include a low-frequency stage. Acoustic calibrations of both hydrophones were made at the Scripps Institution of Oceanography (SIO) and these calibrations were used to convert all acoustic recordings to sound pressure levels.

All recordings were converted to an adapted wav file format (xwav) and decimated by a factor of 20 to yield an effective bandwidth of 10-5000 Hz. Decimated recordings were processed into consecutive non-overlapping 5 s averaged sound pressure spectral density estimates with 1 Hz frequency bin spacing, which were assembled into Long-term Spectral Averages (LTSAs) to facilitate time-frequency analysis. To remove system self-noise resulting from HARP disk writes, the first three and last three 5 s spectra in each 75 s recording were not used for averaging. The retained 5 s spectra were further analyzed using custom Matlab-based (www.Mathworks.com) software to provide average and percentile SPSL, spectrograms, and sound pressure level (SPL) time series for specific frequency bands, including 20-4000 Hz to represent broadband noise radiated by ships and 1/3rd octave frequency bands centered at 250 Hz, 1 kHz, and 3.5 kHz to represent functional hearing of communication signals produced by ringed seals (250 Hz barks) and narwhals (1 kHz burst pulses and 3.5 kHz whistles). All sound pressure level measurements are reported on a logarithmic scale as decibels (dB) with reference pressure 1 μPa; sound pressure spectrum levels are reported in dB re 1 μPa^2/Hz.

4.3.3 Monthly underwater sound levels excluding and including ship transits

To estimate levels of natural and man-made underwater sound, recording periods were selected to exclude and include the presence of ships transiting past the recording site. Sound pressure spectrum levels excluding ship transits were obtained by analyzing all periods when the difference between successive ship transit CPA events was at least 8 h. This duration between ship transits was selected to provide a one-hour buffer before and after all 6 h ship transit windows, reducing inclusion of the long-range components of ship sound in the estimation of natural sound levels. For each period meeting this condition, all 5 s sound pressure spectra were extracted from 4 h after the first ship's CPA to 4 h prior to the second ship's CPA. These inter-transit times will be referred to as periods 'excluding ships'. A monthly random sample of 30,000 5s spectra was selected from the periods excluding ship transits during the shipping season to provide a consistent sample size for each month of shipping operations. Monthly sound pressure spectrum levels of periods excluding ships were evaluated from the 1^{st}, 10^{st}, 50^{st} (median), 90^{st}, and 99^{st} percentiles of all 5 s LTSA subsampled from each time period. The 250 Hz, 1 kHz, and 3.5 kHz $1/3^{rd}$ octave and 20-4000 Hz broadband SPL for all percentiles were calculated from the sum of the squared pressure across the frequency band of the percentile pressure spectra. Sound pressure spectrum levels and percentile SPL measurements were also made for all monthly recording periods during the shipping season. This will be referred to as periods 'including ships'. Measurements of received sound levels excluding and including ships were made for all monthly recorded periods during October 1 to 22, 2018 and between July 18 and September 21, 2019. These periods were selected to include all days of shipping traffic during the 2018 sea ice freeze-up, 2019 sea ice break-up, and two months of the 2019 open water season. Open water recording dates were separated by month to explore differences resulting from seasonal winds, which are higher in September and October than in July and August (Barber et al., 2001). The

duration of monthly periods analyzed differed based on dates of recording and date limits of annual shipping traffic.

4.3.4 Environmental conditions near the recording site

Daily sea ice maps obtained from the Canadian Ice Service, Environment and Climate Change Canada (https://iceweb1.cis.ec.gc.ca/) were used to estimate proportional ice cover near the PI and MI recording sites during periods when acoustic data were analyzed. Wind speed within a 100 km radius of the PI recording site was estimated from 25 km resolution Advanced Scatterometer (ASCAT) measurements processed for 10 m height ocean surface winds by the National Oceanic and Atmospheric Administration, National Environmental Satellite Data and Information Service (https:
manati.star.nesdis.noaa.gov/products/ASCAT.php). Wind vectors were only available for time periods corresponding to ice-free conditions at locations in North Baffin Bay at ranges 25 to 100 km from the recording site. Wind speed was correlated with 1-min average received broadband sound pressure level by selecting all available wind vectors within radius 100 km and time +/- 60 min of SPL_{BB} measurements. Only times during periods excluding ship transits were included to reduce overlap with ship noise. A least-squares regression line was fitted to the data to estimate the relationship between wind speed and SPL_{BB}.

4.3.5 Acoustic characteristics of ship transits

Spectral characteristics of ship transits were analyzed in acoustic recordings at PI from the sound pressure spectrum levels within a 6-hour (6 h) window centered on each ship CPA. Acoustic ship transits were defined as the 6 h period, consisting of 3 h prior to and 3 h after the ship CPA. This time-window around each CPA was selected to include long-range propagation of underwater noise from ship transits and sometimes resulted in multiple ship transits occurring

within the same 6 h window. Site PI recordings were used for ship transit measurements because the continuous recording schedule precluded any gaps in data during all transit windows. Sound pressure levels for the 20-4000 Hz band (SPL_{BB}) and the 250 Hz, 1 kHz, and 3.5 kHz $1/3^{rd}$ octave bands were calculated for each 5 s time bin in the ship transit LTSA data from the sum of the squared pressure across the frequency bands. SPL band one-min average received levels were also computed from the mean of all 5 s SPL values in each one-min time bin across the deployment period. One-min SPL was calculated to facilitate analyses of received level duration and range to ships at specific received levels.

The estimated levels of natural underwater sound occurring sound during each ship transit will be referred to as 'background levels'. The background levels for a ship transit were estimated from the median SPL for all frequency bands and the SPSL during the 30 min from 2.5 to 3 h prior to the ship CPA time. This was intended to provide a reasonable estimate of underwater sound levels prior to each ship transit for comparison with sound introduced by the ship as it transited past the recording site. Received sound pressure spectra and band SPL were calculated for the CPA of each ship transit by averaging the received levels of all 5 s time bins within a data window during which the ship traveled a distance of 1.5 ship lengths with respect to the CPA, similar to the method described in McKenna et al. (2012).

Representative transits were selected for each vessel type to evaluate received level at varying ranges to the different ships and the durations of received levels above the band median and 90^{th} percentile levels during periods excluding ship transits. When available, non-overlapping transits were chosen to represent a vessel type to minimize additional noise from other ships.

4.4 Results

4.4.1 Ship transit information

During Sept 28, 2018 to September 21, 2019 there were 95 unique ships which made 266 transits within 15 km of the Pond Inlet (PI) recording location (Fig. 4.3, Table 1). At the Milne Inlet recording site (MI), 64 unique ships made 240 transits past the recording location (Fig. 4.4, Table 4.1). Ships that transited past the PI site, but not the MI site, were primarily pleasure craft, passenger vessels, military and Canadian Coast Guard vessels. With few exceptions, ship operations during the 6 h transit windows consisted of vessels making way at relatively constant speeds over ground while making minimal course corrections for navigation. Notable exceptions occurred occasionally in October and July when an icebreaker (M/V*Botnica*) approached the recording site then reversed course within 15 km of the site (Fig. 29.b) while engaged in ice assistance activities. These instances of course reversal near the recording site were counted as a single ship transit. At the PI site, the general orientation of vessel traffic was east-west, entering or exiting Eclipse Sound from Baffin Bay (Fig. 4.3). In Milne Inlet, the general orientation of vessel traffic was north-south (Fig. 4.4). Ships were separated into 11 types based on AIS ship-type designation. Among the ship types, cargo vessels, including tankers, represented 74% of all ship transits at PI (n=197) and 79% at MI (n=189). Cargo vessels were separated into four categories to distinguish the three most common cargo sub-types (bulk carrier, general cargo, and tanker) from other less common cargo vessel types (heavy load carrier, deck cargo ship, offshore support vessel). Less common cargo ship types are grouped in Table 4.1 as 'other cargo' ships.

The most common ship type at both locations was the bulk carrier, with 43 unique ships comprising 57% of transits at PI and 63% at MI. After bulk carriers, proportions of ship types differed somewhat between sites. At PI, other ship types with highest transit occurrence were general cargo (9%, n=25), passenger (8%, n=20), icebreaker (7%, n=19), and tanker (6%, n=15). Pleasure craft, and fishing, sailing, tugs, military, Canadian Coast Guard, and other cargo ships

Table 4.1: Summary of AIS ship transits, passing within 15 km of the Milne Inlet (MI) and Pond Inlet (PI) acoustic recording locations between September 28, 2018 and September 21, 2019.

Ship type	Milne Inlet		Pond Inlet	
	Number of transits	Percent of transits	Number of transits	Percent of transits
Bulk Carriers	152	63%	152	57%
General Cargo	21	9%	25	9%
Passenger Ships	0	0%	20	8%
Icebreaker-Support Vessel	39	16%	19	7%
Oil and Chemical Tanker	10	4%	15	6%
Pleasure Craft	1	0%	7	3%
Sailing	0	0%	6	2%
Tug	9	4%	6	2%
Military	2	1%	6	2%
Other Cargo	6	3%	5	2%
CCGS-SAR*	0	0%	5	2%
Total	240		266	

* Canadian Coast Guard Ship - Search and Rescue

together made up the remaining 13% of ship transits (n=35) at site PI.

At site MI, the other types with highest occurrence of transits were icebreaker (16%, n=39), general cargo (9%, n=21), tanker (4%, n=10), and tug (4%, n=9). Other cargo and military ships made up the remaining 3% (n=8). There was a single transit of a 36 m length pleasure craft and no transits of passenger ships, sailing ships, or Search and Rescue ships (SAR; i.e. Canadian Coast Guard Ships) at MI.

4.4.2 Monthly underwater sound levels excluding and including ship transits

Acoustic recordings from site PI totaling 1872 h were analyzed for underwater sound levels from 78 days across four periods of the shipping seasons of 2018 and 2019 (Fig. 4.5). The same set of analysis steps was performed on 1464 h of acoustic recordings from site MI from 61 days across October, 2018, and July and August, 2019. From these data, 870 h (47% of analysis periods) from site PI and 680 h (47% of analysis periods) from site MI were extracted for estimation of sound levels with transient ship noise events excluded (i.e. excluding ships; Fig. 4.5,4.6). Daily durations of continuous recording periods excluding ships ranged from 1 to 24 h. Monthly and annual sound levels for periods including ship transits were calculated from the total recorded hours during each analysis period.

The first analysis period was October 1 to October 22, the last day of 2018 ship transits past sites PI and MI. This period includes the end of the 2018 open water season and the onset of sea ice freeze-up. The second analysis period was from the date of the first ship transit of the year on July 18, 2019, through July 31. This period includes the beginning of 2019 shipping and the onset of continuous sea ice breakup leading to open water. The third and fourth periods at PI included open water shipping during August 1-26 and September 2-21, 2019. Acoustic data were not recorded at PI between August 27 and September 2, 2019. At MI, a third analysis period extended from August 1 to the end of recording on August 18, 2019. No acoustic recordings were

made at site MI in September, 2019.

In all months, noise from ships transiting past the recording sites can be seen in the acoustic recordings as increases in received sound levels of $<$12 h duration with energy concentrated below 2000 Hz, and, with a few exceptions hourly median SPL_{BB} that exceed 110 dB (Figs. 4.7-4.13). Episodic increases in natural underwater sound levels occurred at varying intensities and durations during the periods excluding ship transits. In all months except October, median hourly SPL_{BB} rarely exceeded 110 dB except during ship transits near the recorders. Monthly SPSL excluding ship transits was substantially lower below 200 Hz at MI than PI (Figs 4.14-4.15). Monthly SPL for all frequency bands and percentile levels was lower at site MI than at PI during periods excluding and including ship transits (Table 4.2). Exceptions to this pattern in SPL occurred during several time periods with ship transits, namely the October and July 99th percentile SPL_{BB}, the August 50^{th} and 10^{th} percentile 1 kHz band level, and the August 99^{th} percentile 3.5 kHz band level. Sound levels in the 1^{st} and 10^{th} percentiles represent relatively quiet times during the recording periods. At site PI sound levels during 'quiet' periods were lowest in July and August. At MI, the 1^{st} and 10^{th} percentile SPL were lowest in October.

At site PI, intermittent periods of elevated wind-driven sound are apparent during ice free conditions early to mid-October, 2018 (Fig. 4.7.b.1), in late-August 2019 (Fig. 4.11.b.1), and throughout September 2019 (Fig. 4.13.b.1, b.2). These natural acoustic events can be $>$1 d in duration, as in the October 6-7 period of elevated received levels across the 20-4000 Hz frequency range (Fig. 4.7.b.1). This event generated the highest SPL_{BB} measured during all periods excluding ship transits, with a maximum one-min mean SPL_{BB} of 114 dB re 1 μPa.

Sound pressure spectrum levels from periods excluding ship transits reveal seasonal differences in the natural underwater soundscape (Fig. 4.14 upper panels; Table 4.2). July and August had the lowest levels and included only one period between July 18 and July 20 during which $>$1% sea ice cover remained within a 15 km radius of the recording location. Noise from an icebreaker (M/V*Botnica*) is apparent at 200 Hz in the July 90th and 99th percentile ship-excluded

Table 4.2: 10^{th}, 50^{th} (median) 90^{th}, and 99^{th} percentile SPL (in dB re 1 μPa) in the 250 Hz, 1 kHz, and 3.5 kHz $1/3^{rd}$ octave and 20-4000 Hz frequency bands for monthly periods excluding 6 h ship transit windows in each period ('no ships') and of all recorded times, including ship transits.

Site PI

		October '18					July '19					August '19					September '19				
Frequency Band		1st	10th	50th	90th	99th	1st	10th	50th	90th	99th	1st	10th	50th	90th	99th	1st	10th	50th	90th	99th
20Hz - 4 kHz	no ships	88.0	92.7	102.7	111.4	115.9	89.4	92.4	96.8	102.3	109.1	90.5	93.3	97.7	105.5	110.6	90.5	94.7	101.9	106.6	110.9
	ships		91.7	101.7	110.6	122.5		90.8	95.4	107.7	122.5		91.4	96.6	106.9	119.1		94.4	99.8	108.2	122.4
250 Hz	no ships	74.6	79.3	89.5	97.6	100.8	76.3	79.1	83.3	88.4	96.7	75.7	78.5	83.1	91.0	97.1	76.3	80.3	87.2	92.9	97.5
	ships		78.4	88.8	96.1	106.4		77.0	81.8	95.4	109.3		76.9	82.1	92.3	105.5		79.4	85.5	94.8	109.6
1 kHz	no ships	71.2	77.8	89.5	97.8	100.6	72.9	76.7	82.6	88.9	95.1	70.6	74.3	81.4	94.0	98.4	76.3	82.7	91.8	95.9	98.9
	ships		77.2	87.3	95.6	102.2		74.1	80.3	89.6	105.5		66.7	80.1	91.5	100.1		83.4	89.3	94.1	102.1
3.5 kHz	no ships	71.5	77.4	87.7	96.1	98.8	73.1	76.3	81.3	88.6	93.4	71.0	74.5	81.1	90.3	95.4	72.6	78.4	85.5	91.5	93.8
	ships		75.6	85.3	93.6	97.1		73.3	78.1	86.7	100.0		68.6	78.4	87.3	95.1		78.0	83.2	89.1	95.9

Site MI

		October '18					July '19					August '19					September '19				
Frequency Band		1st	10th	50th	90th	99th	1st	10th	50th	90th	99th	1st	10th	50th	90th	99th	1st	10th	50th	90th	99th
20Hz - 4 kHz	no ships		71.6	86.8	101.8	106.4		81.5	87.7	96.7	101.8		81.6	89.7	97.2	103.7	-	-	-	-	
	ships		72.1	91.0	107.4	123.7		82.3	90.5	103.7	122.8		82.2	90.0	102.9	116.9	-	-	-	-	
250 Hz	no ships		55.3	73.8	89.3	93.6		68.0	73.6	82.4	86.6		67.8	75.5	83.3	89.8	-	-	-	-	
	ships		57.8	79.2	92.2	103.3		69.0	77.1	90.1	107.3		70.0	77.0	90.3	105.2	-	-	-	-	
1 kHz	no ships		57.2	75.2	90.2	94.0		69.8	76.6	85.6	89.8		70.2	79.0	86.5	91.3	-	-	-	-	
	ships		56.1	79.1	93.0	108.9		70.7	79.3	88.9	102.5		70.8	83.4	88.8	99.7	-	-	-	-	
3.5 kHz	no ships		60.4	71.1	86.4	90.6		69.3	76.0	84.5	91.4		69.6	77.8	84.9	94.4	-	-	-	-	
	ships		61.0	73.1	87.3	93.7		70.2	77.8	85.9	94.6		70.0	76.9	86.0	96.3	-	-	-	-	

sound pressure spectrum level (Fig. 4.14), reaching approximately 77 and 89 dB re 1 μPa^2/Hz respectively. This suggests that 200 Hz noise from the ship is detectable at ranges greater than 40 km from the ship in at least some transits. Wind noise (sound pressure spectrum levels above 200 Hz in the 90^{th} and 99^{th} percentiles) rarely appears in August. Median and lower percentiles in August reflect relatively quiet periods above 200 Hz with lower wind noise apparent at those frequencies. September and October periods excluding ship transits had higher sound pressure spectrum levels than July and August. Increased wind-generated noise is apparent during these months by the increased median spectrum levels above 200 Hz, 5 to 8 dB re 1 μPa^2/Hz higher than August. October had the highest sound pressure spectrum levels at all frequencies, with additional broadband noise possibly associated with sea ice formation. Icebreaker harmonic noise at 200 Hz is again visible in October's 99^{th} percentile samples of periods excluding ship transits.

Monthly sound pressure spectrum levels for all analysis periods, including ship transit windows, (Fig. 4.14, Lower panels) were similar to ship-excluded noise spectra in the median and lower percentiles. Ship-inclusive median sound pressure spectrum levels were higher by 1-3 dB in the 50-100 Hz range where the largest contributions from ship noise would be expected. Some additional low-frequency noise <40 Hz was apparent in the ship-inclusive median-level spectra, consistent with cavitation noise from large ship propellers (Ross, 1976). The 90th and 99th percentile ship-inclusive levels for July and October clearly exhibit substantial additional noise consistent with ships and the icebreaker operating in the area during both months. In all months, all one-minute time bins with average SPL_{BB} >115 dB were associated with ship transits. The 99th percentile sound pressure spectrum level including ship transits was higher at all frequencies by 1 to 15 dB than during periods excluding ship noise. The greatest relative differences in spectrum level between ship-excluded and ships-included periods occurred in the 50-250 Hz range.

4.4.3 Environmental correlates with sound levels excluding ship transits

Sound pressure levels above 1 kHz were positively correlated with wind speed from satellite measurements (n=189) at 25 to 100 km from the recording site (Fig. 4.17). A total of 189 5 sec acoustic measurements were made during periods within 2 h of a satellite estimate of sea surface winds. A general pattern is apparent of increasing SPL_{BB} with wind speed. Drawing a linear fit to the data gives an estimate of + 0.8 dB for each increase of 1 m/s in wind speed.

4.4.4 Acoustic characteristics of ship transits

There were 220 ship transits acoustically recorded at site PI during the periods analyzed. Design characteristics, operational information, and acoustic measurements of ships detected at site PI are summarized in Table 4.3.

The five most common ship types (i.e. bulk carrier, general cargo, passenger, fuel and chemical tanker, icebreaker) each had different six-hour long-term spectral averages producing distinctive spectral characteristics of underwater noise (Figs 4.19-32). These ship types represented 87% of transits past site PI (n=231) and 92% of transits past site MI (n=221). Icebreakers (Figs 27-32), fuel and chemical tankers (Figs 24-26), and general cargo ships (Figs 21-23) produced the highest received levels in all frequency bands. For all ship types, the farthest propagating noise occurs in frequencies at or below 200 Hz, including tonal sounds below 100 Hz caused by cavitation of the ship's propeller. Generally, the noise bandwidth extends into higher frequencies as the ship approaches the CPA during a transit and higher-frequency harmonics of the tonal cavitation noise become apparent. The LTSA typically exhibits a U-shaped pattern of ship noise during most close transits of the CPA (e.g. Fig. 4.19; bulk carrier). This effect is also evident in the alternating peaks and valleys in received level across frequency band in the sound spectrum levels near the CPA (e.g. Fig. 19.d; bulk carrier).

As in other studies of underwater noise from ships (e.g. McKenna et al., 2012; Gassmann

Table 4.3: Design characteristics and acoustic measurements of a representative set of ships during transits past the PI recording location. Received broadband sound pressure levels (in dB re 1 μPa)) at ship closest point of approach (CPA) with ranges to the ship for 110 and 120 dB received levels. Where values for bow and stern aspect differ substantially, both are given (i.e. bow range (km), stern range (km)).

Ship information							Acoustic measurements				
Ship type	MMSI number	Ship name	Ship length (m)	Year built	Gross tonnage (10^3)	Deadweight tonnage (10^3)	Speed at CPA (kts)	Range at CPA (km)	Received level at CPA	Range to 110 dB (km)	Range to 120 dB (km)
Bulk Carriers	356364000	NORDIC ODIN	225	2015	41071	76180	8.7	0.9	121	4,7	0.9
	373437000	NORDIC ORION	225	2011	40142	75603	7.5	2	119	5,7	2
	374322000	NORDIC ODYSSEY	225	2010	40142	75603	8.4	1	127	10	3
	538008053	GOLDEN PEARL	225	2013	41718	74300	8.6	0.3	125	5,7	1
	636015651	NS YAKUTIA	225	2013	40972	74559	8.1	1	115	2,3	-
	636015650	NS ENERGY	225	2012	40972	74518	7	3.1	116	4,6	-
	636092901	KAI OLDENDORFF	229	2019	44029	81243	8	1.9	120	4,7	1.9
	255805765	GISELA OLDENDORFF	229	2013	44218	80839	8.8	1	119	3,7	1
	538004978	AM QUEBEC	230	2013	43987	81792	7	1.1	130	10,20	4,5
General Cargo	316015133	ZELADA DESGAGNES	139	2009	9611	12692	12	1.4	132	20,30	4,7
	316011358	ROSAIRE A. DESGAGNES	138	2007	9611	12776	8.2	0.6	127	10,15	3
	246770000	MOLENGRACHT	143	2012	9524	11744	8.9	0.2	135	13,15	4,7
	316015251	SEDNA DESGAGNES	139	2009	9611	12612	12	0.2	134	10,30	3,5
Fuel and Chemical Tankers	316012308	SARAH DESGAGNES	147	2007	11711	17998	9	2	133	10,35	4,16
	316095000	DARA DESGAGNES	124	1992	6262	10511	8.5	0.3	130	7,20	2,4
	316037373	KITIKMEOT W	150	2010	13097	19983	13	3.1	123	10,25	5
Passenger Ships	311000419	OCEAN ENDEAVOUR	137	1982	12907	1762	11	2	122	8,13	3,4
Pleasure Craft	319030600	ARCADIA	36	8	308						
	304977000	HANSE EXPLORER	48	2006	885	198	11	2.7	119	5,6	3,4
Icebreaker	276805000	BOTNICA	97	1998	6370	2850	8.9	0.3	134	14-28	4-10
	276805000	BOTNICA	97	1998	6370	2850	8	2.7	133	18,30	7,16
	265182000	ODEN	108	1989	9605	4906	8	3.4	118	10	4
CCGS-SAR*	316050000	CCGS AMUNDSEN	98	1979	5910	2865	13	1.9	122	9,10	3
	316050000	CCGS AMUNDSEN	98	1979	5910	2865	10	7	119	15,22	8,12
	316122000	TERRY FOX	88	1983	4233	2113	14	0.7	136	20,25	6

* Canadian Coast Guard Ship - Search and Rescue

et al., 2017), there is more energy radiating from the stern than from the bow aspect of ships. The result of this aspect dependence of source level is a longer period with elevated noise levels following a ship transit than preceding it. This pattern is most pronounced in the fuel and chemical tanker example LTSA (e.g. Table 4.3, Figs. 24-26). Relationship between received SPL_{BB} and range to the ships generally was different between ship types, with longer range propagation of noise evident in the icebreaker and tanker ships than in bulk carriers or general cargo ships (Fig. 4.18).

Bulk carriers

Two typical open water transit scenarios for a bulk carrier (*Nordic Orion*) are exemplified in Figures 4.19-4.21, one at about the median background sound level during the transit (September 5, 2019) and one representing 'quieter' background conditions (August 1, 2019). Received sound pressure spectrum level was highest at frequencies between 30 and200 Hz (Figs 4.20.d, 4.21.d) throughout the transits, with energy to >4 kHz also present at ranges closer to the CPA. Low-frequency noise below 50 Hz from transiting bulk carriers was apparent from distances >30 km in both background sound conditions (Figs 4.20.d.1, 4.21.d.1). SPL_{BB} during the August 1 transit was about 6 dB below the median background sound level (Fig. 4.20.a.1) until the ship was at range 15 km from the receiver. SPL_{BB} increased above the relatively quiet transit background sound from 1.5 h prior to CPA to >3 h after CPA (range >40 km), with levels changing more rapidly within 10 km of the ship. The 250 Hz, 1 kHz, and 3.5 kHz band SPL followed a similar pattern during the ship transit with relative increases in frequency band SPL at CPA of 15-25 dB above pre-transit levels (Fig. 4.20.c.). During the September 5 transit, pre-CPA background sound was close to median levels (Fig. 4.21.a and c). SPL_{BB} began increasing about 1.5 h prior to CPA with relative increases in SPL_{BB} and band SPL of 15-25 dB at CPA. Relative changes in all frequency bands and in the SPSL were similar in both transit scenarios. Distance to receiver at SPL_{BB}>110 dB was also similar in both transits and a pattern of higher received levels at the

stern aspect is visible. SPL_{BB} of 110 dB was reached at range to ship of 4 and 7 km from the bow and stern aspects, respectively (Table 4.3, Figs. 4.20.a., 4.21.a.).

Patterns in received level versus range were examined for a subset of 40 bulk carrier transits during which the nearest time to CPA of another ship transit was >2 h and with maximum CPA distance to the receiver of 4 km. SPL_{BB} was greater than 110 and 120 dB at ranges from the recorder of 2-10 and 1-4 km, respectively (Fig. 4.18.a). A notable exception was the ship *AM Quebec* (MMSI 538004978), for which 110 and 120 dB SPL_{BB} occurred 10-20 km and 4-5 km from the ship, respectively. Typical speeds of transiting bulk carriers resulted in duration of received SPL_{BB} >110 dB at the recording location for periods of 0.5-1 h and 120 dB for about 0.5 h. A separate analysis was conducted of received level with range to ship for bulk carriers entering and exiting eastern Eclipse Sound. Bulk carrier ships entering from the east and in route to Milne Port had mean draft 7.6 m, as reported by the ships via AIS transmission. When exiting, presumable after loading at Milne Port, bulk carriers had mean draft 14.2 m. Received level with range was similar in both load states.

General cargo ships

Two transit scenarios are exemplified for general cargo ships in figures 4.22-4.24, one with median background sound levels pre-CPA (*Zelada Desgagnes*, August 23, 2019; Fig. 4.23) and one with relatively noisy (90^{th} percentile background sound level) pre-CPA conditions (*Sedna Desgagnes*, August 24, 2019; Fig. 4.24). General cargo ship received SPSL was highest at frequencies from 20-200 Hz (Figs 4.23.d, 4.24.d) with long-range propagation of 20-30 Hz noise apparent at ranges >30 km from the receiver. Estimated background SPL_{BB} during the August 23 transit was 103 dB (Fig. 4.23.a.1), but determining initial onset of elevated noise at the receiver was complicated by the transit of Canadian Warship *HCMS Kingston* (MMSI 316139000) past the recorder 2 h prior to CPA (Fig. 4.22.a.1, 4.23.c.1). Continuous increase in SPL_{BB} is evident from 1.5 h pre-CPA and SPL_{BB} returned to pre-transit levels 1.5 h after CPA at range 30 km from

the receiver. Duration of >110 dB SPL_{BB} was 2.5 h, starting and ending at ranges 15 and 25 km from the bow and stern aspects, respectively. Duration of SPL_{BB} >120 dB was 0.5 h starting at range 4 km from the bow aspect and ending at range 7 km from stern.

On August 24, 2019, estimated background sound during the transit of the *Sedna Desgagnes* (MMSI 316015251) was close to 90^{th} percentile background sound levels (Fig. 4.24.a.1). SPL_{BB} was elevated above pre-CPA background levels from 0.5 h before to 1.5 h after ship CPA. Duration of >110 dB SPL_{BB} was 2 h, starting and ending at ranges 10 and 25 km from the bow and stern aspects, respectively. Duration of SPL_{BB} >120 dB was 0.4 h starting at range 3 km from the bow aspect and ending at range 5 km from stern. Relative changes in band SPL and in SPSL were smaller and the difference in bow and stern received levels was less visible than in the lower background sound scenario in figure 4.23.

Patterns in received level versus range were examined for a subset of 11 general cargo ship transits during which the nearest time to CPA of another ship transit was >1 h and with maximum CPA distance to the receiver of 2 km. SPL_{BB} was more variable between individual ships and transits with this ship type due to background sound conditions and the presence of other ships within the 6 h ship transit windows. Greater than 110 and 120 dB SPL_{BB} occurred at ranges from the recorder of 2-30 and 1-15 km, respectively (Fig. 4.18.b).

Fuel and Chemical Tankers

Two similar transits of the fuel and chemical tanker, *Sarah Desgagnes* (MMSI 316012308), were selected to exemplify the ship type (Figs 4.25-4.27). This ship made about half of total tanker transits past site PI during the analysis periods. Acoustic characteristics of the ship had higher SPL and SPSL approaching the CPA and longer range and duration of elevated noise levels compared to other cargo ship types. Received SPSL was highest at 30-200 Hz with peak energy at 70-90 Hz (Figs 4.26.d. and 4.27.d.). Low-frequency noise propagation >100 Hz is less apparent at ranges >30 km in transits of this ship type than in bulk carriers. In both representative transits,

background sound levels were within 5 dB of the median SPL_{BB} excluding ship transits. SPL_{BB} increased above estimated pre-CPA background sound from 2 h prior to CPA (range 20-30 km) to >3 h after CPA (range >40 km). The 250 Hz, 1 kHz, and 3.5 kHz band SPL (Fig. 4.26.c,4.27.c) followed a similar pattern during the ship transits with relative increases in SPL at CPA of about 30 dB above pre-transit levels for all bands.

Patterns in received level versus range were examined for a subset of 6 tanker ship transits during which the nearest time to CPA of another ship transit was >4 h and with maximum CPA distance to the receiver of 2 km. Sound levels greater than 110 and 120 dB SPL_{BB} occurred at ranges from the recorder of 7 to >40 km and 2-20 km, respectively (Fig. 4.18.d). At speeds of about 9 knots the duration of SPL_{BB} exceeding 110 dB was from 2.5 to >4 h, persisting at levels of >120 dB for 1.5-2 h.

Icebreaker-Offshore Support Ship

One icebreaker-offshore support ship, *Botnica* (MMSI 276805000), operated in Eclipse Sound and Milne Inlet to assist commercial shipping operations September 29 to October 22, 2018 and July 17 to August 10, 2019, making a total of 19 transits past PI and 39 transits past the MI site (Table 4.1). On most transits, *Botnica* was escorting one or two bulk carriers in convoy. At the end of 2018 and start of 2019 shipping, the icebreaker convoys also included up to two additional ocean tugs. Two representative transits are presented for October (Figs. 4.28-4.30) and two for July to exemplify icebreaker operations in freeze-up and break-up periods with different background sound scenarios (Figs. 4.31-4.33). Generally, icebreaker transit SPSL were distinguished from other ship transits by the presence of strong tonal noise with harmonic bands of fundamental frequency 200 Hz, which extended above 4 kHz as the ship approached the CPA. During typical ambient sound conditions, the 200 and 400 Hz tonal bands were elevated above background levels at distances exceeding 40 km from the receiver from both the bow and stern aspects. When background sound levels were at or below the median, tonal bands up to 1

kHz were apparent throughout the 6 h transit window and to ranges >40 km (e.g. Fig. 4.31). These characteristic bands of noise radiated from the ship were present with and without sea ice in the vicinity, both when the ship was traveling alone and escorting other ships.

A representative multi-ship icebreaker transit was selected during which the 97 m icebreaker *Botnica* escorted bulk carriers *Nordic Oasis* and *Nordic Odin* and tugs *Ocean Taiga* and *Ocean Tundra* at a speed of 8 knots into Eclipse Sound in 2/10 ice cover (Figs 4.31.a and 4.32). The background SPL_{BB} during the transit was estimated as 95 dB re 1 μPa, which was approximately the median SPL_{BB} during July ship-excluded periods. At the CPA, range to the ship was 2.7 km from the recording site and the SPL_{BB} was 130 dB re 1 μPa. In the long-term spectral average (Figure 4.31.a), 200 Hz tonal noise from the ship and harmonics are apparent during the entire 6 h window about the ship CPA. This 200 Hz tonal noise and harmonics at 400, 600, and 800 Hz are also apparent in the background spectrum as well as much higher spectrum levels at the CPA (Fig. 4.32.d.1). During the transit, the SPL_{BB} increased to 110 dB by 1 h pre-CPA and 120 dB at 30 min before the CPA. Durations of received levels greater than 110 and 120 dB were approximately 2.75 and 1.25 hrs. Range to the 110 and 120 dB received levels were 18 and 8 km, respectively as the ships approached (Fig. 4.32.a). After passing, received levels fell below 110 and 120 dB at ranges of 15 and 30 km.

4.5 Discussion

4.5.1 Sound levels in the absence of local ships

This study compared the overall underwater soundscape at two Eclipse Sound locations to monthly estimates of the soundscape with transient ship noise events excluded. At both locations when excluding ship transits, underwater ambient sound levels are variable seasonally and over shorter timescales of days and hours. Much of the variability over timescales of hours to months is likely due to the combined effects of sea ice cover and sea surface wind patterns on sources

and propagation of sound. Excluding ship transits, sound levels are generally higher during open water periods than when sea ice is present, consistent with other studies of Arctic ambient underwater sound levels (Halliday et al., 2020; Roth et al., 2012). The lower received sound levels during ice cover are likely due to the scattering effects of sea ice on propagating sound and the fact that sea ice acts sea surface wave noise.

At site PI, the quietest month of the year was July, a time with relatively low winds (mean 4.7 +/-2.8 m/s). Wind interaction with the sea surface generates noise from 200 Hz to >4 kHz, shows a positive correlation with wind velocity (Wenz, 1962). Although July and August mean wind speeds were within 0.5 m/s of each other, the variability in wind speed increased in August relative to July (Fig. 4.17.b). In August, the sporadic wind-generated noise events become apparent in the $90^{th}$and 99^{th} percentiles of periods excluding ship transits past the recorder (Fig. 4.14). In September and October wind-generated noise becomes a more prevalent feature of the soundscape, raising the median SPSL by 5-10 dB at frequencies above 300 Hz. Median and 90^{th} percentile SPL_{BB} in October increase to 5 and 9 dB, respectively, above July levels.

As October sea ice formation progresses at both sites, SPL_{BB} decreases as expected with increasing ice cover (e.g. Roth et al., 2012; Halliday et al., 2020). Although impulsive natural sound events continue through October at PI, probably in conjunction with sea ice formation and the return of pack ice from N. Baffin Bay, variability in underwater sound levels excluding ship transits decreases as the ice layer forms. Median SPSL at 1 kHz was within 2-4 dB between the sites during July and August, but the two locations strongly differed during October. October SPSL at PI was about 12 dB higher than MI at frequencies >1 kHz, possibly due to the formation of landfast ice within Milne Inlet at that time. Sea ice formation occurred around the same time at both sites, but ice at PI was likely unconsolidated pack ice and subject to dynamics that can generate substantial underwater noise (Kinda et al., 2015; Mahanty et al., 2020). The relatively stable sea ice connected to shore at MI would presumably generate lower levels of sound in comparison to pack ice dynamics.

Except for the August median 1 kHz band level, monthly band percentile and SPSL levels were lower at MI than PI for all periods when ship transits were excluded. Local acoustic propagation and environmental characteristics may explain a significant portion of these differences. The relatively complex bathymetry of MI may act to shelter the site from long-range propagation of sound. In the frequencies below 200 Hz, median SPSL at MI were substantially lower in all months when ships were >30 km from the recording site. For example, at 50 Hz monthly median SPSL was 56-58 dB at MI and 72-76 dB at PI. This difference coincides with frequencies of long-range shipping noise found throughout much of the world ocean and attributed to distant shipping (Hildebrand, 2009). A study in a bathymetrically complex coastal region off California yielded similar results compared to a deeper location nearby that was open to long-range sound propagation (McDonald et al., 2008; McDonald et al. 2006). In the California study, sound levels received at frequencies below 200 kHz were lower than expected, which was attributed to the quieter location being sheltered from long-range propagation of shipping noise. Results of this study suggest a similar sheltering from long-range ship noise at site MI.

4.5.2 Sound levels including ships

A comparison of sound levels during the periods excluding ships with those of periods including ship transits clearly shows the addition of sounds from the ship transits in the upper percentiles of sound pressure spectrum levels and SPL_{BB}. July through August 90^{th} and 99^{th} percentile spectrum levels are up to 10 and 20 dB higher, respectively, in the 20-200 Hz band with ship transit periods included. This is the frequency band in which most underwater acoustic energy from ships occurs (Ross, 1976; McKenna et al., 2012a; Gassman et al., 2017). With each ship transit during July and August, SPL_{BB} reaches levels 10-20 dB higher than the 90^{th} percentile of level excluding ships and up to 40 dB higher than median. These levels are substantially higher than those occurring in the natural acoustic environment and the combined effect of multiple daily ship transits past the recorder is evident in the soundscape. During September and October,

the difference between the natural sound levels excluding ship transits and those including them become less pronounced. For example, the 90^{th} percentile SPL_{BB} excluding and including ship transits during October were 111 and 109 dB.

The highest sound levels from ship transits occurred during October and July, which could be due to the presence of greater numbers of noisier icebreaker, tanker, and general cargo ships. Some contribution may also result from changes in the sound propagation environment. During the times when the noisiest ships are present, the physical properties of the water column may also increase propagation of the ship noise. In July and October, the sea surface temperature is colder and water column more mixed, which increases propagation of radiated sound from ships (Jensen et al., 1993). In summer, the opposite effect may occur as warming of the surface layer creates a sound speed profile that decreases radiated noise (Jensen et al., 1993).

4.5.3 Acoustic characteristics of ship transits

Each of the most common ship types exhibits a different characteristic pattern of underwater noise. The characteristic signals of different ship types also appear in the in the monthly sound pressure spectrum levels. In July and October, the characteristic intense tonal sounds from the icebreaker,*Botnica*, appear in the median to 99^{th} percentile ship-inclusive spectra and some of the 200 Hz tonal sound appears in the sound pressure spectrum levels for the periods excluding ships when ships are >40 km from the recorder. It is apparent that the icebreaker becomes a substantial feature of the acoustic environment when operating in the Eclipse Sound region.

In August and September the sound pressure spectrum levels including ship transits have peaks at 15 and 20 Hz. These peaks are characteristic of cavitation sound associated with rotation of the propeller in the bulk carriers and other cargo ships (Ross, 1976). Cavitation sounds are also apparent in the sound levels during periods excluding ships, suggesting that long-range propagation of ship noise is occurring and potentially adding to ambient sound levels regionally as in other ocean basins with extensive shipping traffic (Hildebrand, 2009).

Other operational characteristics may play a significant role in noise emitted by ships transiting Eclipse Sound. Ore carriers enter the region unloaded with draft c. 7 m and exit loaded with draft c. 14 m after taking on iron ore at the Milne Port. The higher received sound levels of exiting ships than for bulk carriers entering the region is consistent with expectation that the deeper propeller increases dipole source levels. When ships have a shallower draft they are predicted to have lower strength of the dipole source and less underwater radiated noise as a result (Ross, 1976; Wilmut et al., 2007).

Some individual ships had noteworthy signatures. The intense tonal sounds from the icebreaker, *Botnica*, were likely a result of machinery on board the ship and not the cavitation of the propeller. These tones are present and constant in frequency throughout each transit and the pattern of received level from the bow and stern aspects is symmetrical, suggesting that the source is not the propeller that would exhibit the bow/stern asymmetry observed in other studies of ship noise (Gassmann et al., 2017). The intense tones from the icebreaker also add more than other ship types to the $1/3^{rd}$ octave bands chosen to represent some social communication signals used by ringed seal and narwhal. The potential for that ship to have impacts on biologically relevant frequency bands is higher than other ships because of these acoustic characteristics that may result from design or operational parameters. Acoustic characteristics of this ship could be further investigated for potential mitigation or noise abatement measures. Another intense source of man-made sound was the fuel and chemical tanker, *Sarah Desgagnes*, which had higher SPL_{BB} and sound pressure spectrum levels than other ships with similar operational speeds and routes. This ship may also be a good candidate for mitigation measures to address some of the excess sound generating characteristics.

4.5.4 Ship sounds overlap with marine mammal communication frequencies

Acoustic measurements of ship transits demonstrate that underwater sounds from the ships overlap with each of the biologically relevant frequency bands selected to represent ringed seal (250 Hz) and narwhal communication (1 kHz and 3.5 kHz). In most background sound conditions that occurs during ship transits, SPL in the 250 Hz, 1 kHz and 3.5 kHz is elevated above background levels for periods of hours with each ship transit. Levels in this frequency band were elevated for durations of 1-h to >6 h, raising the possibility for communication masking in this species occurring across substantial portions of the day when multiple ships are transiting the region. Bowhead whales are also seasonally present in the study area (Heide-Jørgensen et al., 2006; Chambault et al., 2018) and produce sounds for communication at frequencies below 300 Hz (Clark & Johnson, 1984; Blackwell et al., 2007) where most energy from ship noise occurs. The species should also be considered when evaluating potential communication masking from sounds of ships transiting in the Eclipse Sound and N. Baffin Bay region.

The 1 kHz and 3.5 kHz frequency bands also had elevated levels of sound generated by passing ships, although the duration of measurable noise increases was generally shorter for these bands than at 250 Hz. Tanker and icebreaker ships had higher levels in the 1 kHz and 3.5 kHz bands that extended to longer distances from the ship than for the more common bulk carriers. In the example icebreaker transits (Figs. 4.28-4.33), periods during which these levels were elevated above the pre-transit background range from 1 to 5 h. The maximum duration of elevated 1 or 3.5 kHz levels for the example bulk carrier or general cargo transits was 2 h.

4.6 Conclusions

The natural soundscape of the Eclipse Sound region of North Baffin Island is geographically variable, likely due to differences in bathymetry and sea ice characteristics between the

more interior protected inlets and the waters exposed to the expansive Baffin Bay. Shipping traffic introduces substantial noise to the underwater soundscape in both locations examined in this study. Regional shipping may have a larger effect on the soundscape below 300 Hz in areas more exposed to long-range sound propagation than in bathymetrically complex areas that may be more sheltered acoustically. Individual ship transits through the region introduce transient noise at frequencies from 20 Hz to 4 kHz for periods lasting minutes to several hours. Underwater sound levels from ship transits of the most common ship types are sufficient to cause behavioral disturbance to narwhals along the shipping routes. Disturbance and avoidance behavior by narwhals caused by ship traffic has been observed in previous behavioral response studies in the study region (Golder, 2018; Golder, 2019; Golder, 2020). Underwater sounds from ship transits may also be sufficiently intense to cause masking of communication signals in narwhals, ringed seals, and bowhead whales, especially in the quieter areas like the MI site where levels of natural sounds are low relative to other regions of the ocean. The cumulative impacts to Eclipse Sound marine mammals resulting from repeated daily exposure to noise from transiting ships are unknown but should be further considered given the rapid pace of increasing shipping traffic in the region.

An additional analysis of 2015-2019 Eclipse Sound AIS data was performed for the purpose of historical comparison (Appendix I). Shipping levels during 2019 were 384% and 583% higher at sites PI and MI, respectively, than during 2015. Of the additional ship transits occurring in 2019, 84% passing PI and 99% of additional ships passing MI were transiting to and from the Mary River Mine. Increased iron ore production proposed by the BIMC and under environmental impact review in 2018-20 would double bulk carrier transits through Eclipse Sound by 2022 (BIMC, 2020). Proposed shipping in Eclipse Sound may also include larger Capesize ore carriers with 150,000-250,000 deadweight ton (DWT) capacity, substantially larger ships than the Panamax ships (65,000-85,000 DWT) servicing the mine during 2015-2019. The expectation is that the larger ships with deeper prop depth will have higher radiated sound levels, potentially

with a larger impact on the soundscape than has resulted from commercial ships measured to date. Broadband source level estimates of Capesize ore carrier may be 5-10 dB higher than smaller bulk carriers (Golder, 2018). Additional measurements may be required to determine acoustic characteristics of Capesize ore carriers and impacts of ship speed on radiated noise.

Future studies could analyze previous years of recordings at this and other regional recording sites to compare measurements of the 2018-19 natural underwater soundscape during prior years with substantially lower shipping intensity. This will help to make a more robust estimate of natural soundscape, excluding noise from ships, and facilitate comparison with future measurements. With the results presented here, it may also be possible to predict the relative increase above the baseline natural soundscape that will be caused by higher levels of shipping predicted to occur locally in Eclipse Sound and across the Canadian Arctic.

4.7 Acknowledgements

We thank the Mittimatalik Hunters & Trappers Organization, Pond Inlet, Nunavut, Canada, for annual permission to carry out fieldwork and acoustic recording. Acoustic data collection and fieldwork could not have been completed without expert knowledge and technical, logistical, and ship support provided by Alex Ootoowak. We also thank Sheattie Tagak and Tagak Outfitters for additional ship support. Kristin Westdal and Amanda Joynt of Oceans North were also instrumental in initiating and sustaining this research program. Thanks to Evan Richardson and Environment and Climate Change Canada, for substantial logistical support at the Pond Inlet Research Facility. This project is funded through a private foundation grant to the Marine Physical Laboratory at the Scripps Institution of Oceanography and by Oceans North, with additional support provided by Environment and Climate Change Canada through a grant from the World Wildlife Fund - Canada. We thank members of the Scripps Whale Acoustics Laboratory, including B. J. Thayre, J. Hurwitz, E. O'Neill-Mertz, and S. Wager for assistance with HARP operations

and data processing. Special thanks to Dr. Julie D. Lee, Andrew Mack, Marianne Marcoux, Jeff Hidgon, and Bruce Stewart, who provided helpful comments on this dissertation chapter.

Chapter 4 is currently being prepared for submission for publication of the material. Jones, J. M.; Hildebrand, J. A.; and Wiggins, S. M. The dissertation author was the primary investigator and author of this material.

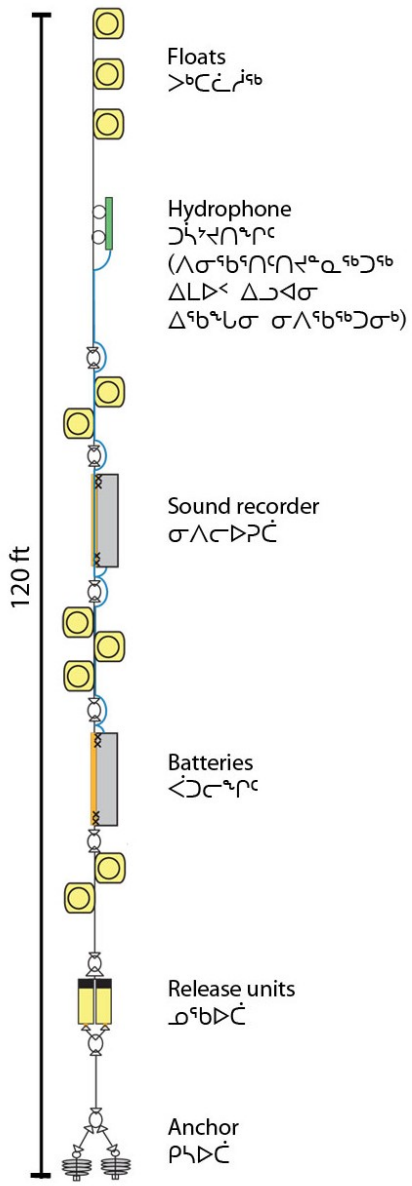

Figure 4.2: High-frequency Acoustic Recording Package (HARP) records underwater sound continuously or on a recording schedule year-round at a sampling rate of 200 kHz. Instrument component labels translated to Inuktitut.

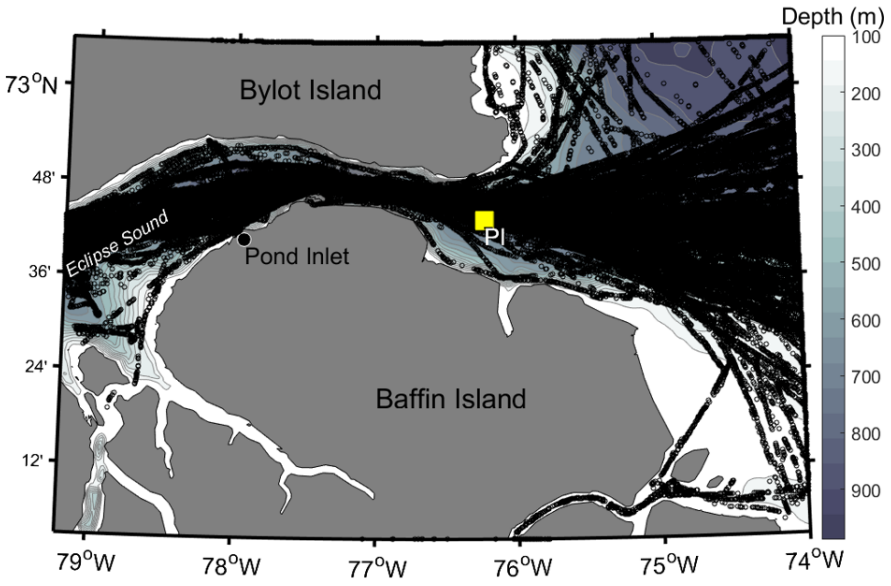

Figure 4.3: All Automated Information System (AIS) locations received by satellite from ships transiting past the Pond Inlet recording location (site PI) with closest point of approach (CPA) <15 km between September 28, 2018 and September 21, 2019. Each black circle represents one AIS message received, which included ship identity, position, and operational information (e.g. heading, speed, draft).

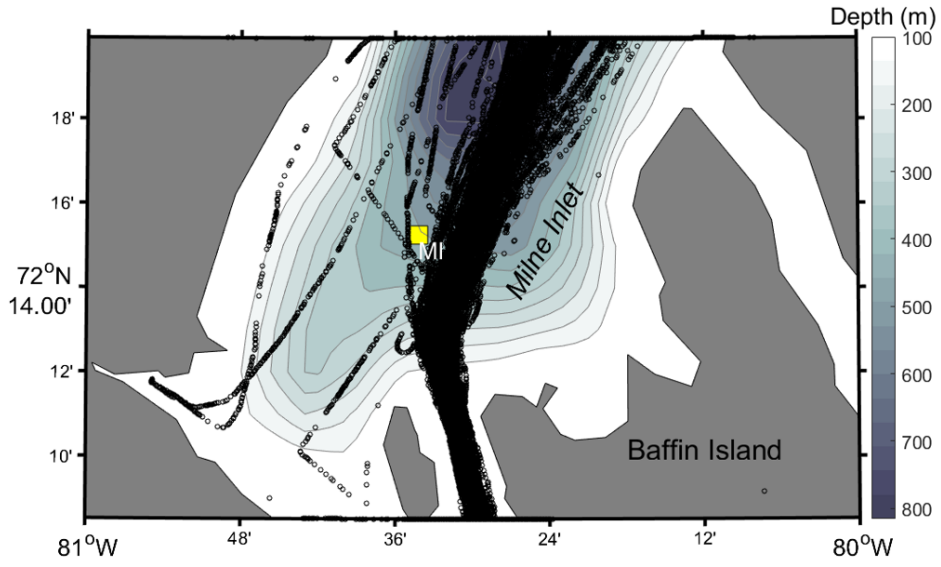

Figure 4.4: All Automated Information System (AIS) locations of ships transiting past the Milne Inlet recording location (MI) with CPA distance <15 km between September 28, 2018 and September 21, 2019. Each black circle represents one AIS message received, which included ship identity, position, and operational information (e.g. heading, speed, draft).

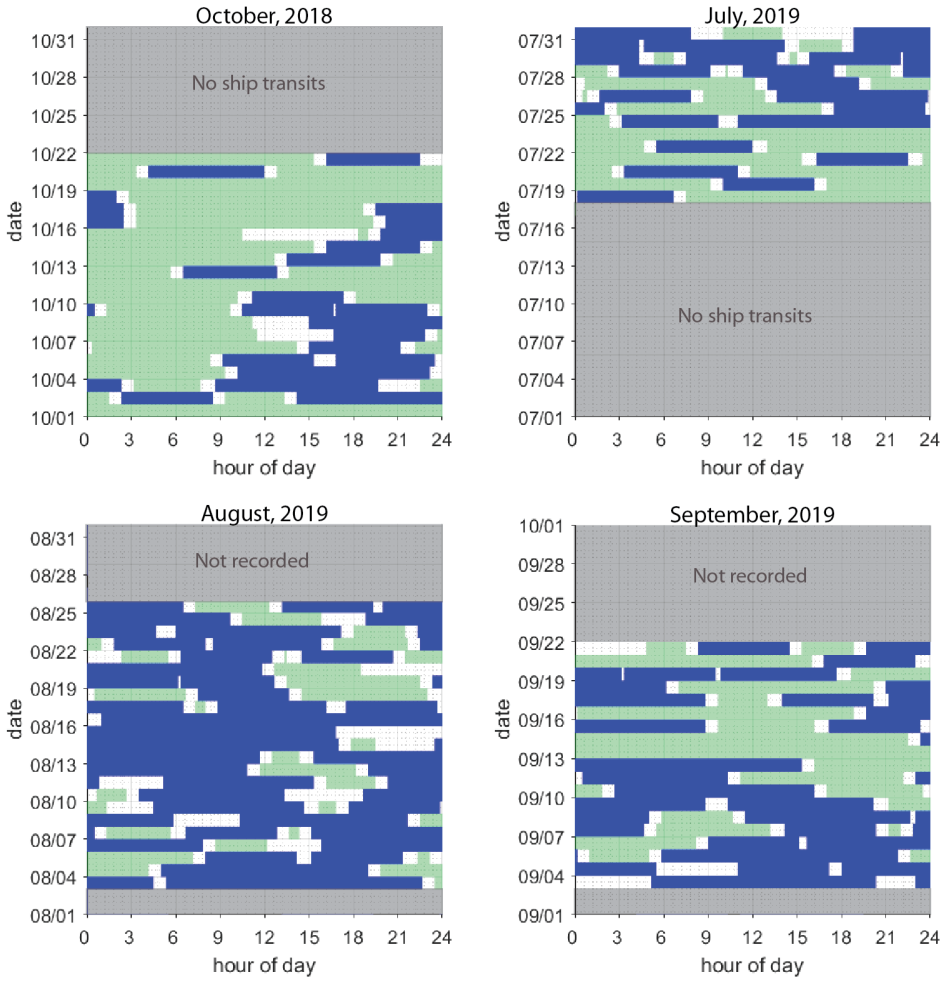

Figure 4.5: Monthly analysis effort for periods excluding and including ship transits at site PI from October, 2018 through Sept, 2019. Blue bars include all 6 h ship transit windows. White bars indicate periods excluding local ships. Gray areas indicate periods either outside of the shipping season (Oct 22-31, 2018 and July 1-17, 2019) or times not recorded. All recording times outside gray areas (blue and white bars) were included in analysis of total monthly sound levels, including ships.

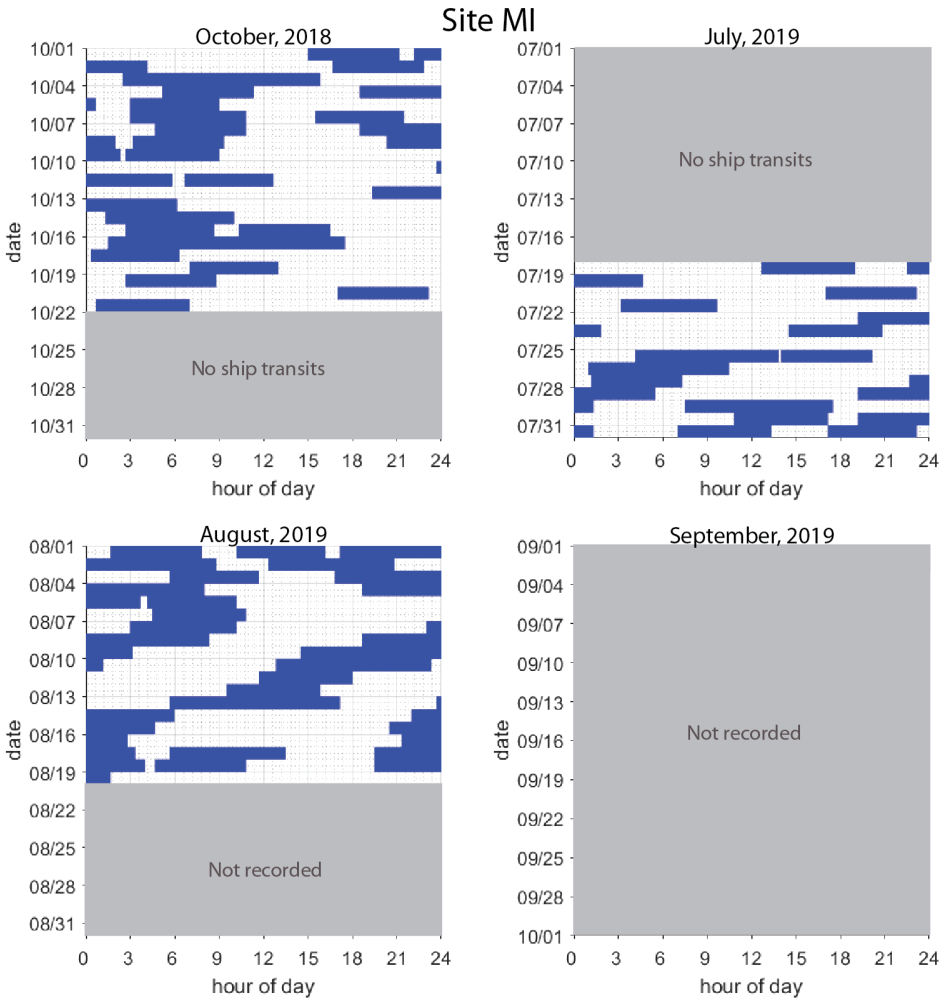

Figure 4.6: Monthly analysis effort for periods excluding and including ship transits at site PI from October, 2018 through Sept, 2019. Blue bars include all 6 h ship transit windows. White bars indicate periods excluding local ships. Gray areas indicate periods either outside of the shipping season (Oct 22-31, 2018 and July 1-17, 2019) or times not recorded. All recording times outside gray areas (blue and white bars) were included in analysis of total monthly sound levels, including ships.

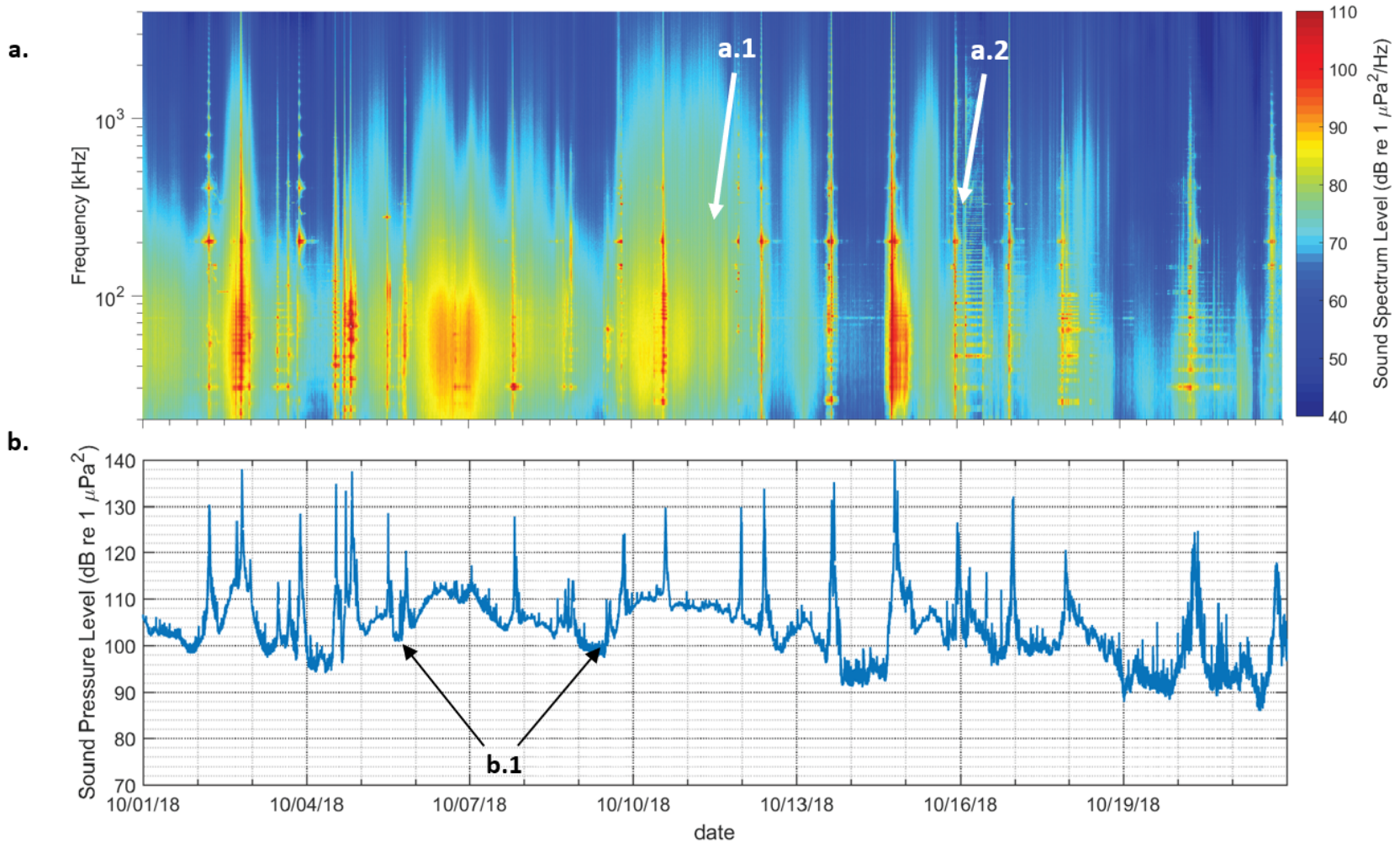

Figure 4.7: Long-term spectral average (LTSA; a) and 1-min average 20-4000 Hz broadband sound pressure level (SPL_{BB}; b) for all recorded periods at the Pond Inlet recording site (PI) from October 1 to the date of last ship transit October 22, 2018. Elevated sound levels from natural sources, likely wind-generated noise, can be seen October 6-7 and October 9-12 (b.1). Example icebreaker transits on October 12 (a.1) and October 16 (a.2).

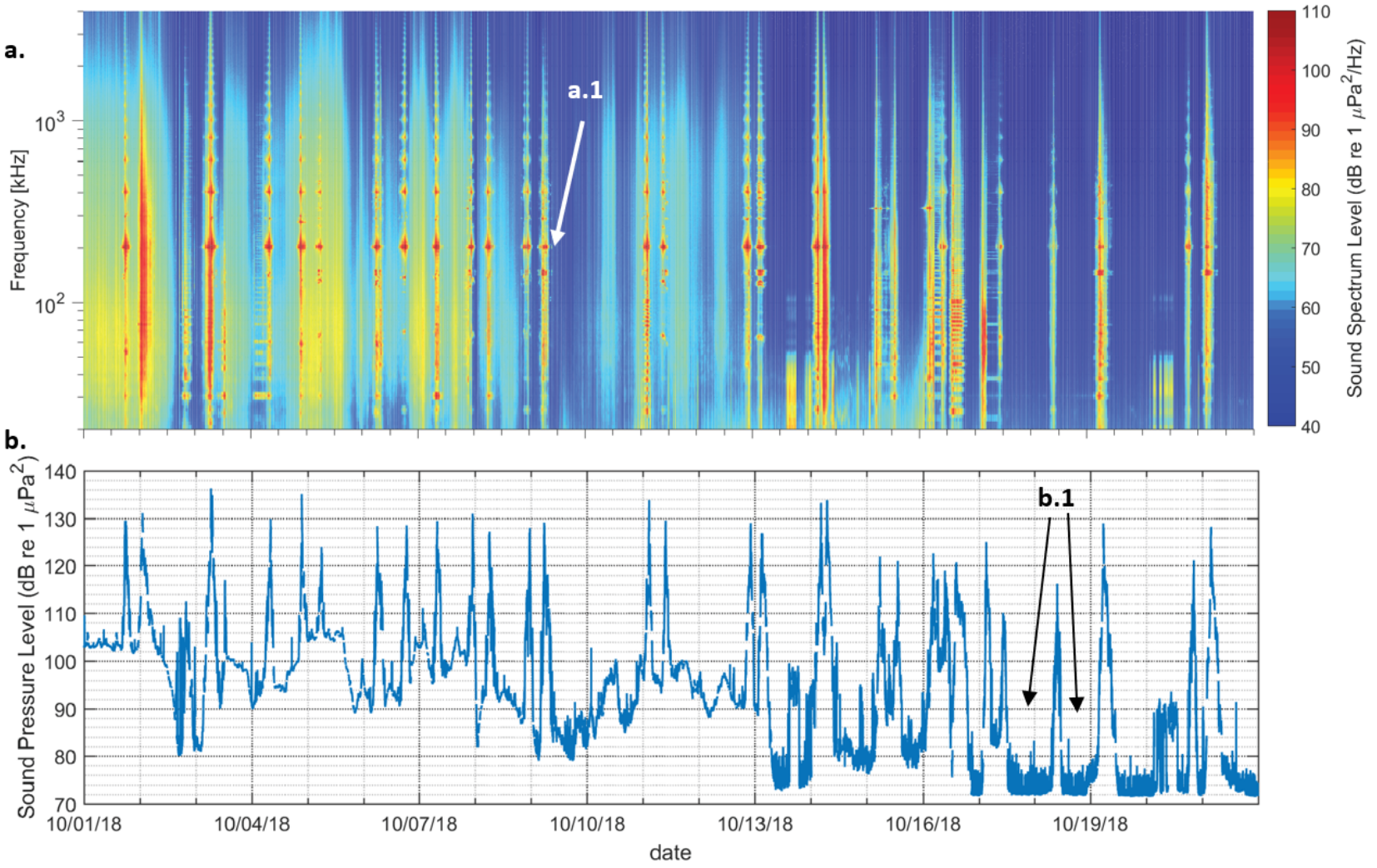

Figure 4.8: Long-term spectral average (LTSA; a) and 1-min average SPL_{BB} (b) for all recorded periods at the Milne Inlet recording site (MI) from October 1 to the date of last ship transit October 22, 2018. Periods of low natural sound levels (b.1) apparent in LTSA and SPL_{BB} after October 13 coincide with sea ice formation. Icebreaker transits identifiable by tonal energy at fundamental frequency 200 Hz (a.1).

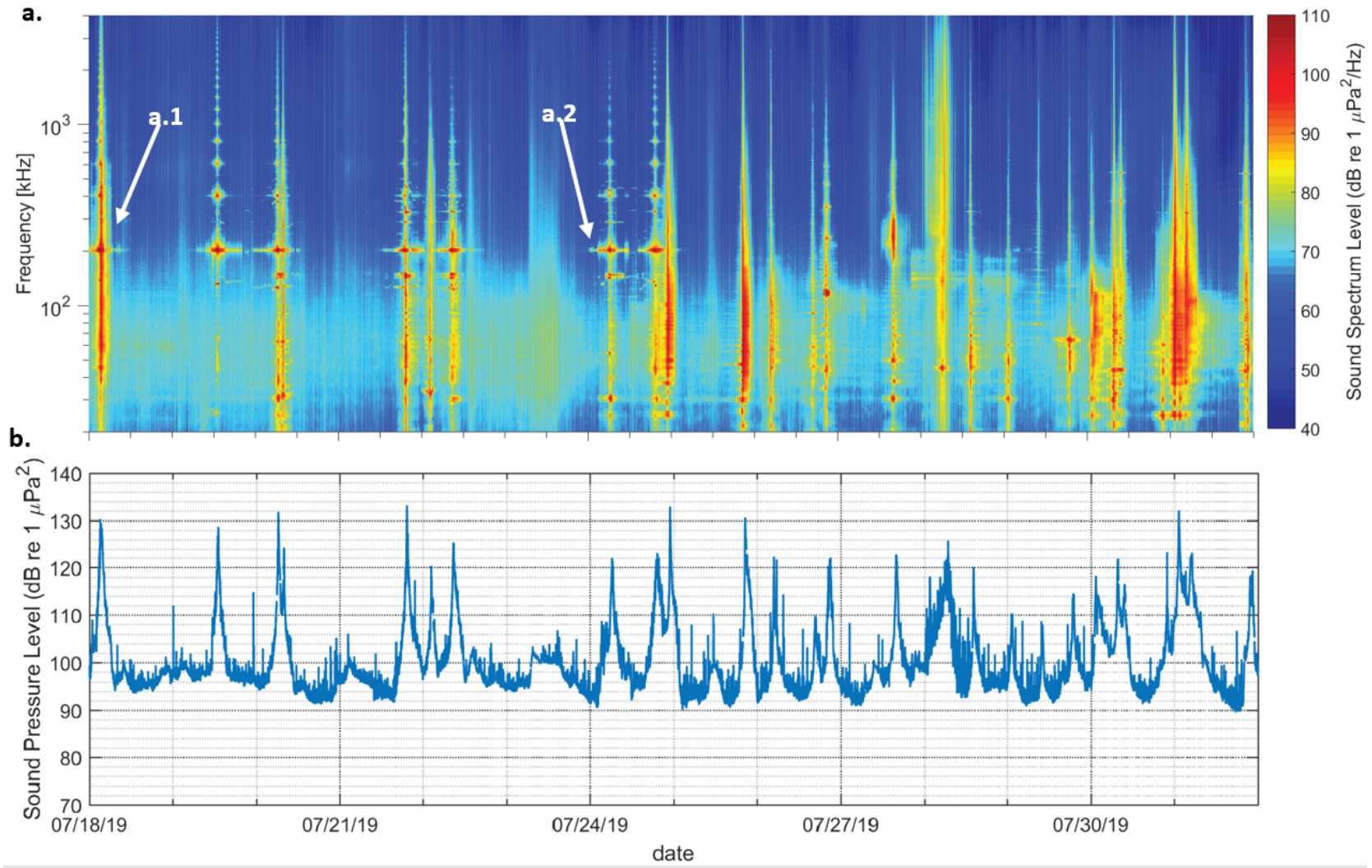

Figure 4.9: LTSA (a) and 1-min average SPL_{BB} (b) for all recorded periods at the Pond Inlet recording site (PI) from July 18, the first ship transit of 2019, to the end of July. Representative transits of the icebreaker,*Botnica*, on July 18 (a.1) and July 24 (a.2).

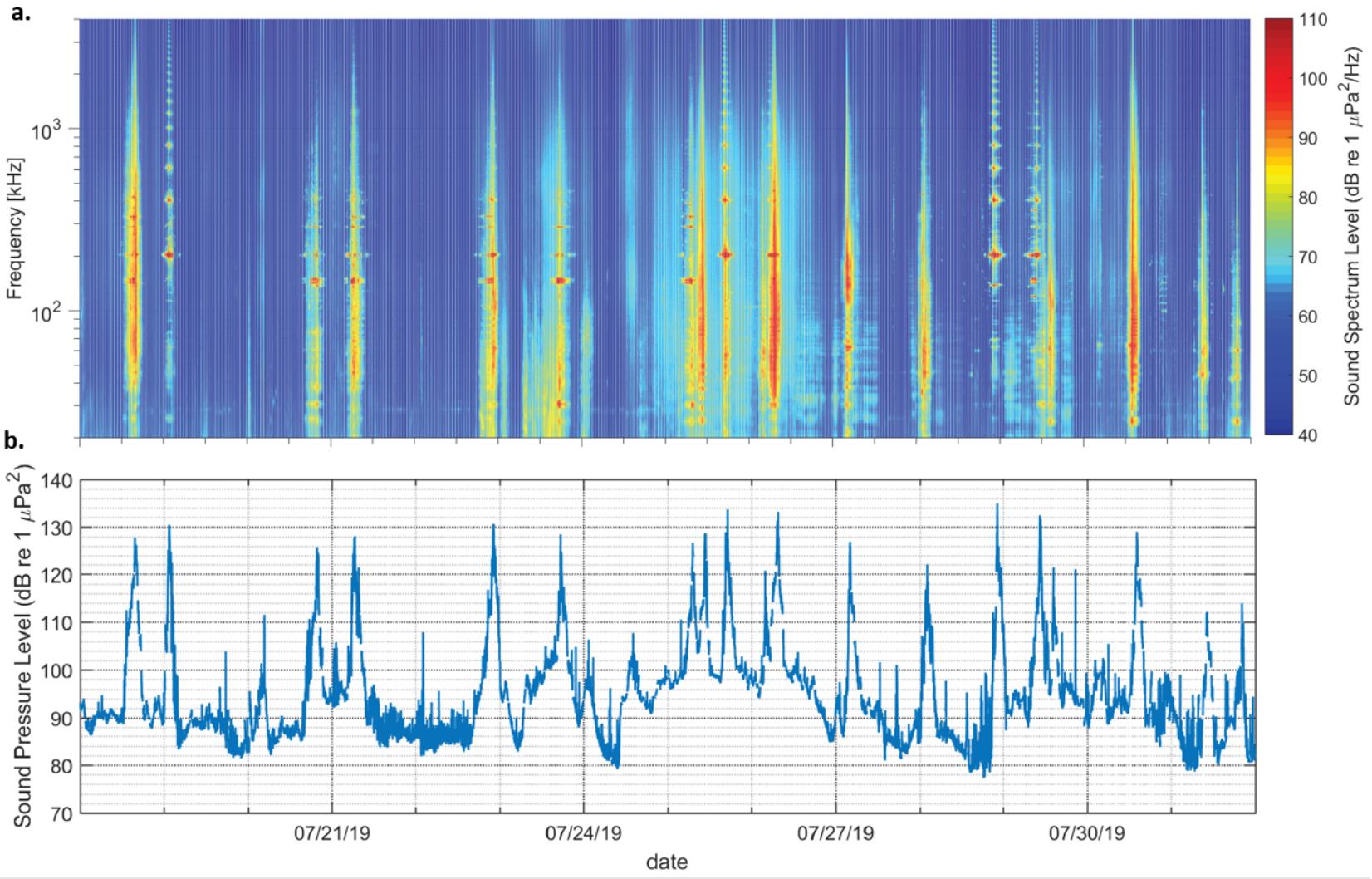

Figure 4.10: LTSA (a) and 1-min average SPL_{BB} (b) for all recorded periods at the Milne Inlet recording site (PI) from July 18, the first ship transit of 2019, to the end of July.

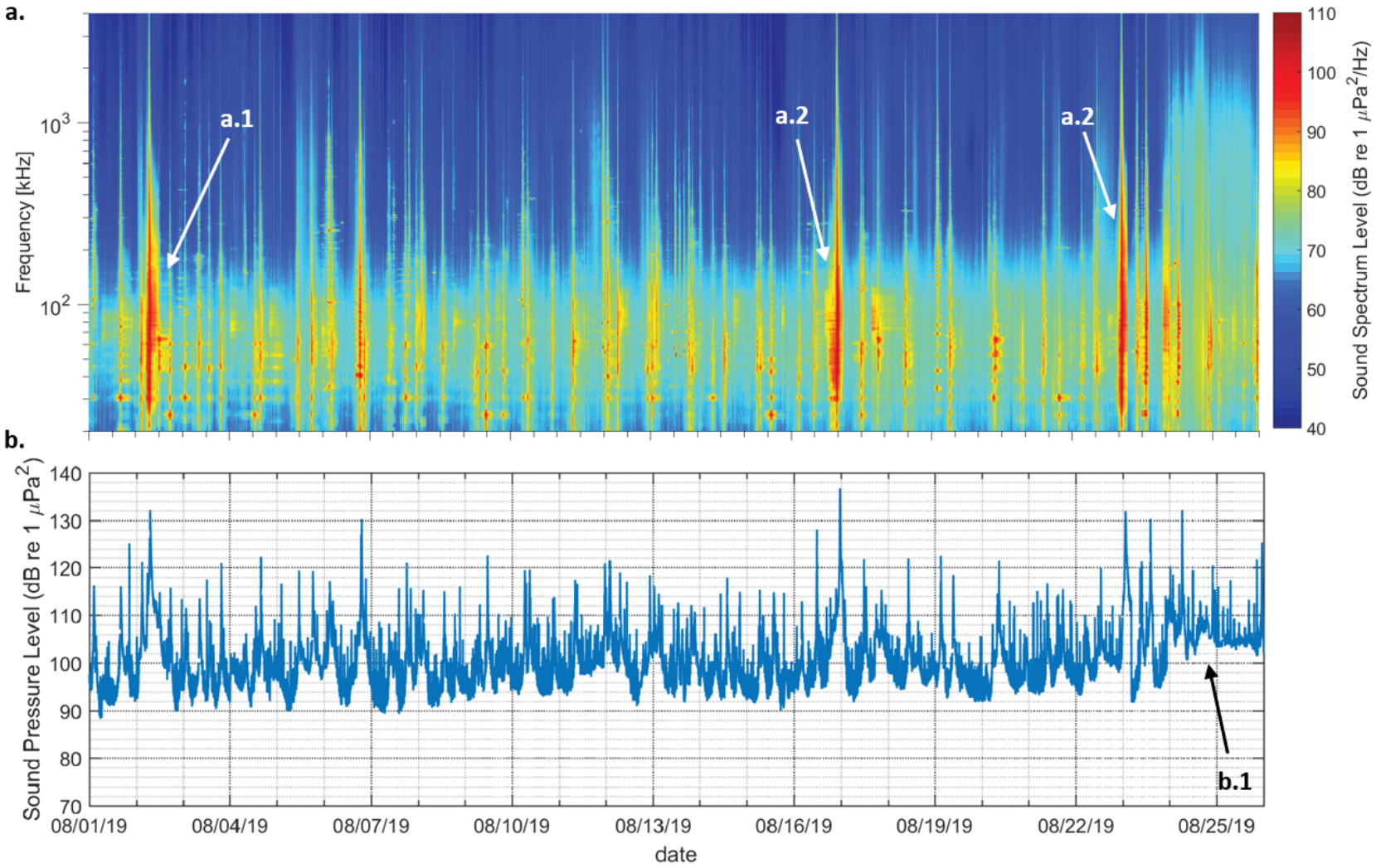

Figure 4.11: LTSA (a) and 1-min average SPL_{BB} (b) for all recorded periods at site PI from August 1 to August 26, 2019 during open water conditions. Example period of elevated sound levels from natural sources, likely wind-generated noise, can be seen August. 24-25 (b.1). Transits of the fuel and chemical tanker,*Sarah Desgagnes* are also indicated (a.1-3).

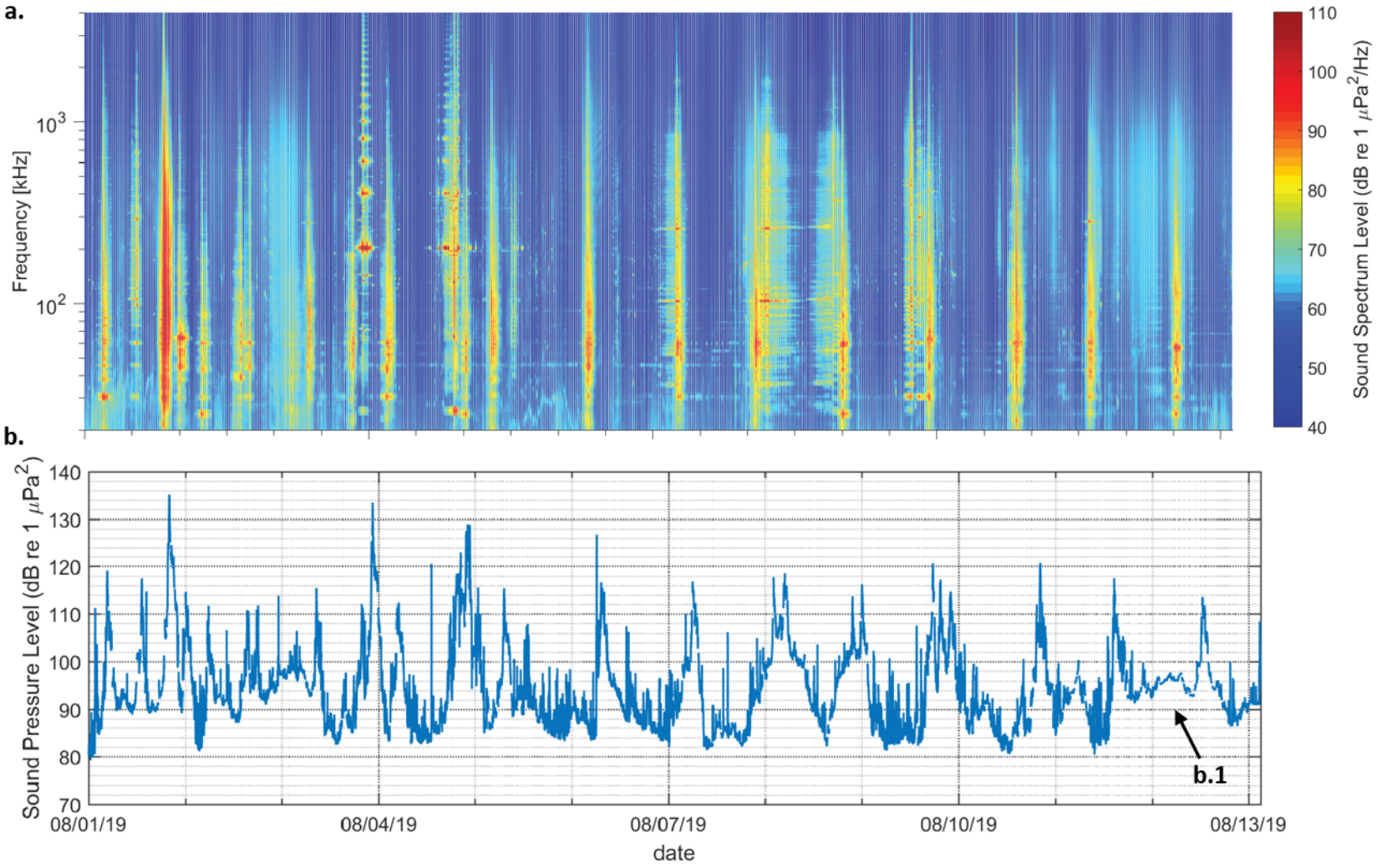

Figure 4.12: LTSA (a) and 1-min average SPL_{BB} (b) for all recorded periods at site MI in August, 2019. Example period of elevated sound levels from natural sources, likely wind-generated noise, can be seen August. 12 (b.1).

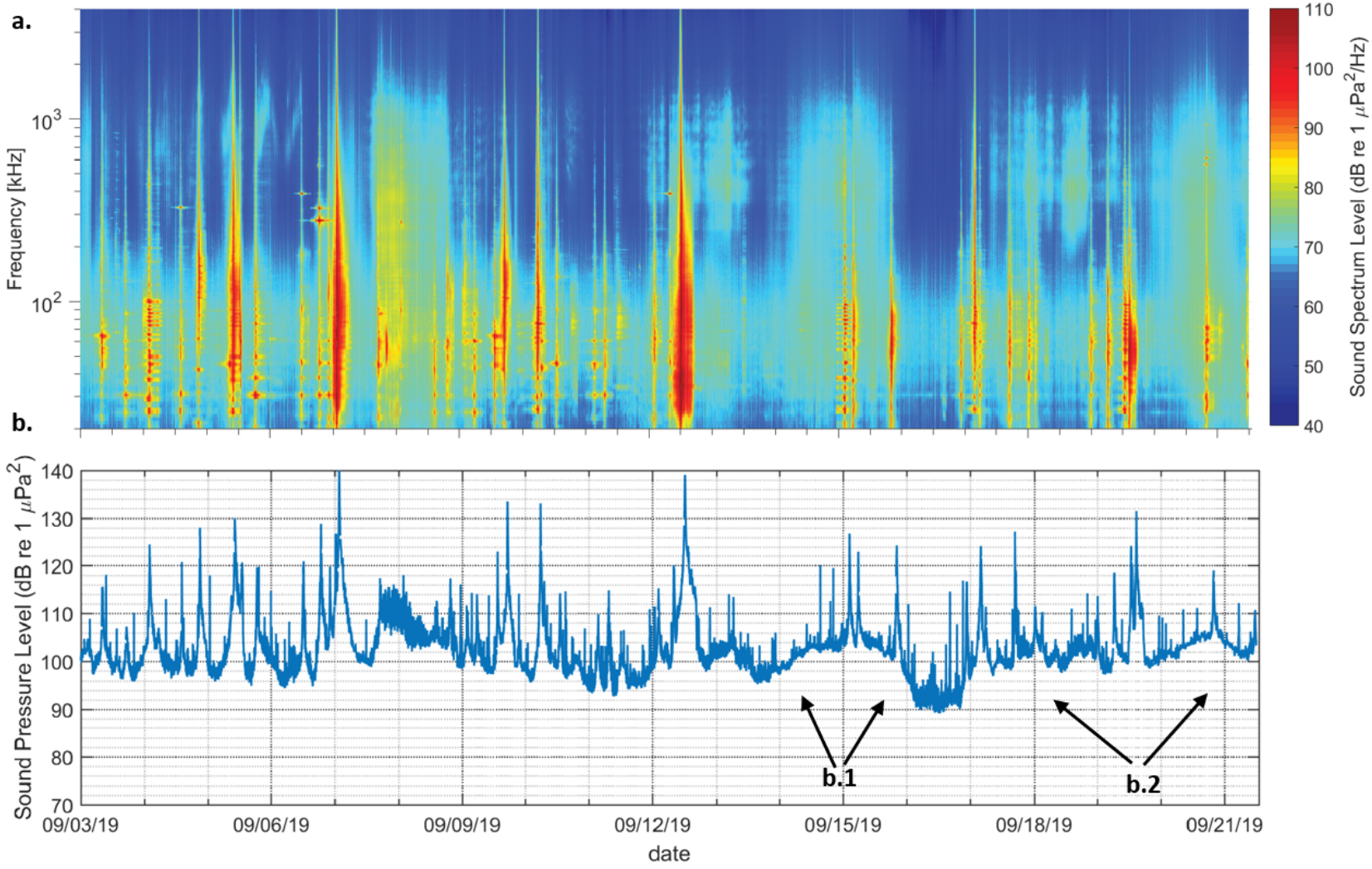

Figure 4.13: LTSA (a) and 1-min average SPL_{BB} (b) for all recorded periods at site PI in September, 2019. Example periods of elevated sound levels from natural sources, likely wind-generated noise, can be seen September. 14-15 (b.1) and September 18-21 (b.2).

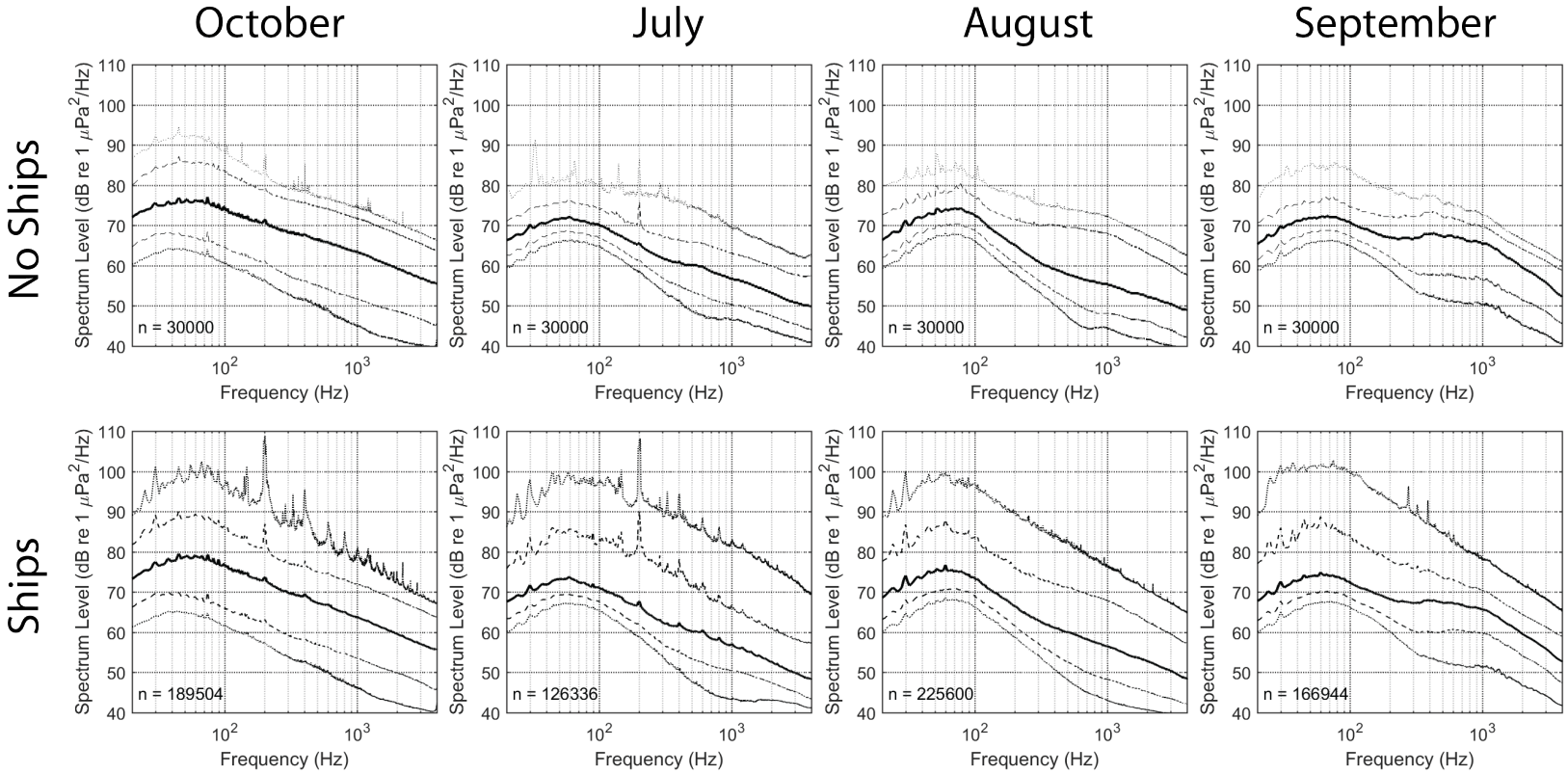

Figure 4.14: Sound pressure spectrum levels at site PI during July, August, and September, 2019 and for October, 2018. Levels are represented by the 1^{st}, 10^{th}, 50^{th} (median), 90^{th}, and 99^{th} percentiles of 30,000 random 5 s samples from times excluding 6 h ship transit windows in each period ('No Ships') and of all recorded times, including ship transits ('Ships').

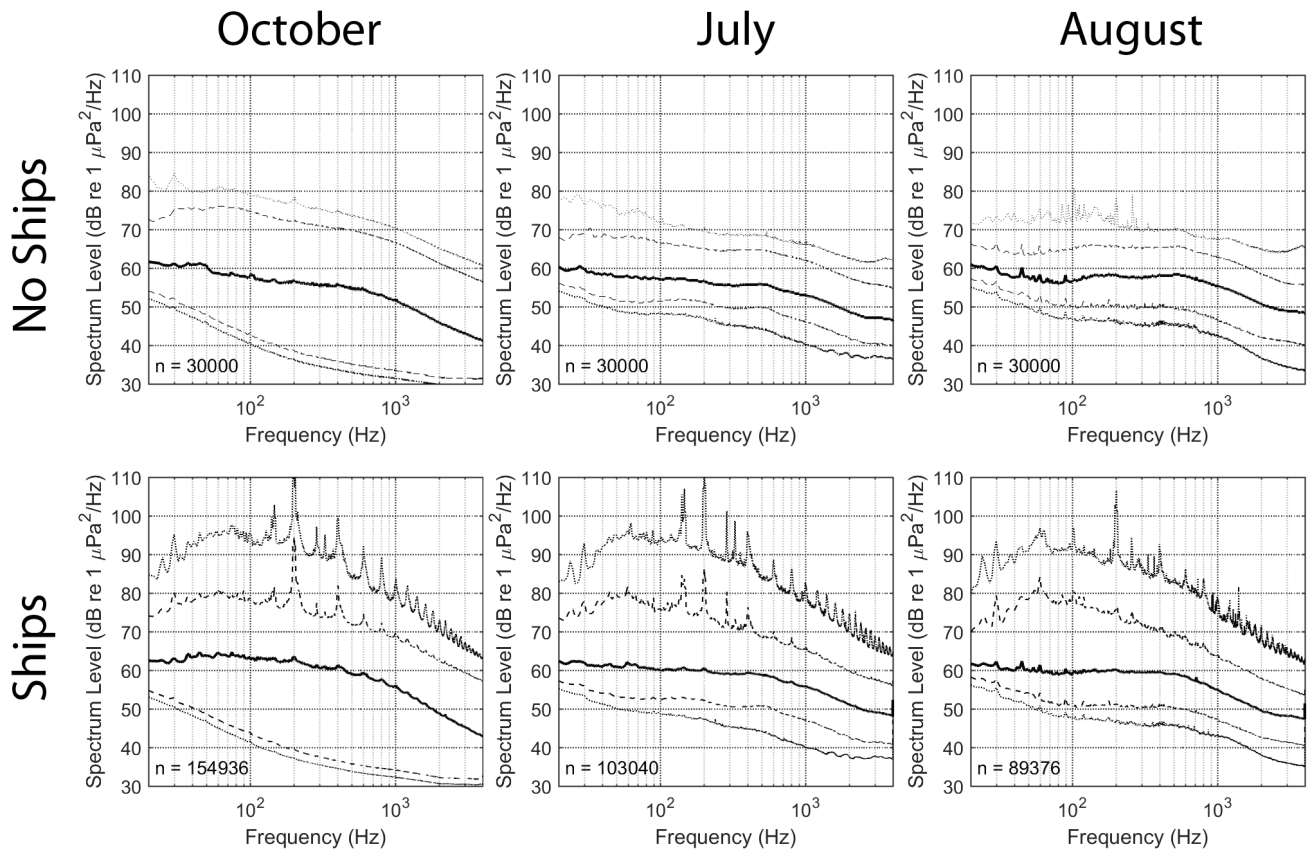

Figure 4.15: SPSL at site MI for periods excluding and including 6 h ship transit windows during monthly analysis periods October, 2018 and July and August, 2019. Levels are represented by the 1^{st}, 10^{th}, 50^{th} (median), 90^{th}, and 99^{th} percentiles of 30,000 random 5 s samples from times excluding 6 h ship transit windows in each period ('no ships') and of all recorded times, including ship transits ('ships').

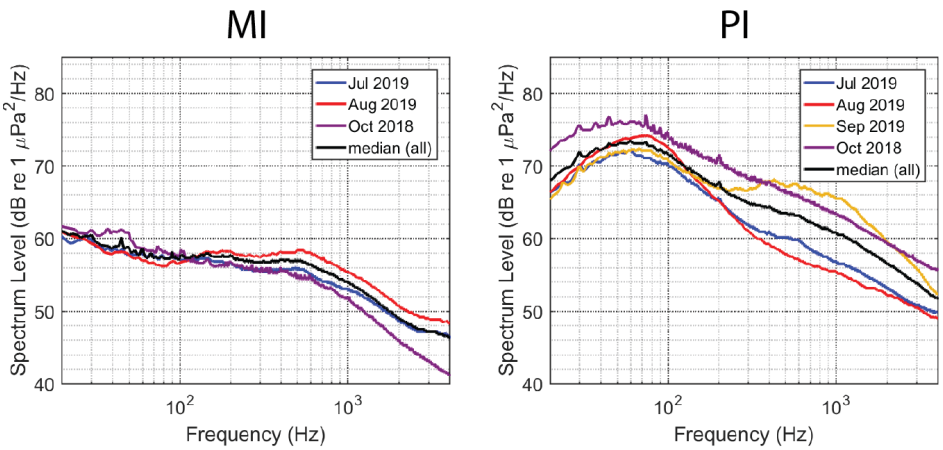

Figure 4.16: Median monthly sound pressure spectrum levels (SPSL) for periods excluding ship transit windows during months of July-Oct in Eclipse Sound. Monthly SPSL based on 30,000 5-sec SPSL selected randomly from all times in each month with nearest ship CPA time and range >4 h and >40 km, respectively.

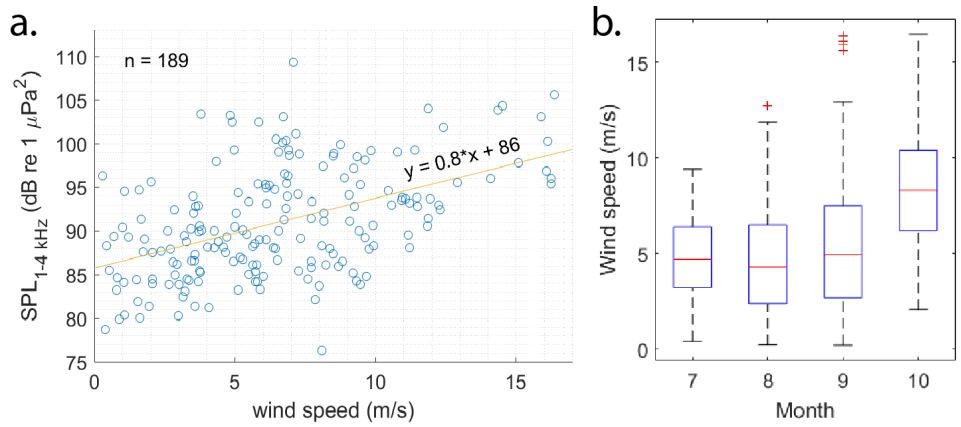

Figure 4.17: One-min averaged sound pressure levels for the 1-4 kHz frequency band versus wind speed for all monthly periods excluding 6 h ship transit windows (a). Wind measurements included within 100 km of the recording site and +/- 2 h from the SPL measurement. A linear fit is plotted (orange line) to estimate the dependence of SPL on wind speed. Box plots (b) with mean (red line), 25^{th} and 75^{th} percentiles (blue box), and most extreme data points (whiskers). Outliers noted with red plus symbol.

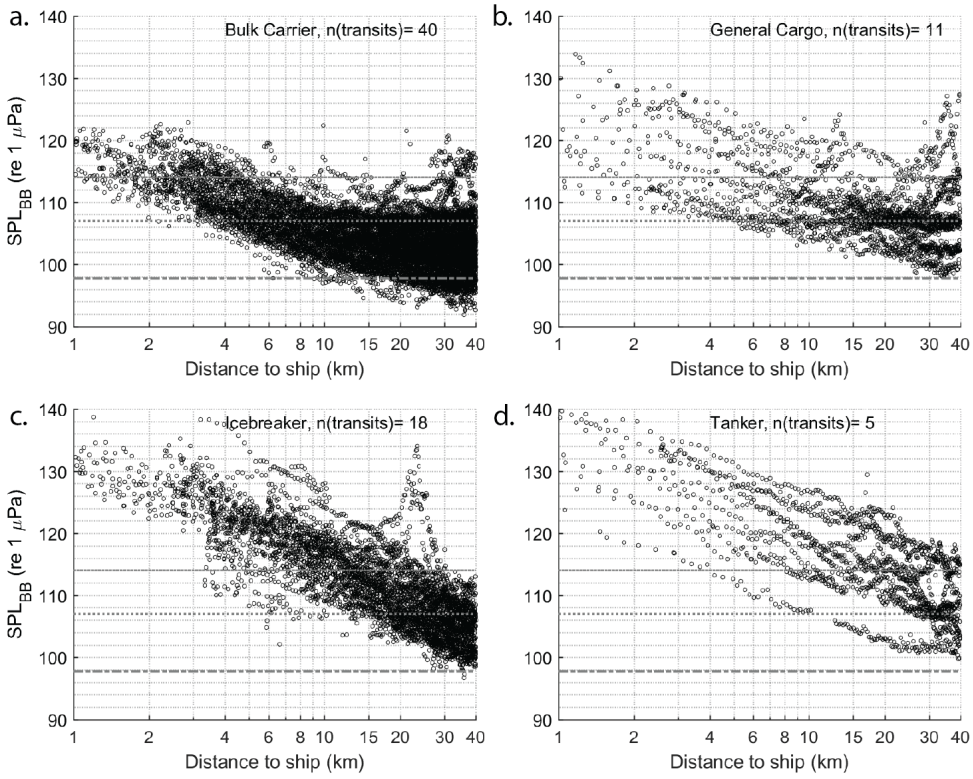

Figure 4.18: Received SPL$_{BB}$ (1-min average) at site PI with range to ship for transit examples in which the closest point of approach (CPA) was within 4 km of the recording location. Transits are separated by ship type. Only transits during open water (no icebreaker) with no other ship CPA within 2 h are included for bulk carrier, and 1 h for tanker and general cargo. Icebreakers were usually transiting with other ships, so all transit events with CPA $<$4 km are plotted. Number of transits plotted (n) is included in each panel title. Median, 90th, and 99th percentile SPL$_{BB}$ of all ship-excluded periods (gray horizontal lines) are plotted for reference.

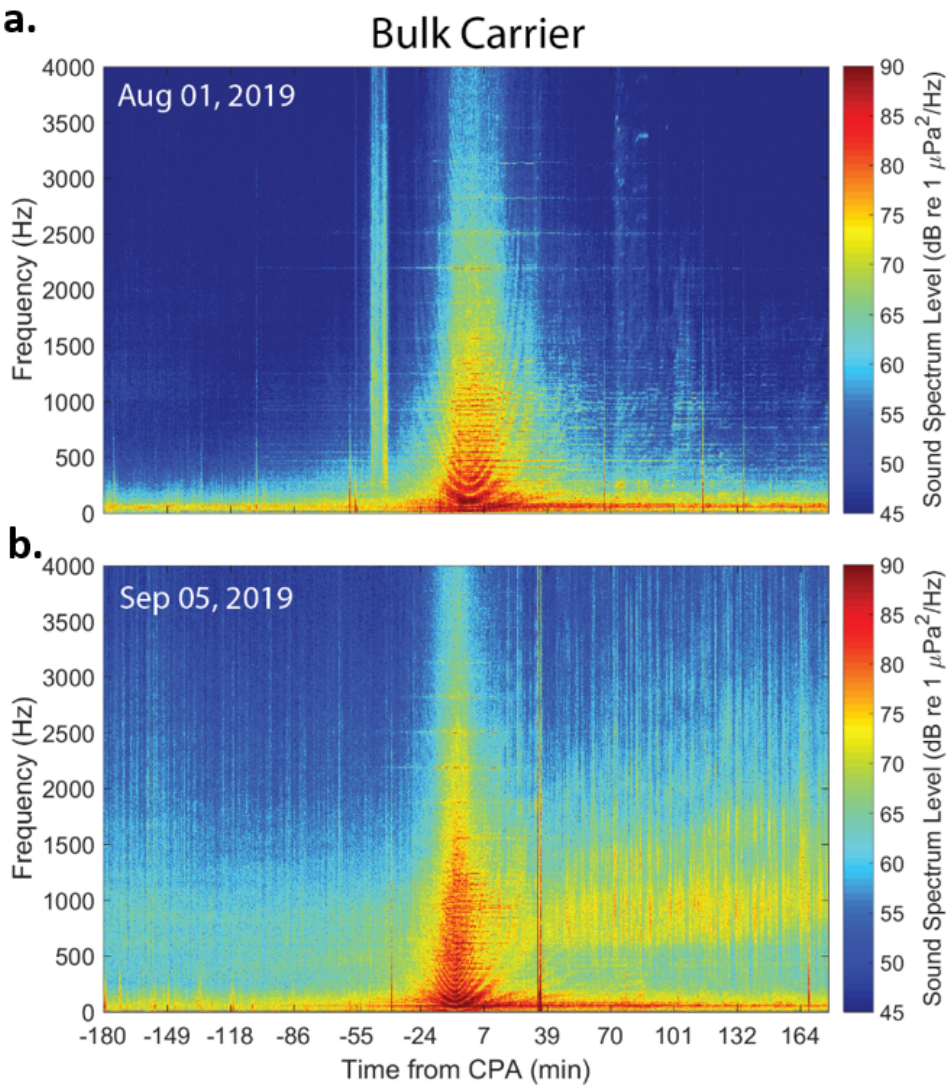

Figure 4.19: Long-term spectral average (LTSA) of the 6 h window about the closest point of approach (CPA) of 225 m bulk carrier *Nordic Orion* (MMSI 373437000) during two transits past the recording location. A transit of the ship August 1, 2019 (a; CPA range 2.4 km) occurs during relatively low background sound levels at the start of the ice-free season. Wind-generated noise below 4 kHz is evident in the September 5, 2019 transit (b; CPA range 2 km).

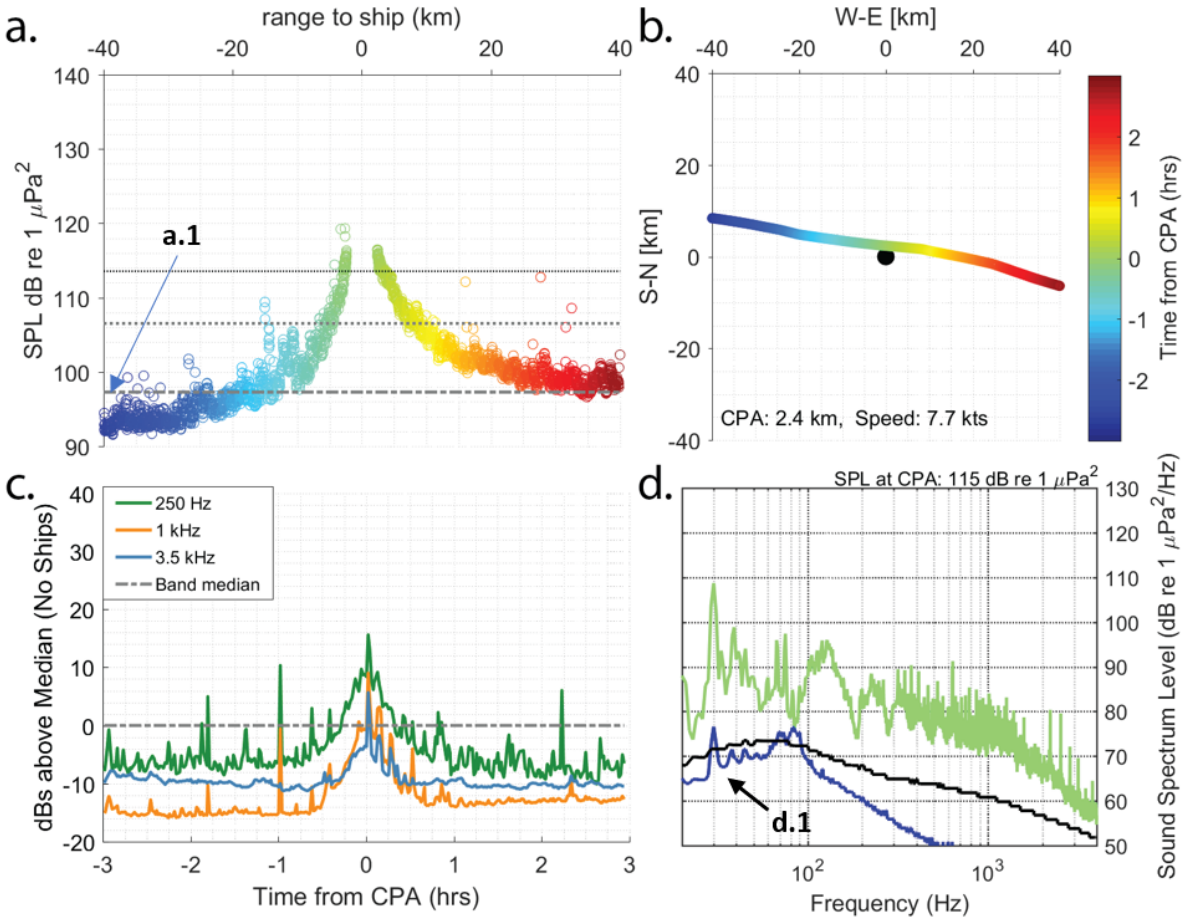

Figure 4.20: Ship transit analysis for bulk carrier *Nordic Orion* August 01, 2019. SPL_{BB} averaged every 5s (a; open circles) increases beginning at approximately range 40 km prior to CPA. SPL_{BB} 115 dB at CPA range 2.4 km. Colors in SPL scatter plot (a) and map showing ship track (b) represent time from CPA. One minute average 250 Hz (c; green line), 1 kHz (orange line), and 3.5 kHz (blue line) $1/3^{rd}$ octave band levels during ship transit plotted relative to median for the frequency band excluding ship transits (dash-dot line). SPSL (d) of CPA period (green line) with median SPSL of the first 30 min of transit plot (blue line) and shipping season median levels during periods excluding ship transits (black line).

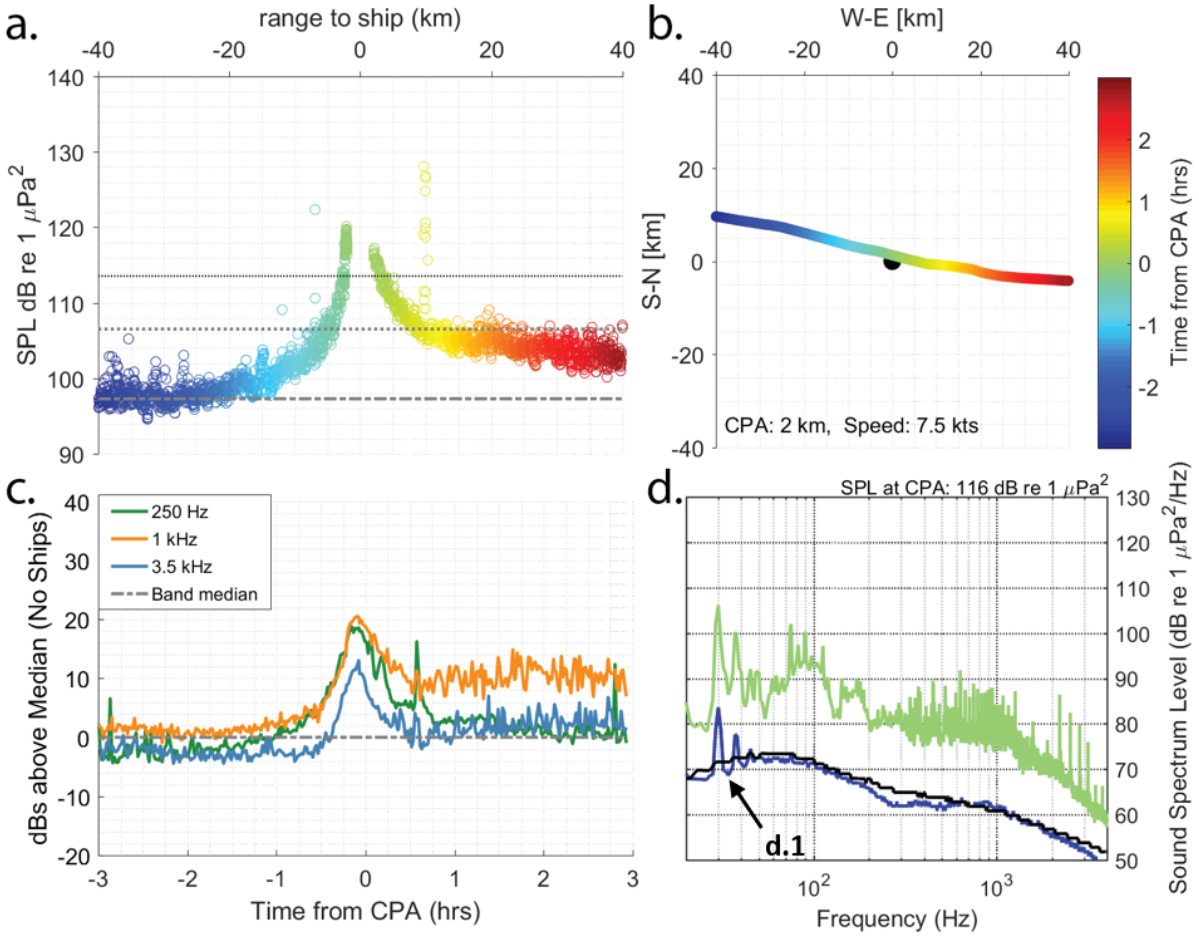

Figure 4.21: Ship transit analysis for bulk carrier *Nordic Orion* September 05, 2019. SPL_{BB} (a, open circles) averaged every 5s increases starting 30 km range to ship pre-CPA. SPL_{BB} was 116 dB at CPA range 2 km. Colors in SPL scatter plot (a) and map showing ship track (b) represent time from CPA. One minute average 250 Hz (c; green line), 1 kHz (orange line), and 3.5 kHz (blue line) $1/3^{rd}$ octave band levels during ship transit plotted relative to median for the frequency band excluding ship transits (dash-dot line). SPSL (d) of CPA period (green line) with median SPSL of the first 30 min of transit plot (blue line) and shipping season median levels during periods excluding ship transits (black line).

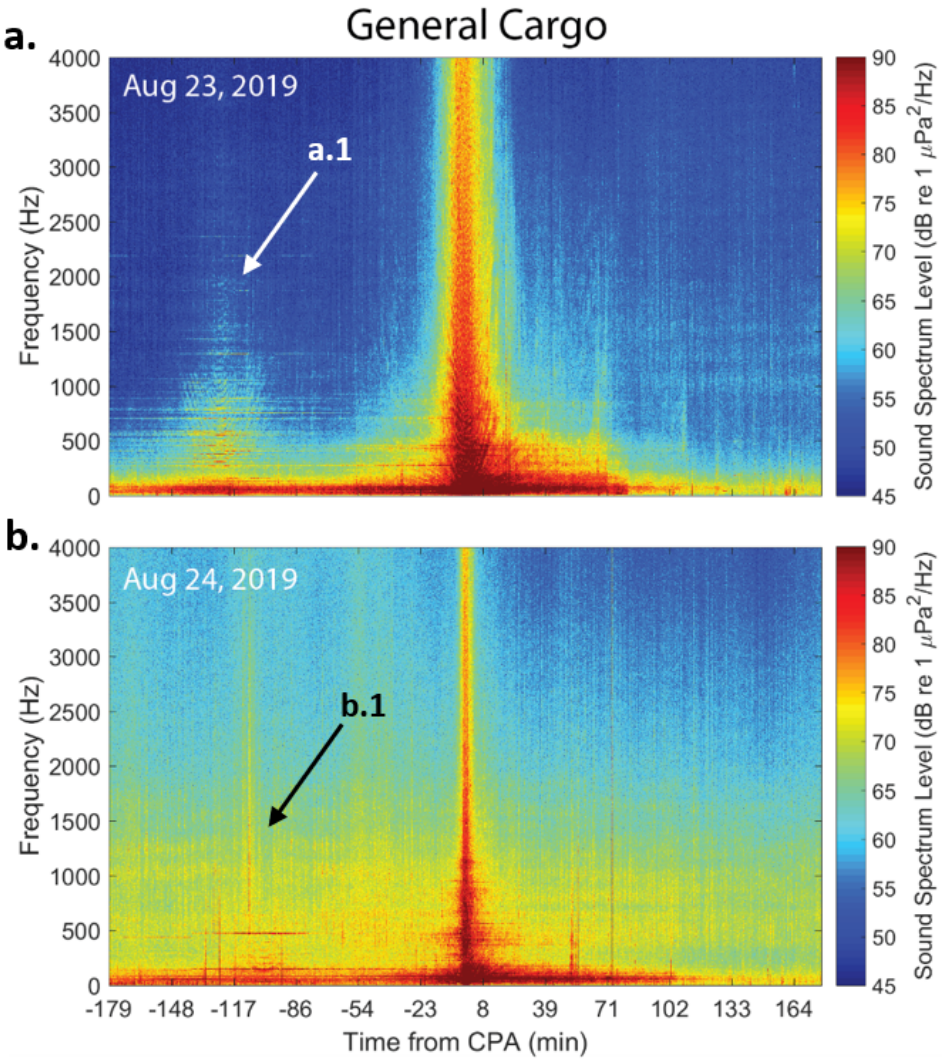

Figure 4.22: LTSA of the 6 h window about the CPA of two general cargo ships transiting past the PI recording site in open water. (a) 139 m general cargo ship, *Zelada Desgagnes* (MMSI 316015133) August 23, 2019 (CPA 1.4 km). Canadian Warship, *HCMS Kingston* (MMSI 316139000) passes at range 1.5 km 2 h prior to CPA (a.1). (b) 139 m general cargo ship *Sedna Desgagnes* (MMSI 316003010) on August 24, 2019. Passenger ship, *Fram* (MMSI 258932000) passes at range 1.6 km from recorder 1.7 h prior to CPA (b.1).

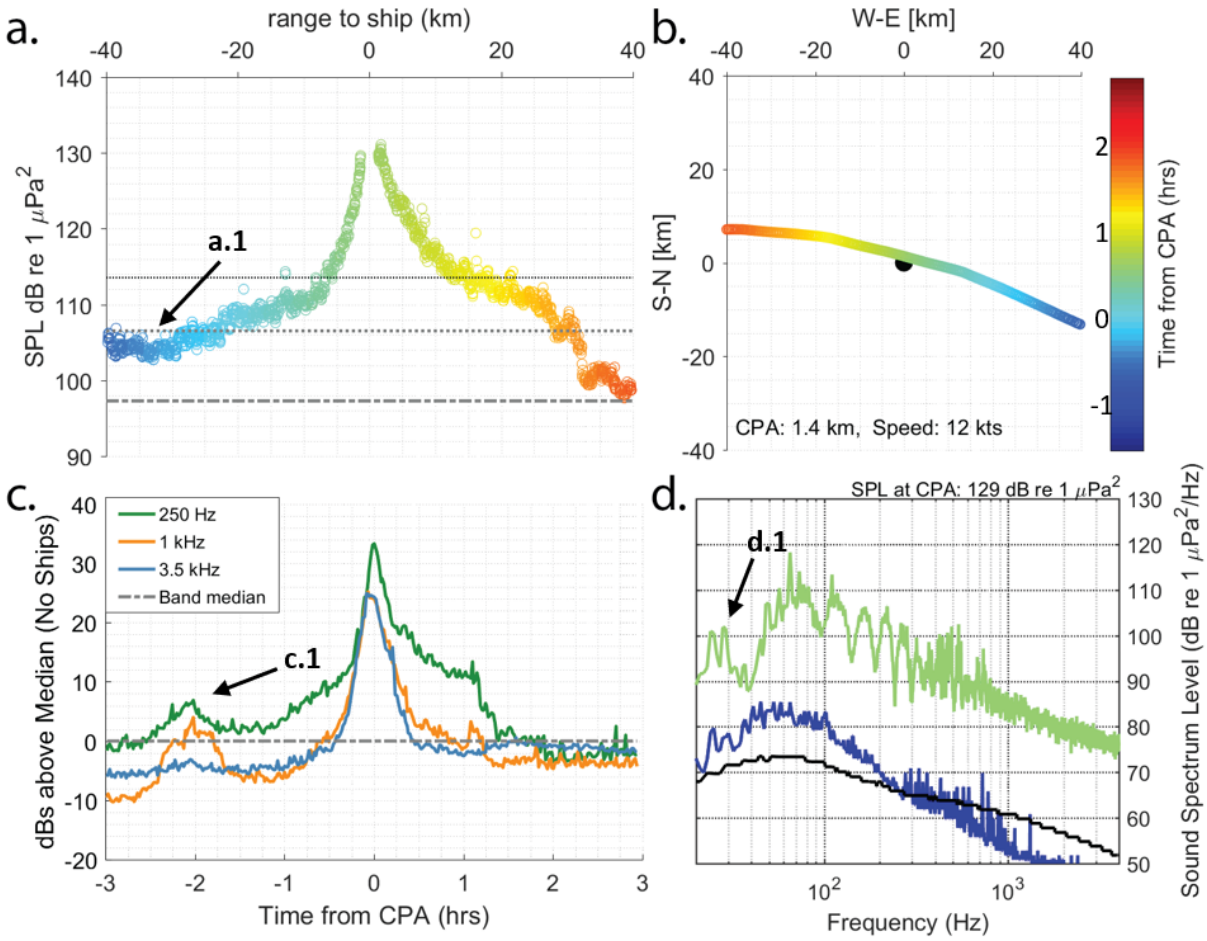

Figure 4.23: Ship transit analysis for general cargo ship, Zelada Desgagnes August 23, 2019. SPL_{BB} (a, open circles) averaged every 5s increases starting 30 km range to ship pre-CPA. SPL_{BB} was 129 dB at CPA range 1.4 km. Colors in SPL scatter plot (a) and map showing ship track (b) represent time from CPA. One minute average 250 Hz (c; green line), 1 kHz (orange line), and 3.5 kHz (blue line) $1/3^{rd}$ octave band levels during ship transit plotted relative to median for the frequency band excluding ship transits (dash-dot line). SPSL (d) of CPA period (green line) with median SPSL of the first 30 min of transit plot (blue line) and shipping season median levels during periods excluding ship transits (black line).

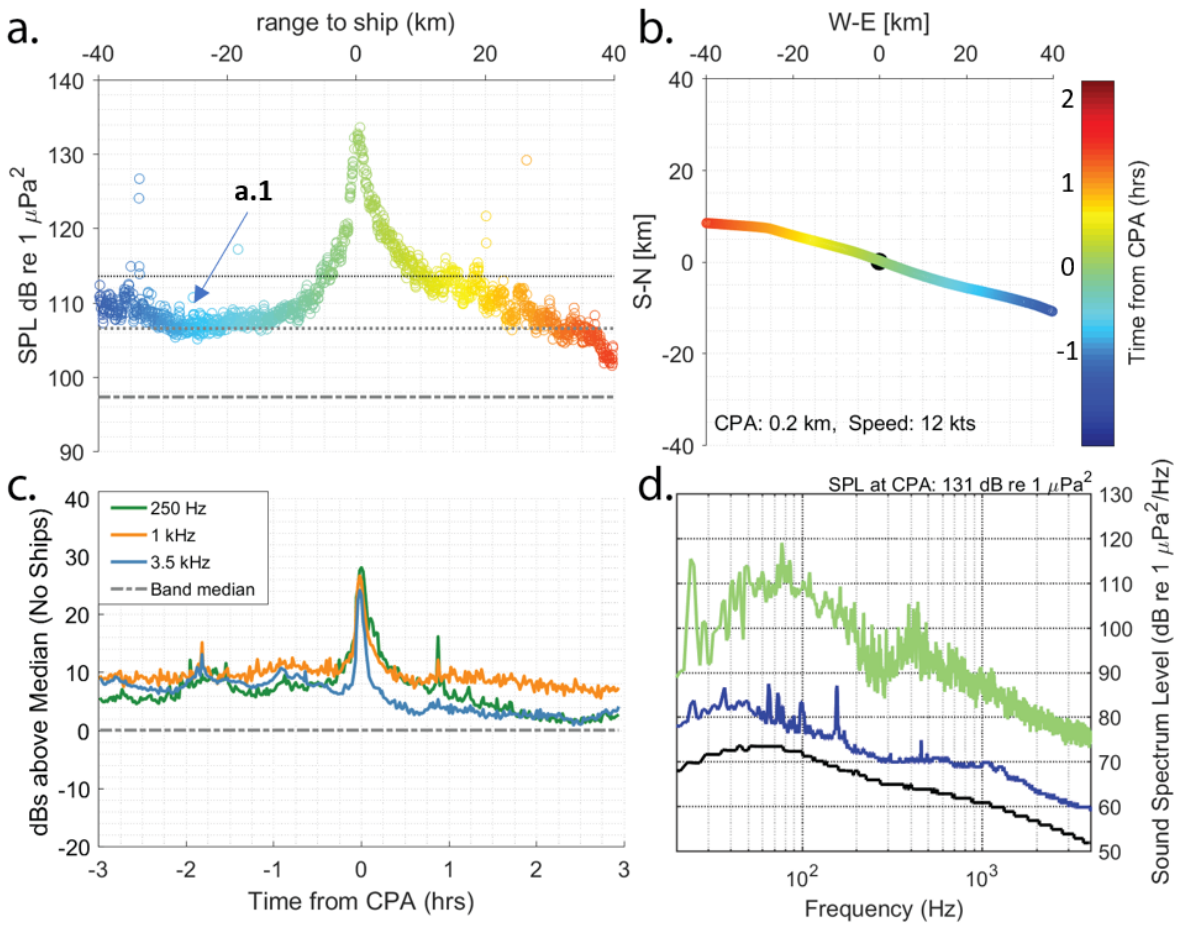

Figure 4.24: Transit of general cargo ship *Sedna Desgagnes* (MMSI 316015251) August 24, 2019. SPL_{BB} (a; open circles) averaged every 5s increases above pre-transit background level (a.1) starting at 10 km range to ship pre-CPA and ending 30 km post-CPA. SPL_{BB} was 131 dB at CPA range 0.2 km. Colors in SPL scatter plot (a) and map showing ship track (b) represent time from CPA. One minute average 250 Hz (c; green line), 1 kHz (orange line), and 3.5 kHz (blue line) $1/3^{rd}$ octave band levels during ship transit plotted relative to median for the frequency band excluding ship transits (dash-dot line). SPSL (d) of CPA period (green line) with median SPSL of the first 30 min of transit plot (blue line) and shipping season median levels during periods excluding ship transits (black line).

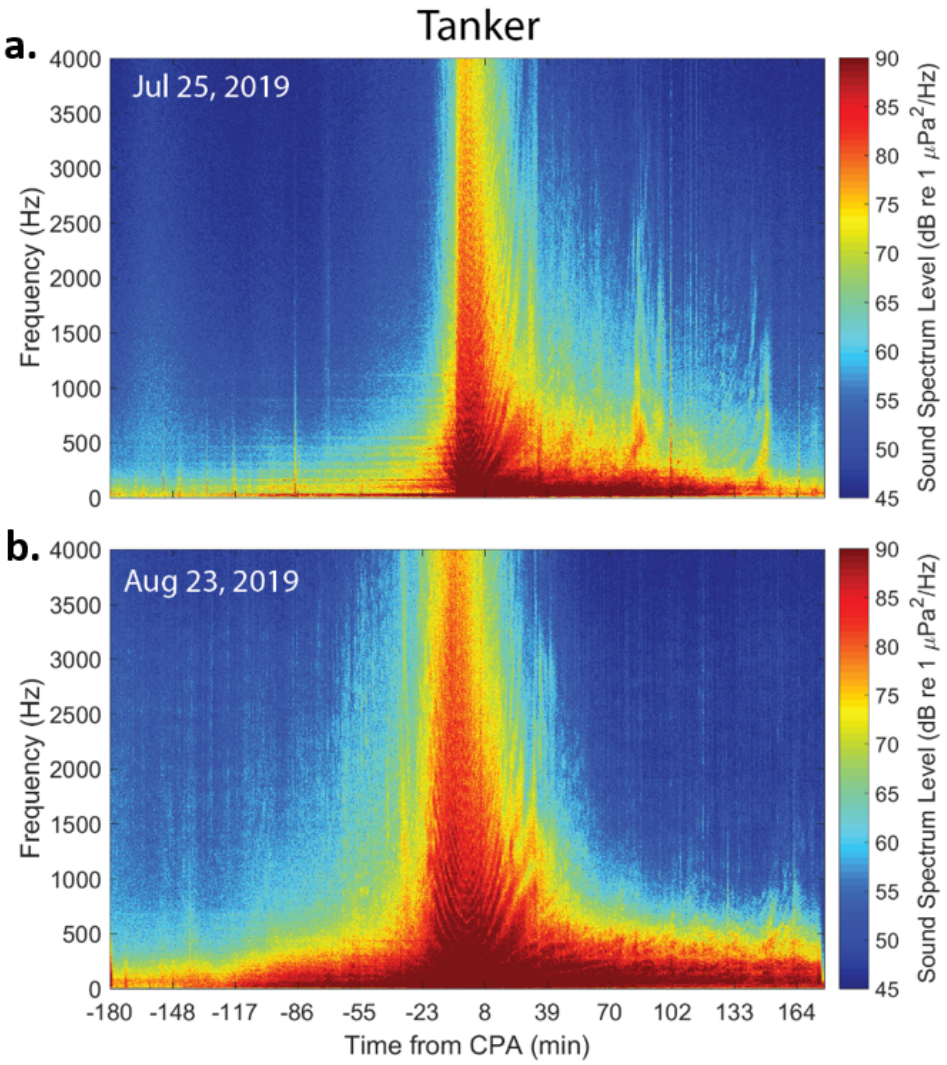

Figure 4.25: Long-term spectral average (LTSA) of the 6 h window for 147 m fuel and chemical tanker *Sarah Desgagnes* (MMSI 316012308) transiting past the PI recording site on July 25 (a) and August 23 (b), 2019. Underwater sound from the ship at $<$200 Hz is evident throughout the transits, with higher levels of low-frequency noise persisting longer at the stern aspect (positive time from CPA) than when ship is approaching (negative time from CPA).

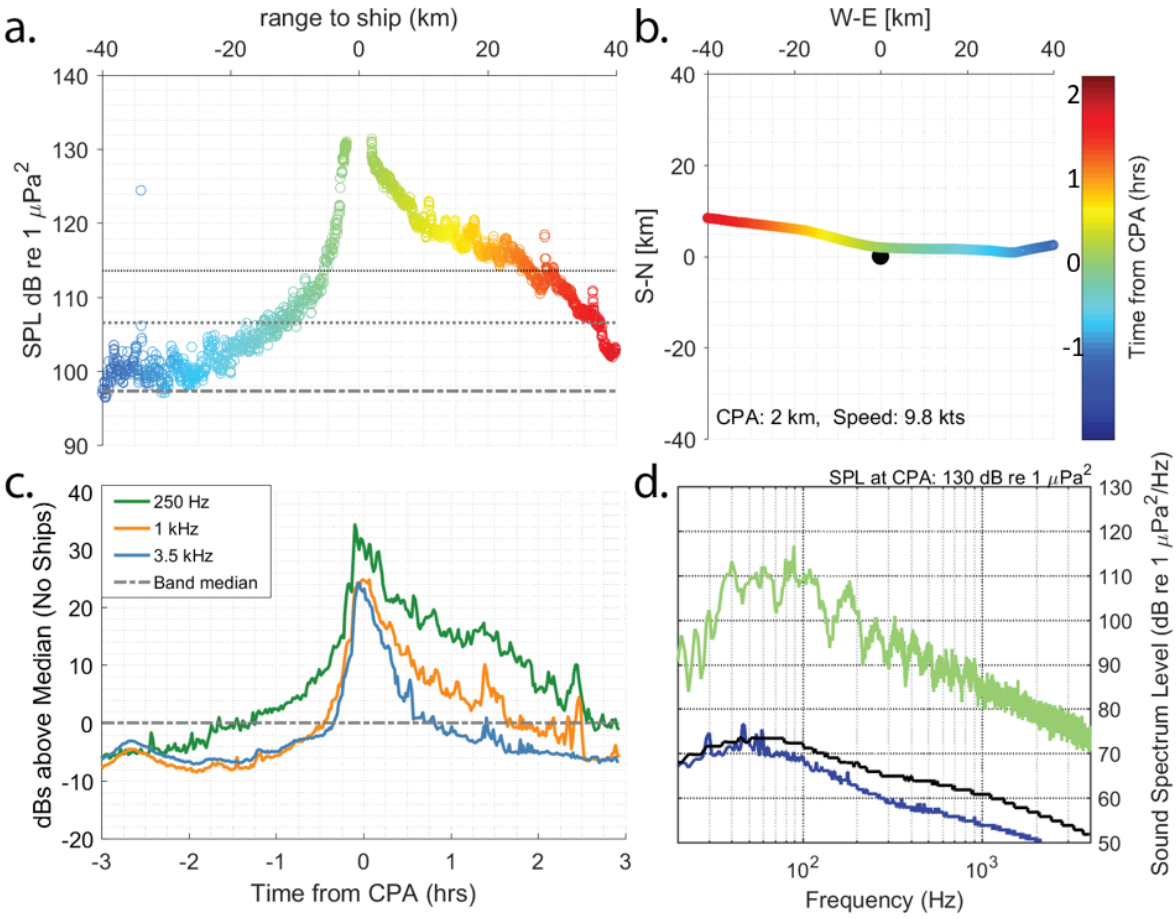

Figure 4.26: Ship transit analysis for fuel and chemical tanker, *Sarah Desgagnes* July 25, 2019. SPL_{BB} (a; open circles) averaged every 5s increases above pre-transit background level starting at 25 km range to ship pre-CPA and ending >40 km post-CPA. SPL_{BB} was 130 dB at CPA range 2 km. Colors in SPL scatter plot (a) and map showing ship track (b) represent time from CPA. One minute average 250 Hz (c; green line), 1 kHz (orange line), and 3.5 kHz (blue line) 1/3rd octave band levels during ship transit plotted relative to 50^{th} percentile for the frequency band excluding ship transits (dash-dot line). SPSL (d) of CPA period (green line) with median SPSL of the first 30 min of transit plot (blue line) and shipping season median levels during periods excluding ship transits (black line).

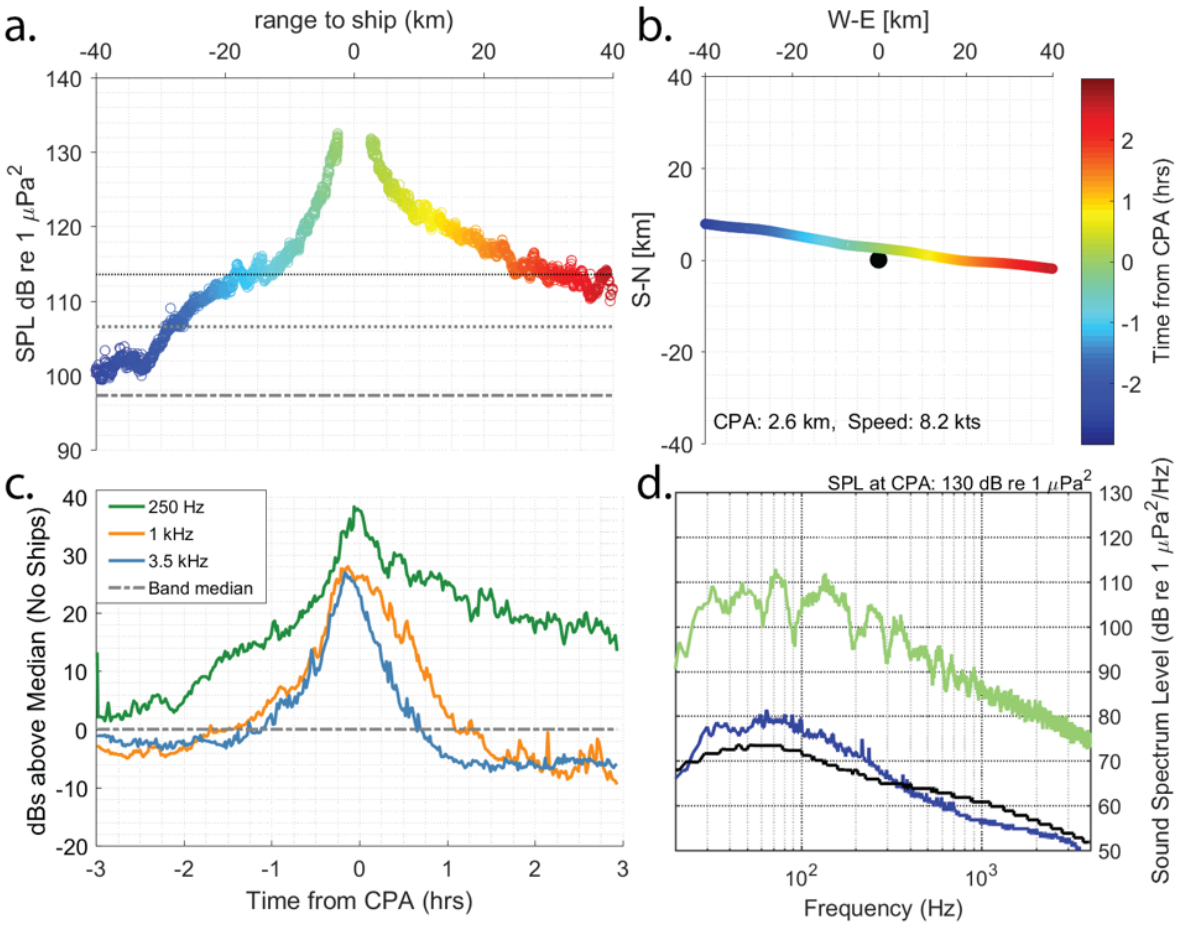

Figure 4.27: Transit of fuel and chemical tanker,*Sarah Desgagnes* August 22, 2019. SPL_{BB} (a; open circles) averaged every 5s increases above pre-transit background level starting at 30 km range to ship pre-CPA and ending >40 km post-CPA. SPL_{BB} was 130 dB at CPA range 2.6 km. Colors in SPL scatter plot (a) and map showing ship track (b) represent time from CPA. One minute average 250 Hz (c; green line), 1 kHz (orange line), and 3.5 kHz (blue line) 1/3rd octave band levels during ship transit plotted relative to 50^{th} percentile for the frequency band excluding ship transits (dash-dot line). SPSL (d) of CPA period (green line) with median SPSL of the first 30 min of transit plot (blue line) and shipping season median levels during periods excluding ship transits (black line).

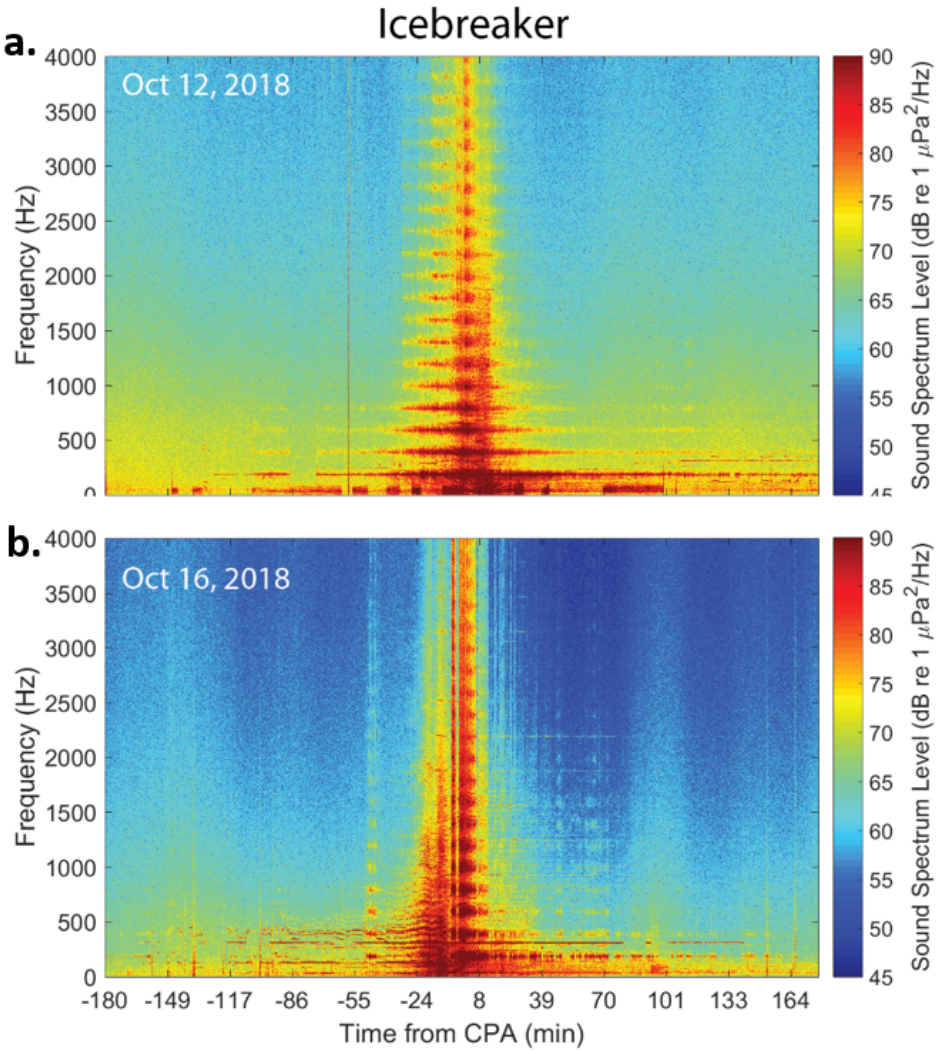

Figure 4.28: LTSA of the 6 h window for the icebreaker *Botnica* (MMSI 276805000) escorting one bulk carrier ship, *Nordic Oshima* (MMSI 357629000), when transiting past the PI recording site in 5/10 to 9/10 ice cover on October 12 (a) and October 16 (b), 2018. Tonal noise from the icebreaker is evident throughout the transit time windows with higher-frequency harmonics extending to above 4 kHz as the ships approach CPA.

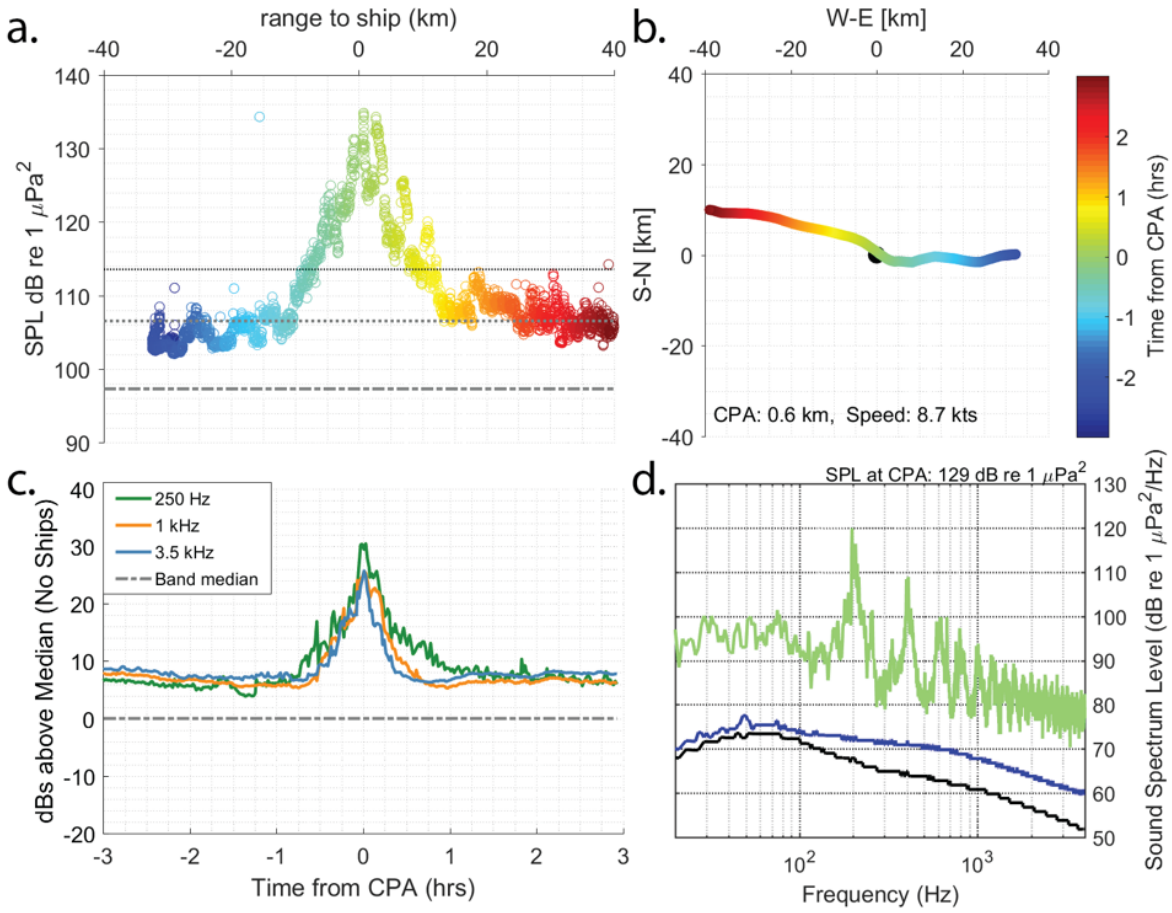

Figure 4.29: Transit of icebreaker *Botnica* escorting the bulk carrier *Nordic Oshima* (MMSI 357629000) into Eclipse Sound from Baffin Bay October 12, 2018 in 5/10 to 9/10 ice cover. Ships separated by 2 km distance and reach their respective CPA to the recorder 8 min apart. SPL_{BB} (a; open circles) averaged every 5s increases above pre-transit background level starting at 20 km range to ship pre-CPA and ending >40 km post-CPA. SPL_{BB} was 129 dB at CPA range 0.6 km. Colors in SPL scatter plot (a) and map showing ship track (b) represent time from CPA. One minute average 250 Hz (c; green line), 1 kHz (orange line), and 3.5 kHz (blue line) $1/3^{rd}$ octave band levels during ship transit plotted relative to median for the frequency band excluding ship transits (dash-dot line). SPSL (d) of CPA period (green line) with median SPSL of the first 30 min of transit plot (blue line) and shipping season median levels during periods excluding ship transits (black line).

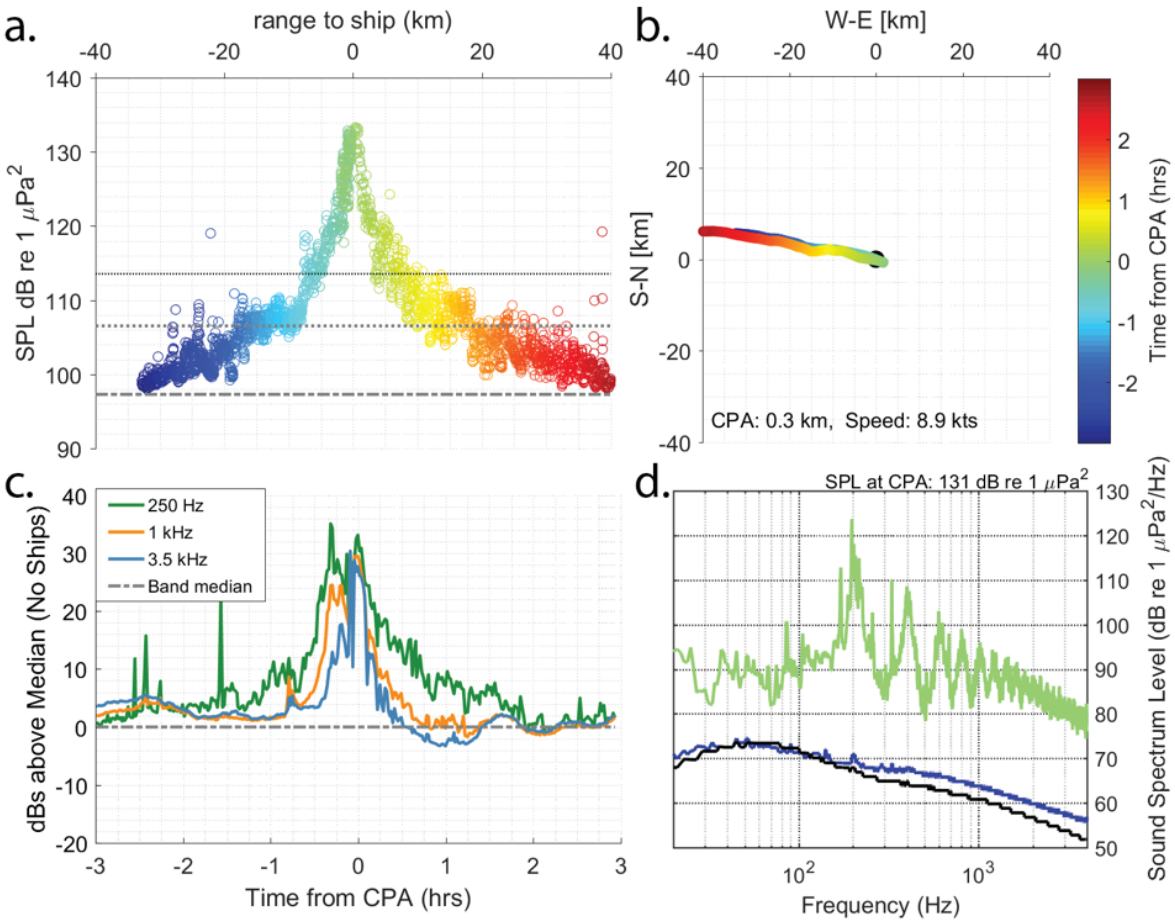

Figure 4.30: Transit of icebreaker *Botnica* escorting the bulk carrier *Nordic Oshima* out of Eclipse Sound toward Baffin Bay October 16, 2018 in 5/10 to 9/10 ice cover with icebreaker maneuvering to reverse course near the recording site. Ships were separated by a 3 km distance and reached their respective CPA to the recorder 11 min apart. SPL_{BB} (a; open circles) averaged every 5 s increased above pre-transit background level at a 20 km distance to the ship pre-CPA and extended to >40 km post-CPA. SPL_{BB} was 129 dB at CPA range 0.6 km. Colors in SPL scatter plot (a) and map showing ship track (b) represent time from CPA. One minute average 250 Hz (c; green line), 1 kHz (orange line), and 3.5 kHz (blue line) $1/3^{rd}$ octave band levels during ship transit plotted relative to median for the frequency band excluding ship transits (dash-dot line). SPSL (d) of CPA period (green line) with median SPSL of the first 30 min of transit plot (blue line) and shipping season median levels during periods excluding ship transits (black line).

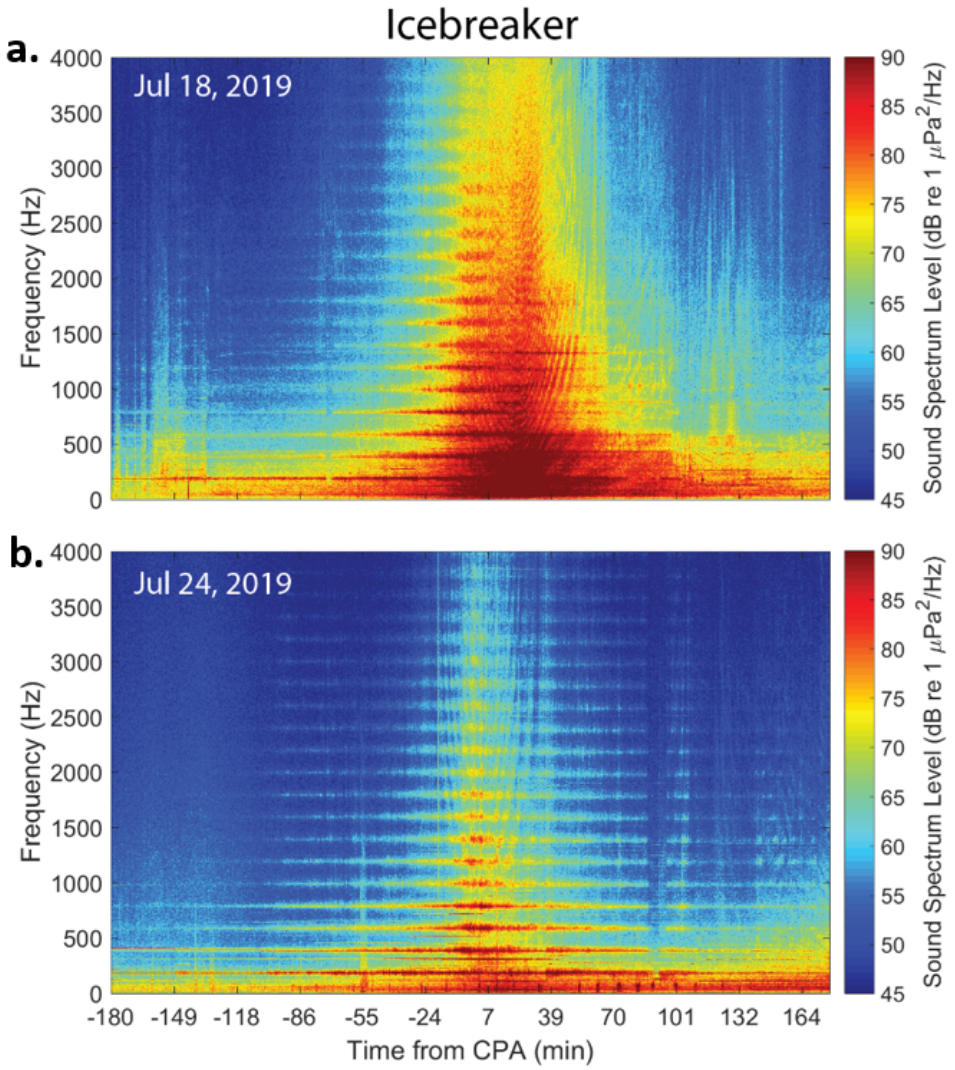

Figure 4.31: LTSA of the 6 h window for icebreaker *Botnica* (MMSI 276805000) escorting two bulk carriers and two tugs in convoy and transiting past the PI recording site on July 18 (a). *Botnica* escorting three bulk carriers on July 24, 2019 (b). Tonal noise up to 1 kHz from the icebreaker is evident throughout the transit time windows with higher-frequency harmonics extending to above 4 kHz as the ships approach CPA. Tonal noise to 3 kHz is evident on July 24 up to 3 h after the CPA.

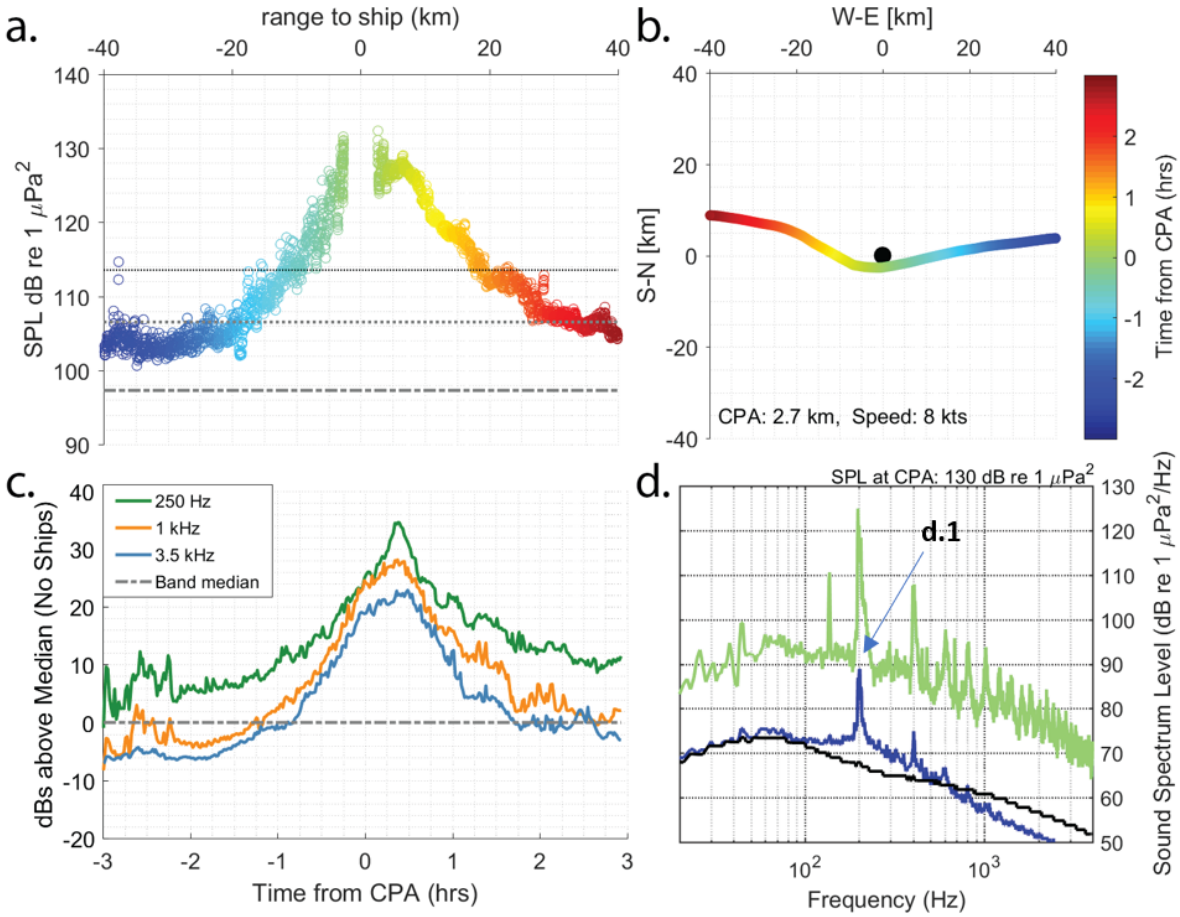

Figure 4.32: Transit of icebreaker *Botnica* escorting bulk carriers *Nordic Odin* (MMSI 356364000) and *Nordic Oasis* (MMSI 374322000) and tugs *Ocean Tundra* (MMSI 316025785) and *Ocean Taiga* (MMSI 316007572) into Eclipse Sound from Baffin Bay July 18, 2019 in 2/10 ice cover. Time from icebreaker passing to last ship CPA was 23 min. SPL_{BB} (a; open circles) averaged every 5s increases above pre-transit background level starting at 30 km range to ship pre-CPA and ending >40 km post-CPA. SPL_{BB} was 130 dB at CPA range 2.7 km. Colors in SPL scatter plot (a) and map showing ship track (b) represent time from CPA. One minute average 250 Hz (c; green line), 1 kHz (orange line), and 3.5 kHz (blue line) $1/3^{rd}$ octave band levels during ship transit plotted relative to median for the frequency band excluding ship transits (dash-dot line). SPSL (d) of CPA period (green line) with median SPSL of the first 30 min of transit plot (blue line) and shipping season median levels during periods excluding ship transits (black line).

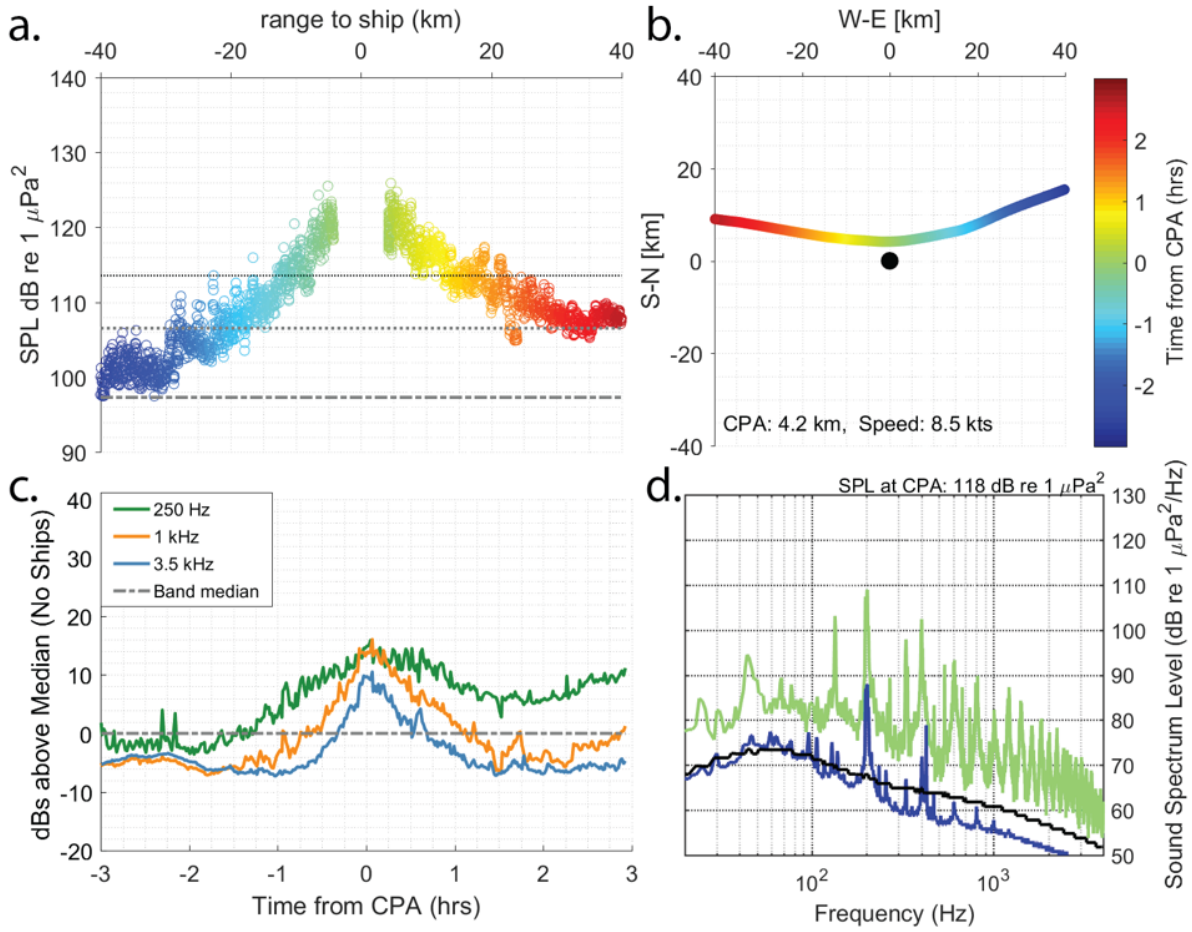

Figure 4.33: Ship transit analysis for icebreaker *Botnica* escorting three bulk carriers (*Nordic Olympic*, *Golden Strength*, and *Golden Ruby*) into Eclipse Sound on July 24, 2019 at a speed of 8.5 knots in 0/10 ice cover. Time from icebreaker passing to last ship CPA was 28 min. SPL_{BB} (a; open circles) averaged every 5s increases above pre-transit background level starting at 30 km range to ship pre-CPA and ending >40 km post-CPA. SPL_{BB} was 118 dB at CPA range 4.2 km. Colors in SPL scatter plot (a) and map showing ship track (b) represent time from CPA. One minute average 250 Hz (c; green line), 1 kHz (orange line), and 3.5 kHz (blue line) $1/3^{rd}$ octave band levels during ship transit plotted relative to median for the frequency band excluding ship transits (dash-dot line). SPSL (d) of CPA period (green line) with median SPSL of the first 30 min of transit plot (blue line) and shipping season median levels during periods excluding ship transits (black line).

Chapter 5

Conclusions

5.1 General Overview

This research focuses on improving methods for year-round autonomous underwater passive acoustic monitoring of marine mammals in Arctic waters. I develop a method to provide spatial context for acoustic detections of bowhead whale sounds, enabling more direct comparisons of acoustic presence across different locations and environmental conditions. The description of nearly one million echolocation signals of both belugas and narwhals improves confidence in acoustic detection and discrimination between the species. Measurements of the underwater soundscape within a core summer habitat of a large population of narwhal provides an assessment of underwater noise added as a result of rapidly increasing commercial ship traffic in that region. Each of these findings and their methodologies prepare the way for future studies, proposed in this chapter. Finally, there is a discussion of implications of these results in the context of a rapidly changing Arctic where resource management decisions can benefit from these results and findings.

5.1.1 Chapter 2: Bowhead Detection Probability and Spatial Normalization of Acoustic Detections

A key question when conducting passive acoustic monitoring is the distance that marine mammal calls may be detected by an acoustic sensor and how detection capabilities might change with environmental conditions. I utilize acoustic propagation modeling and detection probability theory to develop a method for correcting bowhead whale call detection time series at two acoustically different recording locations in the offshore region of the northeast Chukchi Sea. Acoustic detections are corrected for the site-specific effects of sound propagation on the received signal and the effects of noise on the probability of acoustic signal detection. Modeling results reveal that the presence of sea ice cover has a large effect on detection probability. Uncorrected bowhead whale acoustic presence is overestimated after the onset of continuous sea ice melt and prior to the onset of sea ice freeze-up due to increased probability of detection during open water. The corrected estimates of bowhead whale call density are highest at both Chukchi Sea locations one to two months prior to sea ice break-up (June-July) and during the week of rapid freeze-up (October). Bowhead presence begins in April and increases through early June. These results are important because this area is not understood to be an important part of the Western Arctic bowhead population spring (April-May) migratory corridor, although there is growing evidence that it may be important for this population during Arctic summer in June-July (Olnes et al., 2020). The effective call detection distance is 10-25 km from the hydrophone during periods of ice cover, suggesting that migrating Western Arctic bowhead whales are farther offshore during April-May than previously understood from aerial and ice-based surveys. Their offshore movements during this time also occur within large areas of $>$90% sea ice cover.

Accounting for differences in instrument and environmental noise characteristics, as well as site-specific sound propagation, facilitates more direct comparison between multiple recording locations and increases confidence in acoustic detection time series. s These advancements make

possible an assessment of the movements of bowhead whales and their responses to habitat factors, such as sea ice, on seasonal and shorter time scales through integration of acoustic detections from numerous widely separated acoustic recorders. Seasonal patterns in movements have been expected to change with rapid reductions in sea ice, especially within the range of the Western Arctic bowhead whale population (Druckenmiller et al., 2018). Further, the presence of bowhead whales during periods of nearly 100% ice cover across a large area coupled with the confidence that the listening area with ice cover is only 20 km in diameter, suggests that bowheads are utilizing heavy close pack ice farther offshore in this area prior to annual sea ice breakup than expected based on previous studies.. The previous inference was that there are fewer bowhead whales present during the period of ice cover, then when the ice melts a pulse of bowhead whales is observed. When we account for the effects of sea ice on the propagation of bowhead whale sounds we learn that there appear to be more bowhead whales when there is ice cover. This is a surprising result because traditional ecological knowledge (Huntington & Quakenbush, 2009) and 30 years of bowhead whale mark-recapture surveys (Givens et al., 2018) would indicate that bowhead whales do not use the offshore area that far north of point Barrow for their spring migration. However, it is likely that animals migrating this far offshore during April and May have not been accounted for by previous researchers in abundance estimation of this population.

5.1.2 Chapter 3: Description and Discrimination Between Echolocation Clicks of Narwhals and Belugas

Another important issue that needs to be addressed for the use of passive acoustic monitoring is the construction of a complete catalog of the sounds that are produced by marine mammals in a given region. Using combination of automated and semi-automated approaches, large numbers of echolocation clicks were detected and analyzed at two widely-separated Arctic locations. One location was in the northeast Chukchi Sea that is predominantly occupied by beluga whales. The other location in the eastern Canadian Arctic is a well-known summering

area for a large population of narwhal, where acoustic detections of beluga are rare. The same calibrated hydrophone and analysis methods for recordings from both locations were used to allow direct comparison of the echolocation signals of these two species. The resultant analyses showed that beluga and narwhal echolocation clicks differ substantially in frequency content and in rhythmic patterns. Acoustic energy of beluga echolocation is concentrated at frequencies between 30 and 80 kHz and inter-click-intervals (ICI) are tightly distributed around a modal value of 0.06 s. Narwhal echolocation also covers frequencies from 30 to 80 kHz, but with more acoustic energy extending down the frequency spectrum to a distinctive peak at 22.5 kHz. Narwhal ICI is more variable than that of belugas and has a bimodal distribution, with one mode less than 0.06 s and a second mode at 0.14 s. These characteristics allow discrimination between the two species, which was confirmed through analyses of acoustic recordings at a third location in the Canadian High Arctic where the ranges of these two species overlap (Fig. 3.1).

Characteristics of echolocation clicks of both species studied exhibit a downward shift in peak frequency and broader -10 dB frequency bandwidth as the received level of the clicks decreases. This feature of monodontid click detection raises important considerations for positive identification of detected echolocation signals. Failure to account for effects of animal orientation and frequency-dependent sound absorption by seawater could lead to missed acoustic detections or misidentification of their echolocation signals. A review of results from all previous studies of beluga and narwhal echolocation suggested that pulse durations may differ substantially between the species. Applying a single method of analysis yielded significantly different cumulative distributions of click durations, but with means within one standard deviation of one another. This characteristic is less distinctive for species discrimination than click frequency spectrum or ICI distributions.

Using large datasets of approximately one million echolocation signals per location allowed for comparative analysis of recorded distributions of frequency content, rhythmic patterns, and pulse duration.. This method yields arguably more consistent results for comparison with

future research than using relatively small sets of recorded echolocation clicks. Coupled with an improved understanding of the relationship between received level of the clicks and their frequency content, these methods improve confidence in detection and identification of species in long-term acoustic recordings made in Arctic waters. While there is uncertainty about the seasonal movements and distribution of monodontid species populations, the advances in acoustic methods for species identifications and discriminations developed in this study create opportunities for improved analysis of existing and future recordings for studies of beluga and narwhal movements.

5.1.3 Chapter 4: Underwater Soundscape and Acoustic Characteristics of Ships, Eclipse Sound, Nunavut

Anthropogenic sounds, primarily due to commercial shipping, have the potential to dramatically alter the acoustic environment of the Arctic with unknown impacts on marine mammals. This study addresses a set of questions raised during an environmental assessment related to development of an iron ore mine within Eclipse Sound, Nunavut. Iron ore is transported to market using marine shipping within an isolated fiord that is a known habitat for narwhals. Canadian federal, territorial, and local agencies are engaged in a decision-making process regarding a proposed expansion of ore production and shipping. The questions answered in this chapter arise due to a rapid increase in commercial shipping traffic related to the mine and occurring within this summering ground for one of the largest populations of narwhals in the world. There are three primary foci of this chapter, all generally centered around the impacts of underwater noise from ships on Arctic marine mammals and their acoustic environment. The first priority was to measure the monthly underwater soundscape including and, to the extent possible, excluding underwater sound from local ships transiting past the recording sites. Secondly, the results here describe the characteristics of underwater sounds generated by the four most common ship types (bulk carrier, general cargo, fuel and chemical tanker, and icebreaker). Lastly, recordings from this study document measurements of acoustic characteristics of ship transits within frequency

bands most commonly used for social communication by ringed seal and narwhal, the most abundant marine mammal species within the study region. Recordings from two locations in Eclipse Sound were analyzed during time periods spanning all commercial shipping traffic from October, 2018 through October, 2019. The two recording locations were selected to represent both: (1) protected inlets and (2) open water and deeper areas along the shipping route.

The natural soundscape, excluding sounds from nearby ships, was dominated seasonally by the presence or absence of sea ice. Months with sea ice cover (July and October) were relatively quiet when compared with open water months. The presence of wind-generated underwater noise substantially increased natural sound levels above 300 Hz during ice-free periods at both locations. Sound levels below 300 Hz were lower in all months at the protected location, while long-range sound from regional shipping was apparent during times excluding nearby ships at the location exposed to sound propagation from Baffin Bay and Eclipse Sound. Large ship transits past the recording locations elevated sound levels above median levels of natural sounds for periods ranging from 30 minutes to up to more than four hours. Individual ship types had distinctive sound characteristics. Icebreakers, general cargo, and tanker ships radiated more underwater noise from longer distances than bulk carriers. Two ships in particular had notably high underwater noise levels: a commercial icebreaker and a tanker vessel. These ships may represent good candidates for targeted efforts to identify and reduce sources of unintentional noise introduced into the marine environment. Sound levels in the three biologically relevant frequency bands analyzed were elevated within 1 to ¿30 km from transiting ships, suggesting that potential interference with narwhal and ringed seal communication should be investigated further. Sounds from ships overlapped substantially with all three frequency bands. Finally, the relative changes in underwater sound levels caused by transiting ships are greater at the protected location than at the deeper, more exposed site. While the more exposed location is an area where narwhal pass during their annual migration, the more protected site is part of their core summer use area. Narwhal in the interior acoustically sheltered areas of Eclipse Sound may be more susceptible to

disturbance and communication masking not only as a result of repeated daily shipping traffic, but due to the greater difference between their natural underwater soundscape and the soundscape when affected by sounds from ships.

5.2 Practical Implications for Passive Acoustic Monitoring in Arctic Waters

Accounting for the limitations of acoustic recording systems, influences of the environment, and the effect of noise on detection and characteristics of recorded signals of interest can improve the strength of inference drawn from long-term underwater sound recordings. Consideration should be given to the effects of sound transmission loss on the received characteristics of the signals of interest. Failing to do this means that passive acoustic studies may misidentify those signals or misinterpret what they tell us about the presence or the behavior of marine mammals when we are not able to visually observe the animals. Bowhead sounds that travel long distances underwater are particularly susceptible to influences of the environment, especially the presence of sea ice. Detection of these sounds is a function of environmental influences and of the relative levels of noise that may mask acoustic detection. Echolocation clicks of belugas and narwhals rapidly attenuate over shorter distances and the received characteristics also change rapidly across those distances. Behavioral aspects, such as orientation of the animals also influence the recorded signals. Taking these factors into consideration when interpreting acoustic detection time series will improve confidence in the identification of marine mammal sounds and provide greater spatial context for their acoustic presence when utilizing passive acoustic monitoring to learn about species relationships with habitat or responses to potential stressors such as ship traffic.

5.3 Future Implications

The Arctic is changing rapidly: sea ice cover is declining, marine ecosystems are changing, and non-Arctic species are predicted to make increasing incursions into areas with greater annual occurrence of ice-free conditions. At the same time, human activities such as shipping are increasing rapidly in some areas, like the eastern Canadian Arctic. Marine resource managers are faced with the difficult task of understanding both Arctic marine mammal adaptation to impacts of climate change and the added potential stress from increasing regional ship traffic. Acoustic monitoring offers a promising avenue to help address these research needs in a region with numerous physical and logistical limitations for other research methods, such as ship-based observation of marine mammals.

Recent developments in density estimation for marine mammal populations using single hydrophones (e.g. Hildebrand et al., 2019) can be applied to beluga and narwhal based on the improved understanding of their echolocation signals and increased confidence in their identification in long-term acoustic recordings. A growing volume of data from tags placed on the animals is providing a better understanding of their underwater behavior, including their use of echolocation and other aspects of diving behavior (Blackwell et al., 2018). These insights into beluga and narwhal underwater behavior can be combined with high-confidence time series of echolocation clicks recorded in the far field to acoustically estimate abundance of these species at locations where other methods of density estimation are not practical.

Another important aspect of marine mammal research in a changing Arctic is to understand species relationships with and responses to sea ice on a range of spatial and temporal scales. The development of spatially explicit measures of bowhead whale acoustic presence that can be directly compared across multiple recording locations opens avenues of research into their habitat use. A next step from the work presented here is to use the improved spatial context for call detections to investigate bowhead whale responses to sea ice characteristics on a range of

timescales. Acoustic recordings similar to those analyzed here have been made annually at up to 114 locations over a period of ten years or more throughout the range of the Western Arctic bowhead whale population (Clark et al., 2015). With site-specific detection time series corrected for noise and environmental effects it will be possible to integrate seasonal acoustic presence at numerous sites. Collaborative research like this has previously been limited largely due to the difficulties presented by comparison between different types of acoustic recorders and different environmental conditions.

On shorter timescales of a day to a week, bowhead whales and other Arctic marine mammal species likely respond to local environmental conditions such as the concentration, thickness and dynamics of sea ice. Applying the methods from this research allows combining acoustic detections of bowhead whale sounds with sea ice data from remote sensing to investigate their relationships with habitat factors that are changing across large areas of the Arctic. Understanding these finer temporal and spatial scale responses of bowheads to habitat factors will help in predicting future changes in their distribution and seasonal movements that may result from large scale effects of climate change in the Arctic.

While marine mammals are likely responding to large scale changes across Arctic waters, the resilience of their populations to these changes may also be impacted by local stressors such as increasing shipping traffic. Methods developed here for detection of beluga and narwhal echolocation signals and measurement of underwater sound generated by individual ship transits should be applied to investigate behavioral responses of the monodontid species to ship traffic. Behavioral responses to underwater noise include impacts on foraging behavior or displacement from areas around transiting ships. Generalized Additive Models are commonly utilized to investigate relationships between marine mammals and independent variables in time series data (e.g. Becker et al., 2020; Forney et al., 2012), such as those collected in Eclipse Sound and presented in this dissertation. Management and decision-making processes are now underway regarding proposed increases in shipping traffic in the Eastern Canadian Arctic. There is a clear

need and opportunity to better understand narwhal behavioral responses to ships making use of the methods advanced in this study.

Bibliography

Ainslie, M. A. (2013). Neglect of bandwidth of Odontocetes echo location clicks biases propagation loss and single hydrophone population estimates. Journal of the Acoustical Society of America, 134(5), 3506-3512.

Alexander, P., Duncan, A., Bose, N., and Smith, D. (2013). Modeling acoustic transmission loss due to sea ice cover. Acoustics Australia, 41(1), 79-87.

Ariak, E., and Olson, R. (2019). *Qikiqtani Inuit Association's Tusaqtavut for Phase 2 Application of the Mary River Project*. Qikiqtani Inuit Association Final Report. https://www.nirb.ca/portal/dms/script/dms_download.php?fileid=325450&applicationid=124701&sessionid=b83etr131bg3jvioocef51h393 (accessed 12/14/2020).

Arrigo, K. R. and van Dijken, G. L. (2015). Continued increases in Arctic Ocean primary production. Progress in Oceanography 136:60-70.

Au, W. W. L., Carder, C. A., Penner, R. H., and Scronce, B. L. (1985). Demonstration of adaptation in beluga echolocation signals. Journal of the Acoustical Society of America, 77(2), 726-730.

Au, W. W. L., Moore, P. W. B., and Pawloski, D. (1986). Echolocation transmitting beam of the Atlantic bottlenose dolphin. Journal of the Acoustical Society of America, 80(2), 688-691.

Au, W. W. L., Penner, R. H., and Turl, C. W. (1987). Propagation of beluga echolocation signals. Journal of the Acoustical Society of America, 82(3), 807-813.

Au, W. W. L., Pawloski, J. L., and Nachtigall, P. E. (1995). Echolocation signals and transmission beam pattern of a false killer whale (*Pseudorca crassidens*). Journal of the Acoustical Society of America, 98(1), 51-59.

Au., W. L., Ford, J. K. B., Horne, J. K., and Newman Allman, K. A. (2004). Echolocation signals of free-ranging killer whales (*Orcinus orca*) and modeling of foraging for chinook salmon (*Oncorhynchus tshawytscha*). Journal of the Acoustical Society of America, 115(2), 901-909.

Baffinland Iron Mines Corporation. (2015, August 10). *First shipment of Baffinland's Mary River iron ore*. https://www.baffinland.com/media-centre/news-releases/2015/first-shipment-of-baffinlands-mary-river-iron-ore (accessed 12/14/2020).

Baffinland Iron Mines Corporation. (2018, August 16). *Baffinland submits Final Environmental Impact Statement Addendum for Phase 2.* https://www.baffinland.com/media-centre/news-releases/2018/baffinland-submits-final-environmental-impact-statement-addendum-for-phase-2 (accessed 12/23/2020).

Baffinland Iron Mines Corporation. (2020a). *Phase 2 Proposal Updated Information Package.* https://www.nirb.ca/portal/dms/script/dms_download.php?fileid=327957&applicationid=124701&sessionid=b83etr131bg3jvioocef51h393 (accessed 12/14/2020)

Barber, D. G., Hanesiak, J. M., and Piwowar, J. (2001). Sea-ice and meteorological conditions in Northern Baffin Bay and the North Water Polynya between 1979 and 1996. Atmosphere-Ocean, 39(3), 343-359.

Barrett-Lenard, L. G., Ford, J. K. B., and Heise, K. A. (1996). The mixed blessing of echolocation: Differences in sonar use by fish-eating and mammal-eating killer whales. Animal Behaviour, 51, 553-565.

Baumann-Pickering, S., McDonald, M. A., Simonis, A. E., Solsona Berga, A., Oleson, E. M., Roch, M. A., Wiggins, S. M., Rankin, S., Yack, T. M., and Hildebrand, J. A. (2013). Species-specific beaked whale echolocation signals. Journal of the Acoustical Society of America, 134(3), 2293-2301.

Becker, E. A., Carretta, J. V., Forney, K. A., Barlow, J., Brodie, S., Hoopes, R., Jacox, M. G., Maxwell, S. M., Redfern, J. V., Sisson, N. B., Welch, H., and Hazen, E. L. (2020). Performance evaluation of cetacean species distribution models developed using generalized additive models and boosted regression trees. Ecology and Evolution, 10(2020), 5759-5784.

Blackwell, S. B., Richardson, W. J., Greene, C. R., and Streever, B. (2007). Bowhead whale (*Balaena mysticetus*) migration and calling behavior in the Alaskan Beaufort Sea, Autum 2001-04: An acoustic localization study. Arctic, 60(3), 255-270.

Blackwell, S. B., Nations, C. S., McDonald, T. L., Thode, A. M., Mathias, D., Kim, K. H., Greene, C. R., and Macrander, M. (2015). Effects of airgun sounds on bowhead calling rates:Evidence for two behavioral thresholds. PLoS ONE, 10(6), e0125720.

Blackwell, S. B., Tervo, O. M., Conrad, A. S., Sinding, M. H. S., Hansen, R. G., Ditlevsen, S., and Heide-Jørgensen, M. P. (2018). Spatial and temporal patterns of sound production in East Greenland narwhals. PLoS ONE, 13(6), e0198295.

Booth, C. G., Sinclair, R. R., and Harwood, J. (2020). Methods for monitoring for the population consequences of disturbance in marine mammals: A review. Frontiers in Marine Science, 7, 115.

Brown, J. R., and Milne A. R. (1967). Reverberation under Arctic sea-ice. Journal of the Acoustical Society of America, 42(1), 78-82.

Buckland, S., Anderson, D., Burnham, K., Laake, J., and Thomas, L. (2001). *Introduction to Distance Sampling: Estimating Abundance of Biological Populations* (Oxford University Press, New York), pp. 1-444.

Cate, J. R., Smultea, M., Blees, M., Larson, S., Simpson, S., Jefferson, T.,and Streckler, D. (2014). 90-day report of marine mammal monitoring and mitigation during a 2D seismic survey by TGS in the Chukchi Sea, August through October 2013. AES Doc. No. 15416-04 13-185. Prepared by ASRC Energy Services, Smultea Environmental Sciences, Clymene Enterprises and Entiat River Technologies for TGS-NOPEC Geophysical Company, National Marine Fisheries Service and U.S. Fish and Wildlife Service. 122 p. + Appendices.

Chambault, P., Moesgaard Albertsen, P., Patterson, T. A., Hansen, R. G., Tervo, O., Laidre, K. L., and Heide-Jørgensen, M. P. (2018). Sea surface temperature predicts the movements of an Arctic cetacean: the bowhead whale. Nature: Scientific Reports, 2018(8), 9658.

Chapman, R. P., and Harris, J. H. (1962). Surface backscattering strengths measured with explosive sound sources. Journal of the Acoustical Society of America, (34)10, 1592-1597.

Citta, J. J., Quakenbush, L. T., George, J. C., Small, R. J., Heide-Jørgensen, M. P., Brower, H., Adams, B., and Brower, L. (2012). Winter movements of bowhead whales (*Balaena mysticetus*) in the Bering Sea. Arctic, 65(1):13-34.

Citta, J. J., Quakenbush, L. T., Okkonen, S. R., Druckenmiller, M. L., Maslowski, W., Clement-Kinney, J., George, J. J., Brower, H., Small, R. J., Ashjian, C. J., Harwood, L. A., and Heide-Jørgensen, M. P. (2014). Ecological characteristics of core-use areas used by Bering-Chukchi-Beaufort (BCB) bowhead whales, 2006-2012. Progress in Oceanography 136, 201-222.

Clark, C. W., and Johnson, J. H. (1984). The sounds of the bowhead whale *Balaena mysticetus*, during the spring migration of 1979 and 1980. Canadian Journal of Zoology, 62, 1436-1441.

Clark, C. W., Ellison, W. T., Southall, B. L., Hatch, L., Van Parijs, S. M., Frankel, A., and Ponirakis, D. (2009). Acoustic masking in marine ecosystems: intuitions, analysis, and implication. Marine Ecological Progress Series 395, 201-222.

Collins, M. D. (1993) A split-step Padé solution for the parabolic equation method. Journal of the Acoustical Society of America, (93)4, 1736-1742.

Cummings, W. C. and Holliday, D. V. (1987). Sounds and source levels from bowhead whales off Pt. Barrow, Alaska. Journal of the Acoustical Society of America, 82(3), 814-821.

Clark, C. W., Berchok, C. L., Blackwell, S. B., Hannay, D. E., Jones, J., Ponirakis, D., and Stafford, K. M. (2015). A year in the acoustic world of bowhead whales in the Bering, Chukchi, and Beaufort Seas. Progress in Oceanography, 136, 223-240.

Clarke, J., Stafford, K., Moore, S. E., Rone, B., Aerts, L., and Crance, J. (2013). Subarctic cetaceans in the southern Chukchi Sea: Evidence of recovery or response to a changing ecosystem. Oceanography, 26(4), 136-149.

Corlett, W. B. and Pickart, R. S. (2017). The Chukchi slope current. Progress in Oceanography, 153(2017), 50-65.

COSEWIC. (2004). COSEWIC assessment and update status report on the beluga whale *Delphinapterus leucas* in Canada. Committee on the Status of Endangered Wildlife in Canada. Ottawa. ix +70 pp. (https://wildlife-species.canada.ca/species-risk-registry/virtual_sara/files/cosewic/sr_beluga_whale_e.pdf; accessed 12/30/2020).

Dawson, J., Pizzolato, L., Howell, S., Copland, L., & Johnston, M. (2018). Temporal and Spatial Patterns of Ship Traffic in the Canadian Arctic from 1990 to 2015. Arctic, 71(1), 15-26.

Deecke, V., Ford, J. K. B., and Slater, P. (2005). The vocal behaviour of mammal-eating killer whales: Communicating with costly calls. Animal Behaviour, 69, 395-405.

Delarue, J., Laurinolli, M., and Martin, B. (2009). Bowhead whale (*Balaena mysticetus*) songs in the Chukchi Sea between October 2007 and May 2008. Journal of the Acoustical Society of America, 126(6), 3319-3328.

Diachok, O. (1976). Effects of sea-ice ridges on sound propagation in the Arctic Ocean. Journal of the Acoustical Society of America, 59(5), 1110-1120.

Diachok, O. I. and Winokar, R. S. (1974). Spatial variability of underwater ambient noise at the Arctic ice-water boundary. Journal of the Acoustical Society of America, 55(4), 750-753.

Doniol-Valcrose, T., Gosselin, J., Pike, D. G., Lawson, J. W., Asselin, N. C., Hedges, K., and Ferguson, S. H. (2020). Narwhal abundance in the Eastern Canadian High Arctic in 2013. NAMMCO Scientific Publications, 11. https://doi.org/10.7557/3.5100.

Druckenmiller, M. L., Citta., J. J., Ferguson, M. C., Clarke, J. T., George, J. C., and Quakenbush, L. (2018). Trends in sea-ice cover within bowhead whale habitats in the Pacific Arctic. Deep-Sea Research Part II, 152(2018), 95-107.

Duncan, A. J. and Maggi, A. L. (2006). A consistent, user-friendly interface for running a variety of underwater acoustic propagation codes. *Proceedings of Acoustics 2006*, pp. 471-477.

Duncan, A. J., Gavrilov, A. N., McCauley, R. D., and Parnum, I. M. (2013). Characteristics of sound propagation in shallow water over an elastic seabed with a cap-rock layer. Journal of the Acoustical Society of America, 134(1), 207-215.

Dietz, R., Heide-Jørgensen, M. P., Richard, P., Orr, J., Laidre, K., and Schmidt, H. C. (2008). Movements of narwhals (*Monodon monoceros*) from Admiralty Inlet monitored by satellite telemetry. Polar Biology, 31(2008), 1295-1306.

Duckworth, G., LePage, K., and Farrell, T. (2001). Low-frequency propagation and reverberation in the central Arctic: Analysis of experimental results. Journal of the Acoustical Society of America, 110(2),747-760.

Eskesen, I. G., Wahlberg, M., Simon, M., and Larsen, O. N. (2011). Comparison of echolocation clicks from geographically sympatric killer whales and long-finned pilot whales. Journal of the Acoustical Society of America, 130(1), 9-12.

Eguiluz, V. M., Fernandez-Garcia, J., Irigoien, X., and Duarte, C. M. (2016). A quantitative assessment of Arctic shipping in 2010-2014. Nature: Scientific Reports, 6, 30682.

Erbe, C., Reichmuth, C., Cunningham, K., Lucke, K., and Dooling, R. (2016). Communication masking in marine mammals: A review and research strategy. Marine Pollution Bulletin, 103, 15-38.

Farmer, D. M. and Xie, Y. (1988). The sound generated by cracks in sea ice. Journal of the Acoustical Society of America, 85(4), 1489-1500.

Finley, K. J., Miller, G. W., Davis, R. A., and Greene, C. R. (1990). Reactions of belugas, *Delphinapterus leucas*, and narwhals, *Monodon monoceros*, to ice-breaking ships in the Canadian High Arctic. Canadian Bulletin of Fisheries and Aquatic Sciences, 224, 97-117.

Finneran, J. J., Carder, D. A., Dear, R., Belting, T., McBain, J., Dalton, L., & Ridgway, S. H. (2005). Pure tone audiograms and possible aminoglycoside-induced hearing loss in belugas (Delphinapterus leucas). The Journal of the Acoustical Society of America, 117(6), 3936-3943.

Fofonoff, N. P. and Millard, R. C. Jr. 1983. Algorithms for computation of fundamental properties of seawater. Unesco Technical Papers in Marine Science, 44, 55 pp.

Ford, J. K. B. and Fischer, H. D. (1978). Underwater acoustic signals of the narwhal (*Monodon monoceros*). Canadian Journal of Zoology, 56, 552-560.

Forney, K. A., Ferguson, M. C., Becker, E. A., Fielder, P. C., Redfern, J. V., Barlow, J., Vilchis, I. L., Balance, L. T. (2012). Habitat-based spatial models of cetacean density in the eastern Pacific Ocean. Endangered Species Research, 16, 113-133.

Frasier, K. E., Wiggins, S. M., Harris, D., Marques, T. A., Thomas, L., and Hildebrand, J. A. (2016). Delphinid echolocation detection probability on near-seafloor sensors. Journal of the Acoustical Society of America, 140(3), 1918-1930.

Frasier, K. E., Roch, M. A., Soldevilla, M. S., Wiggins, S. M., Garrison, L. P., and Hildebrand, J. A. (2017). Automated classification of dolphin echolocation click types from the Gulf of Mexico. PLoS Computational Biology, 13(12): e1005823.

Frey, K. F., Moore, G. W. K., Cooper, L. W., and Grebmeier, J. M. (2015). Divergent patterns of recent sea ice cover across the Bering, Chukchi, and Beaufort seas of the Pacific Arctic Region. Progress in Oceanography, 136(2015), 32-49.

Frouin-Muoy, H., Kowarski, K., Martin, B., and Broker, K., (2017). Seasonal trends in acoustic detection of marine mammals in Baffin Bay and Melville Bay, Northwest Greenland. Arctic, 70(1), 59-76.

Frouin-Mouy, H., E.E. Maxner, M.E. Austin, and S.B. Martin. (2019). Baffinland Iron Mines Corporation– Mary River Project: 2018 Passive Acoustic Monitoring Program. Document 01720, Version 4.0. Technical report by JASCO Applied Sciences for Golder Associates Ltd.

Frouin-Mouy, H., C.C. Wilson, K.A. Kowarski, and M.E. Austin. (2020). Baffinland Iron Mines Corporation – Mary River Project: 2019 Passive Acoustic Monitoring Program – Draft Report. Document 02007, Version 2.2. Technical report by JASCO Applied Sciences for Golder Associates Ltd.

Gavrilov, A. N. and Mikhalevsky, P. N. (2006). Low-frequency acoustic propagation loss in the Arctic Ocean: Results of the Arctic climate observations using underwater sound experiment. Journal of the Acoustical Society of America, 119(6), 3694-3706.

Gassmann, M., Henderson, E. E., and Wiggins, S. M. (2013). Offshore killer whale tracking using multiple hydrophone arrays. Journal of the Acoustical Society of America, 134(5), 3513-3521.

Gassmann, M., Wiggins, S. M., & Hildebrand, J. A. (2017). Deep-water measurements of container ship radiated noise signatures and directionality. The Journal of the Acoustical Society of America, 142(3), 1563-1574.

George, J. C., Clark, C., Carroll, G. M., and Ellison, W. T. (1989). Observations on the ice-breaking and ice navigation behavior of migrating bowhead whales (*Balaena mysticetus*) near Point Barrow, Alaska, Spring 1985. Arctic, 42(1), 24-30.

Givens, G. H., Edmonson, S. L., George, J. C., Suydam, R., Charif, R. A., Rahaman, A., Hawthorne, D., Tudor, B., DeLong, R. A., and Clark, C. W. (2013). Estimate of 2011 abundance of the Bering-Chukchi-Beaufort Seas bowhead whale population. Paper SC/65a/BRG01 presented to the IWC Scientific Committee June, 2013 Cheju, Republic of Korea.

Givens, G.H., Mocklin, J.A., Brattstrom, L. V., Tudor, B. J., Koski, W. R., Zeh, J. E., Suydam, R., and George, J. C. (2018). Adult survival rate and 2011 abundance of Bering-Chukchi-Beaufort Seas bowhead whales from photo-identification data over three decades. Submitted as paper SC/67B/AWMP/01 REV1 to the Scientific Committee of the International Whaling Commission, May 2018.

Goff, J. A. (1995). Quantitative analysis of sea ice draft 1.Methods for stochastic modeling. Journal of Geophysical Research, 100(C4),6993-7004.

Golder Associates Ltd. (2018). Baffinland Iron Mines Corporation Mary River Project - Phase 2 Proposal Technical Supporting Document No.24, Marine Mammal Effects Assessment. https://www.nirb.ca/portal/dms/script/dms_download.php?fileid=320584&applicationid=124701&sessionid=b83etr131bg3jvioocef51h393 (accessed 12/14/2020).

Golder Associates Ltd. (2019). Final Report – Bruce Head Shore-based Monitoring Program. 2014-2017 Integrated Report. Baffinland Iron Mines Corporation Mary River Project. 1663724-081-R-Rev1-12000.

Golder Associates Ltd. (2020). Draft 2017-2018 Integrated Narwhal Tagging Study – Technical Data Report. Mary River Project, Baffin Island, Nunavut. 1663724-188-R-RevB.

Gomez, C., Lawson, J. W., Wright, A. J., Tollit, B. D., and Lesage, V. (2016). A systematic review on the behavioural responses of wild marine mammals to noise: the disparity between science and policy. Canadian Journal of Zoology, 94, 801-819.

Gong, D. and Pickart, R. S. (2015). Summertime circulation in the eastern Chukchi Sea. Deep-Sea Research II, 118,18-31.

Greene, C. R., and Buck, B. M. (1964). Arctic ocean ambient noise. Journal of the Acoustical Society of America, 36(6), 1218–1220.

Guisan, A., Reid, T., Baumgartner, J. B., Naujokaitis-Lewis, I., Sutcliffe, P. R., Tulloch, A. I. T., Regan, T. J., Brotons, L., McDonald-Madden, E., Mantyka-Pringle, C., Martin, T. G., Rhodes, J. R., Maggini, R., Setterfield, S. A., Elith, J., Schwartz, M. W., Wintle, B. A., Broennimann, O., Austin, M., Ferrier, S., Kearney, M. R., Possingham, H. P., and Buckley, Y. M. (2013). Predicting species distributions for conservation decisions. Ecology Letters, 16:1424-1435.

Halliday, W. D., Pine, M. K., Muoy, X., Kortsalo, P., and Insley, S. J. (2020). The coastal Arctic marine soundscape near Ulukhaktok, Northwest Territories, Canada. Polar Biology 43:623-636.

Hannay, D. E., Delarue, J., Muoy, X., Martin, B. S., Leary, D., Oswald, J. N., and Vallarta, J. (2013). Marine mammal acoustic detections in the northeastern Chukchi Sea, September 2007-July 2011. Continental Shelf Research, 67(2013), 127-146.

Hatch, L. T., Clark, C. W., Van Parijs, S. M., Frankel, A. S., & Ponirakis, D. W. (2012). Quantifying loss of acoustic communication space for right whales in and around a US National Marine Sanctuary. Conservation Biology, 26(6), 983-994.

Hauser, D. W., Laidre, K. L., Suydam, R. S., and Richard, P. R. (2014). Population-specific home ranges and migration timing of Pacific Arctic beluga whales (*Delphinapterus leucas*). Polar Biology, 37(2014), 1171-1183.

Hauser, D. D. W., Laidre, K. L., Stern, H. L., Moore, S. E., Suydam, R. S., and Richard, P. R. (2017). Habitat selection by two beluga whale populations in the Chukchi and Beaufort Seas. PLoS ONE 12(2), e0172755, p19.

Helble, T. A., D'Spain, G. L., Campbell, G. S., and Hildebrand, J. A. (2013). Calibrating passive acoustic monitoring: Correcting humpback whale call detections for site-specific and time-dependent environmental characteristics. Journal of the Acoustical Society of America, 134(5), EL400

Helble, T. A., D'Spain, G. L., Hildebrand, J. A., and Campbell, G. S. (2013). Site-specific probability of passive acoustic detection of humpback whale calls from single fixed hydrophones. Journal of the Acoustical Society of America, 134(3), 2556-2570.

Heide-Jørgensen, M. P., Laidre, K. L., Jensen, M. V., Dueck, L., and Postma, L. D. (2006). Dissolving stock disctreteness with satellite tracking: Bowhed whales in Baffin Bay. Marine Mammal Science, 22(1), 34-45.

Heimrich, A. F., Halliday, W. D., Frouin-Muoy, H., Pine, M. K., Juanes, F., and Insley, S. J. (2020). Vocalizations of bearded seals and their influence on the soundscape of the western Canadian Arctic. Marine Mammal Science, 2020, 1-20.

Higdon, J. H., Westdal, K. H., and Ferguson, S. (2013). Distribution and abundance of killer whales (Orcinus orca) in Nunavut, Canada – an Inuit knowledge survey. Journal of the Marine Biological Association of the UK, 94(6), 1293-1304.

Hildebrand, J. A., Frasier, K. E., Baumann-Pickering, S., Wiggins, S. M., Merkens, K. P., Garrison, L. P., Soldevilla, M. S., and McDonald, M. A. (2019). Assessing seasonality and density from passive acoustic monitoring of signals presumed to be from pygmy and dwarf sperm whales in the Gulf of Mexico. Frontiers in Marine Science, 6:66, p.11.

Hildebrand, J. A. (2009). Anthropogenic and natural sources of ambient noise in the ocean. Marine Ecology Progress Series, 395, 5-20.

Hildebrand, J.A., Frasier, K.E., Baumann-Pickering, S., Wiggins, S.M., Merkens, K.P., Garrison, L.P., Soldevilla, M.S., and Mcdonald, M.A. (2019). Assessing seasonality and density from passive acoustic monitoring of signals presumed to be from pygmy and dwarf sperm whales in the Gulf of Mexico. Frontiers in Marine Science, 6(66),1-11.

Hildebrand, J. A., Baumann-Pickering, S., Frasier, K. E., Trickey, J. S., Merkens, K. P., Wiggins, S. M., McDonald, M. A., Garrison, L. P., Harris, D., Marques, T. A., and Thomas, L. (2015). Passive acoustic monitoring of beaked whale densities in the Gulf of Mexico. Scientific Reports, 5:16343.

Hoeg-Guldberg, O., and Bruno, J. F. (2010). The impact of climate change on the world's marine ecosystems. Science, 328, 1523-1528.

Huntington, H.P. and Quakenbush, T. T. (2009). Traditional knowledge of bowhead whale migratory patterns near Kaktovik and Barrow, Alaska. Final report to the Barrow and Kaktovik Whaling Captains Associations, the Alaska Eskimo Whaling Commission, ConocoPhillips, and the Minerals Management Service. 13pp.

Huntington, H. P., Quakenbush, L. T., and Nelson, M. (2016). Effects of changing sea ice on marine mammals and subsistence hunters in northern Alaska from traditional knowledge interviews. Biology Letters, 12:20160198.

Jakobsson, M., Macnab, R., Mayer, L., Anderson, R., Edwards, M., Hatzky, J., Schenke, H. W., and Johnson, P. (2012). An improved bathymetric chart of the Arctic Ocean: Implications for ocean modeling and geological, geophysical and oceanographic analyses. Geophysical Research Letters, 35, L07602.

Jensen, F. B. and Kupperman, W. A. (1983). Optimum frequency of propagation in shallow water environments. Journal of the Acoustical Society of America, 73(3), 813-819.

Jensen, F. B., Kuperman, W. A., Porter, M. B., and Schmidt, H. (1994). *Computational Ocean Acoustics* (AIP Press, New York), pp. 256-260.

Jin, G., Lynch, J. F., Pawlowicz, R., and Worcester, P. (1994). Acoustic scattering losses in the Greenland Sea marginal ice zone during the 1988-89 tomography experiment. Journal of the Acoustical Society of America, 96(5), 3045-3053.

Johnson, H. D., Stafford, K. M., George, J. C., Ambrose, W. G. Jr., and Clark, C. W. (2015). Song sharing and diversity in the Bering-Chukchi-Beaufort population of bowhead whales (*Balaena mysticetus*), spring 2011. Marine Mammal Science, 31(3), 902-922.

Jones, J. M., Thayre, B. J., Roth, E. H., Mahoney, M., Sia, I, Merculief, K., Jackson, C., Zeller, C., Clare, M., Bacon, A., Weaver, S., Gentes, Z., Small, R. J., Stirling, I., Wiggins, S. M., and Hildebrand, J. A. (2014). Ringed, bearded, and ribbon seal vocalizations north of Pt. Barrow, Alaska: Seasonal presence and relationship with sea ice. Arctic, 67(2), 203-222.

Kahru, M. 2000. Windows Image Manager: Image display and analysis program for Microsoft Windows with special features for satellite images. http://wimsoft.com.

Keen, K. A., Thayre, B. J., Hildebrand, J. A., and Wiggins, S. M. (2018). Seismic airgun sound propagation in Arctic Ocean waveguides. Deep-sea Research Part I, 141, 24-32.

Kinda, G. B., Simard, Y., Gervaise, C., Mars, J. I., and Fortier, L. (2015). Arctic underwater noise transients from sea ice deformation: Characteristics, annual time series, and forcing in the Beaufort Sea. Journal of the Acoustical Society of America, 138(4). 2034-2045.

Koblitz, J. C., Stilz, P., Rasmussen, M. H., and Laidre, K. L. (2016). Highly directional sonar beam of narwhals (*Monodon monoceros*) measured with a vertical 16 hydrophone array. PLoS ONE, 11(11), e0162069.

Krishfield, R., Toole, J., Proshutinsky, A., and Timmermans, M. L. (2008). Automated ice-tethered profilers for seawater observations under pack ice in all seasons. Journal of Atmospheric and Ocean Technology, 25, 2091-2105.

Küsel, E. T., Mellinger, D. K., Thomas, L., Marques, T. A., and Ward, J. (2011). Cetacean population density estimation from single fixed hydrophone sensors using passive acoustics. Journal of the Acoustical Society of America, 129(6), 3610-3622.

Kwok, R. (2018). Arctic sea ice thickness, volume, and multiyear ice coverage: losses and coupled variability (1958-2018). Environmental Research Letters, 13(2018), 105005.

Kwok, R. and Cunningham, G. F. (2015). Variability of Arctic sea ice thickness and volume from CryoSat-2. Philosophical Transactions of the Royal Society A, 373, 20140157.

Laidre, K. L., Stern, H., Kovacs, K. M., Lowry, L., Moore, S. E., Regehr, E. V., Ferguson, S. H., Wiig, Ø., Boveng, P., Angliss, R. P., Born, E. W., Litvoka, D., Quakenbush, L., Lydersen, C., Vongraven, D., and Ugarte, F. (2015). Arctic marine mammal population status, sea ice loss, and conservation recommendations for the 21st century. Conservation Biology, 29(3), 724-737.

LeFort, K. J., Garroway, C. J., and Ferguson, S. H. (2020). Killer whale abundance and predicted narwhal consumption in the Canadian Arctic. Global Change Biology, 2020(26), 4276-4283.

Lewis, K. M., van Dijken, G. L., and Arrigo, K. R. (2020). Changes in phytoplankton concentration now drive increased Arctic Ocean primary production. Science, 369, 198-202.

Li, M., Pickart, R. S., Spall, M. A., Weingartner, T. J., Lin, P., Moore, G. W. K., and Yiquan, Q. (2019). Circulation of the Chukchi Sea shelfbreak and slope from moored time series. Progress in Oceanography, 172(2019), 14-33.

Ljungblad, D. K., Würsig, B., Swartz, S. L., and Keene, J. M. (1988). Observations on the behavioral responses of bowhead whales (*Baleana mysticetus*) to active geophysical vessels in the Alaskan Arctic. Arctic, 41(3), 183-194.

Livingston, E. and Diachok, O. (1989). Estimation of average under-ice reflection amplitudes and phases using matched-field processing. Journal of the Acoustical Society of America, 86(5), 1909-1919.

Macaulay, G. J., Chu, D., and Ona, E. (2020). Field measurements of acoustic absorption in seawater from 38 to 360 kHz. Journal of the Acoustical Society of America, 148(1), 100-107.

Mahanty, M. M., Latha, G., Venkatesan, R., Ravichandran, M., Atmanand, M. A., Thirunavukarasu, A., and Raguraman, G. (2020). Underwater sound to probe sea ice melting in the Arctic during winter. Nature: Scientific Reports, 10(1), 16047.

Marques, T. A., Thomas, L., Ward, J., DiMarzio, N., and Tyack, P. L. (2009). Estimating cetacean population density using fixed passive acoustic sensors: An example with Blainville's beaked whales. Journal of the Acoustical Society of America, 124(4), 1982-1994.

Marcoux, M., Auger-Méthé, M., & Humphries, M. M. (2009). Encounter frequencies and grouping patterns of narwhals in Koluktoo Bay, Baffin Island. Polar Biology, 32(12), 1705-1716.

Marcoux, M., Auger- Méthé, M., and Humphries, M., M. (2012). Variability and context specificity of narwhal (*Monodon monoceros*) whistles and pulsed calls. Marine Mammal Science, 28(4), 649-665.

Markus, T., Stroeve, J. C., and Miller, J. (2009). Recent changes in Arctic sea ice melt onset, freezeup, and melt season length. Journal of Geophysical Research, 114, C12024.

Marques, T. A., Munger, L., Thomas, L., Wiggins, S., and Hildebrand, J. A. (2011). Estimating North Pacific right whale *Eubalaena japonica* density using passive acoustic cue counting. Endangered Species Research, 13, 163-172.

Marques, T. A., Thomas, L., Martin, S. W., Mellinger, D. K., Ward, J. A., Moretti, D. J., Harris, D., and Tyack, P. L. (2013). Estimating animal population density using passive acoustics. Biological Reviews, 88, 287-309.

Matkin, C. O., Barrett-Lenard, L. G., Yurk, H., Ellifrit, D., and Trites, A. W. (2007). Ecotypic variation and predatory behavior among killer whales (*Orcinus orca*) off the eastern Aleutian Islands, Alaska. Fishery Bulletin, 105(1), 74-87.

McDonald, M. A., Hildebrand, J. A., and Wiggins, S. M. (2006). Increases in deep ocean ambient noise in the Northeast Pacific west of San Nicolas Island, California. Journal of the Acoustical Society of America, 120(2), 711-718.

McDonald, M. A., Hildebrand, J. A., Wiggins, S. M., and Ross, D. (2008). A 50-year comparison of ambient ocean noise near San Clemente Island: A bathymetrically complex coastal region off Southern California. Journal of the Acoustical Society of America, 124(4), 1985-1992.

McKenna, M. F., Ross, D., Wiggins, S. M., & Hildebrand, J. A. (2012). Underwater radiated noise from modern commercial ships. The Journal of the Acoustical Society of America, 131(1), 92-103.

Melcón, M. L., Cummins, A. J., Kerosky, S. M., Roche, L. K., Wiggins, S. M., and Hildebrand, J. A. (2012). Blue whales respond to anthropogenic noise., PLoS ONE, 7(2), e32681.

Mellen, R. H., Scheifele, P. M., and Browning, D. G. (1987). Global model for sound absorption in seawater. Naval Underwater Systems Center, Technical Report 7923. Published by the Naval Underwater Systems Center (1987), p. 58.

Mesinger, F., G. DiMego, E. Kalnay, K. Mitchell, & Coauthors. (2006). North American Regional Reanalysis. Bulletin of the American Meteorological Society, 87, 343–360.

Milne, A. R., and Ganton, J. H. (1964). Ambient noise under Arctic-Sea ice. The Journal of the Acoustical Society of America, 36(5), 855-863.

Miller, L. A., Pristed, J., Møhl, B., and Surlykke, A. (1995). The click sounds of narwhals (*Monodon monoceros*) in Inglefield Bay, Northwest Greenland. Marine Mammal Science, 11(4), 491-502.

Millero, F. J., Feistel, R., Wright, D. G. and McDougall, T. J. (2008). The composition of Standard Seawater and the definition of the Reference-Composition Salinity Scale. Deep-Sea Research, 55:50-72

Moore, S. E., and Huntington, H. P. (2008). Arctic marine mammals and climate change: Impacts and resilience. Ecological Applications, 18(2), S157-S165.

Moore, S. M., Stafford, K. M., and Munger, L. M. (2010). Acoustic and visual surveys for bowhead whales in the western Beaufort and northeastern Chukchi Seas. Deep-Sea Research, 57, 153-157.

Moore, S. E., Stafford, K. M., Melling, H., Berchok, C., Wiig, Ø. Kovacs, K. M., Lydersen, C., Richter-Menge, J. (2012). Comparing marine mammal acoustic habitats in Atlantic and Pacific sectors of the High Arctic: year-long records from Fram Strait and the Chukchi Plateau. Polar Biology, 35, 475-480.

Moorse, S. E., and Laidre, K. L. (2006). Trends in sea ice cover within habitats used by bowhead whales in the western Arctic. Ecological Applications, 16(3), 932-944.

Morrissey, R. P., Ward, J., DiMarzio, N., Jarvis, S., and Moretti, D. J. (2006). Passive acoustic detection and localization of sperm whales (*Physeter macrocephalus*) in the Tongue of the Ocean. Applied Acoustics, 67(2006), 1091-1105.

Nielsen, N. H., Laidre, K., Larsen, R. S., and Heide-Jørgensen, M. P. (2015). Identification of potential foraging areas for bowhead whales in Baffin Bay and adjacent waters. Arctic, 68(2):169-179.

Nowacek, D. P., Thorne, L. H., Johnston, D. W., & Tyack, P. L. (2007). Responses of cetaceans to anthropogenic noise. Mammal Review, 37(2), 81-115.

O'Brien, K. L. and Leichenko, R. M. (2000). Double exposure: assessing impacts of climate change within the context of economic globalization. Global Environmental Change, 10(2000), 221-232.

Olnes, J., Citta, J. J., Quakenbush, L. T., George, J. C., Harwood, L. A., Lea, E. V., and Heide-Jørgensen, M. P. (2020). Use of the Alaskan Beaufort Sea by bowhead whales (*Balaena mysticetus*) tagged with satellite transmitters, 2006-18. Arctic, 73(3), 278-291.

Overland, J. E., Hanna, E., Hanssen-Bauer, I., Kim, S. J., Walsh, J. E., Wang, M., Bhatt, U. S., Thoman, R. L., and Ballinger, T. J. (2019). Surface air temperature. *Arctic Report Card 2019*, Richter-Menge, J., Druckenmiller, M. L., and Jeffries, M., Eds. http://www.arctic.noaa.gov/Report-Card.

Payne, R. S. and McVay, S. (1971). Songs of humpback whales. Science, 173(3997), 585-597.

Pickart, R. S., Moore, G. W. K., Mao, C., Bahr, F., Nobre, C., and Weingartner, T. J. (2016). Circulation of winter water on the Chukchi shelf in early summer. Deep-Sea Research II, 130(2016), 56-75.

Pine, M. K., Hannay, D. E., Insley, S. J., Halliday, W. D., & Juanes, F. (2018). Assessing ship slowdown for reducing auditory masking for marine mammals and fish of the western Canadian Arctic. Marine Pollution Bulletin, 135, 290–302. https://doi.org/https://doi.org/10.1016/j.marpolbul.2018.07.031

Pine, M., K.A. Nikolich, B. Martin, C. Morris, and F. Juanes. (2020). Assessing auditory masking for management of underwater anthropogenic noise. Journal of the Acoustical Society of America, 147, 3408-3417.

Pizzolato, L., Howell, S. E., Dawson, J., Laliberté, F., & Copland, L. (2016). The influence of declining sea ice on shipping activity in the Canadian Arctic. Geophysical Research Letters, 43(23), 12-146.

Pirotta, E., Milor, R., Quick, N., Moretti, D., Di Marzio, N., Tyack, P., Boyd, I., and Hastie, G. (2012). Vessel noise affects beaked whale behavior: results of a dedicated acoustic response study. PLoS ONE, 7(8), e42535.

Ramirez, F., Coll, M., Navarro, J., Bustamante, J., and Green, A. J. (2018). Spatial congruence between multiple stressors in the Mediterranean Sea may reduce its resilience to climate impacts. Nature: Scientific Reports, 8(2018), 14871.

Rasmussen, M. H., Koblitz, J. C., and Laidre, K. L. (2015). Buzzes and high-frequency clicks recorded from narwhals (*Monodon monoceros*) at their wintering ground. Aquatic Mammals, 41(3), 256-264.

Richard, P. R., Laake, J. L., Hobbs, R. C., Heide-Jørgensen, M. P., Asselin, N. C., and Cleator, H. (2010). Baffin Bay narwhal population distribution and numbers: Aerial surveys in the Canadian High Arctic, 2002-04. Arctic, 63(1), 85-99.

Robertson, F. C., Koski, W. R., and Trites, A. W. (2016). Behavioral responses affect distribution analyses of bowhead whales in the vicinity of seismic operations. Marine Ecology Progress Series, 549, 243-262.

Rocktröm, J., Steffen, W., Noone, K., Persson, Å., Chapin F. S., Lamblin, E. F., Lenton, T. M., Scheffer, M., Folke, C., Schellenhuber, H. J., Nykvist, B., de Wit, C. A., Hughes, T., van der Leeuw, S., Rodhe, H., Sörlin, S., Snyder, P. K., Costanza, R., Svedin, U., Falkenmark, M., Karlberg, L., Corell, R. W., Fabry, V. J., Hansen, J., Walker, B., Livberman, D., Richardson, K., Crutzen, P., and Foley, J. A. (2009). A safe operating space for humanity. Nature, 461(24), 472-475.

Ross, L. G. (1976). *Mechanics of underwater noise*. Pergamon Press, New York.

Roth, E. H., Hildebrand, J. A., and Wiggins, S. M. (2012). Underwater ambient noise on the Chukchi Sea continental slope from 2006-2009. Journal of the Acoustical Society of America, 131(1), 104-110.

Roy, N., Simard, Y., and Gervaise, C. (2010). 3D tracking of foraging belugas from their clicks: Experiment from a coastal hydrophone array. Applied Acoustics, 71(2010), 1050-1056.

Shapiro, A. D. (2006). Preliminary evidence for signature whistles in free-ranging narwhals (*Monodon monoceros*). Journal of the Acoustical Society of America ,120(3), 1695-1705.

Silber, G. K., Lettrich, M. D., Thomas, P. O., Baker, J. D., Baumgartner, M., Becker, E. A., Boveng, P., Dick, D. M., Feichter, J., Forcada, J., Forney, K. A., Griffis, R. B., Hare, J. A., Hobday, A. J., Howell, D., Laidre, K. L., Mantua, N., Quakenbush, L., Santora, J. A., Stafford, K. M., Spencer, P., Stock, C., Sydeman, W., Van Houtan, K., Waples, R. S. (2017). Projecting marine mammal distribution in a changing climate. Frontiers in Marine Science, 4, 413.

Sills, J. M., Southall, B. L., & Reichmuth, C. (2015). Amphibious hearing in ringed seals (Pusa hispida): underwater audiograms, aerial audiograms and critical ratio measurements. Journal of Experimental Biology, 218(14), 2250-2259.

Simon, M., Wahlberg, M., and Miller, L. A. (2007). Echolocation clicks from killer whales (*Orcinus orca*) feeding on herring (*Clupea harengus*) (L). Journal of the Acoustical Society of America, 121(2), 749-752.

Širović, A., Hildebrand, J. A., and McDonald, M. A. (2016). Ocean ambient sound south of Bermuda and Panama Canal traffic. Journal of the Acoustical Society of America, 139(5),2417-2423.

Širović, A., and Hildebrand, J. A. (2011). Using passive acoustics to model blue whale habitat off the Western Antarctic Penninsula. Deep-Sea Research II, 58(2011), 1719-1728.

Širović, A., Hildebrand, J. A., Wiggins, S. M., McDonald, M. A., Moore, S. E., and Thiele, D. (2004). Seasonality of blue and fin whale calls and the influence of sea ice in the Western Antarctic Peninsula. Deep-Sea Research II, 51,2327-2344.

Skovrind, M., Castruita, J. A. S., Haile, J., Treadaway, E. C., Gopalakrishnan, S., Westbury, M. V., Heide-Jørgensen, M. P., Szpak, P., and Lorenzen, E. D. (2019). Hybridization between two high Arctic cetaceans confirmed by genomic analysis. Nature: Scientific Reports, 9(2019), 7729.

Smith, L. C., & Stephenson, S. R. (2013). New Trans-Arctic shipping routes navigable by midcentury. Proceedings of the National Academy of Sciences, 110(13), E1191-E1195.

Southall, B. L., Bowles, A. E., Ellison, W. T., Finneran, J. J., Gentry, R. L., Greene, C. R., Kastak, D., Ketten, D. R., Miller, J. H., Nachtigall, P. E., Richardson, W. J., Thomas, J. A., and Tyack, P. L. (2007). Marine mammal exposure criteria: Initial scientific recommendations. Aquatic Mammals, 33(4), 411-521.

Spreen, G., L. Kaleschke & G. Heygster. (2008). AMSR-E ASI 6.25 km sea ice concentration data, v.5.4. Hamburg Germany: Institute of Oceanography, University of Hamburg.

Stirling, I. (1973). Vocalizations in the ringed seal (*Phoca hispida*). Journal of the Fisheries Research Board of Canada, 30(10), 1592-1594.

Stafford, K. M. (2019). Increasing detections of killer whales (*Orcinus* orca) in the Pacific Arctic. Marine Mammal Science, 35(2), 696-706.

Stafford , K., M., Laidre, K. L., and Heide-Jørgensen, M. P. (2012). First acoustic recordings of narwhals (*Monodon monoceros*) in winter. Marine Mammal Science, 28(2), e197-e207.

Stafford, K. M., Ferguson, M. C., Hauser, D. D. W., Okkonen, S. R., Berchok, C. L., Citta, J. J., Clarke, J. T., Garland, E. C., Jones, J., and Suydam, R. S. (2017). Beluga whales in the western Beaufort Sea: Current state of knowledge on timing, distribution, habitat use, and environmental drivers. Deep-Sea Research II, 152, 182-194.

Stafford, K. M., Moore, S. E., Berchok, C. L., Wiig, Ø., Lydersen, C., Hansen, E., Kalmbach, D., and Kovacs, K. M. (2012). Spitsbergen's endangered bowhead whales sing through the polar night. Endangered Species Research, 18, 95-103.

Stanistreet, J. E., Nowacek, D. P., Bell, J. T., Cholewiak, D. M., Hildebrand, J. A., Hodge, L. E. W., Van Parijs, S. M., and Read, A. J. (2018). Spatial patterns in acoustic detections of sperm whales *Physeter macrocephalus* along the continental slope in the western North Atlantic Ocean. Endangered Species Research, 35, 1-13.

Stirling, I., Calvert, W., and Cleator, H. (1983). Underwater vocalizations as a tool for studying the distribution and relative abundance of wintering pinnipeds in the High Arctic. Arctic, 36(3), 262-274.

Stroeve, J. C., Markus, T., Boisvert, L., Miller, J., and Barrett, A. (2014). Changes in Arctic melt season and implications for sea ice loss. Geophysical Research Letters, 41, 1216-1225.

Stroeve, J., and Notz, D. (2018). Changing state of Arctic sea ice across all seasons. Environmental Research Letters, 13(2018), 103001

Theocharis, D., Pettit, S., Rodriguez, V. S., and Haider, J. (2018). Arctic shipping: A systematic literature review of comparative studies. Journal of Transport Geography,69, 112-128.

Thode, A. M., Blackwell, S. B., Seger, K. D., Conrad, A. S., Kim, K. H., and Macrander, A. M. (2016). Source level and calling depth distributions of migrating bowhead whale calls in the shallow Beaufort Sea. Journal of the Acoustical Society of America, 140(6), 4288-4297.

Thode, A. M., Blackwell, S. B., Conrad, A. S., Kim, K. H., and Macrander, A. M. (2017). Decadal-scale frequency shift of migrating bowhead whale calls in the shallow Beaufort Sea. Journal of the Acoustical Society of America, 142(3), 1482-1502.

Tittensor, D. P., Mora, C., Jetz, W., Lotze, H. K., Ricard, D., Berghe, E. V., and Worm, B. (2010). Global patterns and predictors of marine biodiversity across taxa. Nature, 466(26), 1098-1102.

Tivy, A., Howell, S. E. L., Alt, B., McCourt, S., Chagnon, R., Crocker, G., Carrieres, T., and Yackel, J. J. (2011). Trends and variability in summer sea ice cover in the Canadian Arctic based on the Canadian Ice Service Digital Archive, 1960-2008 and 1968-2008. Journal of Geophysical Research, 116, C03007, p25.

Toole, J. M., Krishfield, R. A., Timmermans, M. L., and Proshutinsky, A. (2011). The ice-tethered profilier: Argo of the Arctic. Oceanography, 24(3), 126-135.

Von Brenda-Beckmann, A. M., Thomas, L., Tyack, P. L., and Ainslie, M. A. (2018). Modeling the broadband propagation of marine mammal echolocation clicks for click-based population density estimates. Journal of the Acoustical Society of America, 143(2), 954-967.

Walsh, C., Lazarou, N., Traut, M., Price, J., Raucci, C., Sharmina, M., Agnolucci, P., Mander, S., Gilbert, P., Anderson, K., Larkin, A., and Smith, T. (2019). Trade and trade-offs: Shipping in changing climates. Marine Policy, 106(2019), 103537.

Warner, G. A., Dosso, S. E., Dettmer, J., and Hannay, D. E. (2015). Bayesian environmental inversion of airgun modal dispersion using a single hydrophone in the Chukchi Sea. Journal of the Acoustical Society of America, 137(6),3009-3023.

Wartzok, D., Popper, A. N., Gordon, J, and Merrill, J. (2003). Factors affecting the responses of marine mammals to acoustic disturbance. Marine Technology Society Journal, 37(4), 6-15.

Weingartner, T., Aagaard, K., Woodgate, R., Danielson, S., Sasaki, Y., and Cavalieri, D. (2005). Circulation on the north central Chukchi Sea shelf. Deep-sea Research, 52(2005), 3150-3174.

Wenz, G. M. (1962). Acoustic ambient noise in the ocean: Spectra and sources. Journal of the Acoustical Society of America, 34(12), 1936-1956.

Wiggins, S.M., and Hildebrand, J.A. 2007. High-frequency Acoustic Recording Package (HARP) for broad-band, long-term marine mammal monitoring. International Symposium on Underwater Technology 2007 and International Workshop on Scientific Use of Submarine Cables & Related Technologies 2007. Tokyo: Institute of Electrical and Electronics Engineers. 551 – 557.

Willoughby, A. L., Ferguson, M. C., Stimmelmayr, R., Clarke, J. T., and Brower, A. A. (2020). Bowhead whale (Balaena mysticetus) and killer whale (Orcinus orca) co-occurrence in the U.S. Pacific Arctic, 2009-2018: evidence from bowhead whale carcasses. Polar Biology, 2020(43), 1669-1679.

Wilmut, M. J., Chapman, N. R., Heard, G. J., and Ebbeson, G. R. (2007). Inversion of Lloyd Mirror Field for determining a source's track. IEEE Journal of Ocean Engineering, 32, 940-947.

Xiangmei, M., Guanbao, L., Guozhong, H., and Guangming, K. (2015). Sound velocity and related properties of seafloor sediments in the Bering and Chukchi Sea. Acta Oceanologica Sinica, 34(5), 75-80.

Yang, T. C. and Votaw, C. W. (1981). Under-ice reflectivities at frequencies below 1 kHz. Journal of the Acoustical Society of America, 70(3), 841-851.

Yurkowski, D. J., Young, B. G., and Ferguson, S. H. (2018). Spring distribution of ringed seals (*Pusa hispida*) in Eclipse Sound and Milne Inlet, Nunavut: implications for potential icebreaking activities. Arctic Science, 5(2019), 54-61.

Zhu, C., Garcia, H., Kaplan, A., Schinault, M., Handegard, N. O., Godø, O. R., Huang, W., and Ratilal, P. (2018). Detection, localization, and classification of multiple mechanized ocean ships over continental-shelf scale regions with passive ocean acoustic waveguide remote sensing. Remote Sensing, 2018(10), p26.